

AMERICAN UNIVERSITY OF BEIRUT

COMPARATIVE ASSESMENT OF DIFFERENT STATIC
MIXERS USING CFD

by
RANIM MOUDASER CHAKLEH

A thesis
submitted in partial fulfillment of the requirements
for the degree of Master of Engineering
to Baha and Walid Bassatne Department of Chemical Engineering
and Advanced Energy
of the Maroun Semaan Faculty of Engineering and Architecture
at the American University of Beirut

Beirut, Lebanon
April 2022


AMERICAN UNIVERSITY OF BEIRUT

THESIS RELEASE FORM

Student Name: ___ Chakleh ___ Ranim ___ Moudaser ___
Last First Middle

I authorize the American University of Beirut, to: (a) reproduce hard or electronic copies of my thesis; (b) include such copies in the archives and digital repositories of the University; and (c) make freely available such copies to third parties for research or educational purposes:

- As of the date of submission
- One year from the date of submission of my thesis.
- Two years from the date of submission of my thesis.
- Three years from the date of submission of my thesis.

 _____ May 5, 2022
Signature Date

ACKNOWLEDGEMENTS

First, I would like to express my deepest gratitude to my advisor Prof. Fouad Azizi. The accomplishment of this thesis would not have been possible without your patience, endless encouragement, valuable guidance, and great support. Thank you for your insightful comments and for taking the time to read through this thesis and answer my endless questions.

I would also like to thank Prof. Joseph Zeaiter and Prof. Marwan Darwish for accepting to be on my committee.

I am very thankful to Dr. Walid Abou Hweij for providing me with the geometry of the new mixer. I appreciate your guidance throughout this thesis and I am very grateful for the endless and fruitful discussions we had.

My sincere gratitude goes to the MCF scholarship program for its financial and academic support. Special thanks go to Ms. Patil Yessayan, you believed in me from day 1.

My gratitude extends to the IT department and the HPC-support group at the American University of Beirut.

I can't forget to thank Sabah, Mariam, Elham, and Siham. You lifted me up when I was about to give up!

I am forever grateful to my mom, Najwa, and my sister Ghadir. You never fail to show me love. Thank you for all your sacrifices to make me happy and successful. I am blessed to have you as a great support system!

My deepest gratitude goes to Moudaser's immortal soul, to the forever closest to my heart, to my role model and source of inspiration, my beloved Dad... you taught me to keep moving in this life and challenge myself... I always recall my last promise to you ...yet, sometimes "in the midst of the chaos", we are forced to slow down... who knows, "*peut être on doit parfois s'égarer pour mieux se retrouver!*" ... I hope you are proud of your little girl!

Last but not least, I owe it all to GOD, my source of peace and countless blessings!

ABSTRACT OF THE THESIS OF

Ranim Moudaser Chakleh

for

Master of Engineering

Major: Chemical Engineering

Title: Comparative Assessment of Different Static Mixers Using CFD

A numerical investigation was carried out to compare the hydrodynamics and the mixing performance of three variants of static mixers under turbulent flow conditions where the pipe Reynolds numbers varied between 5,000 and 30,000. The investigated mixers are the standard helical Kenics mixer, the corrugated Sulzer SMV mixer and a modified geometry of the screen-type static mixer. This new geometry is based on the use of specially located divergent inserts downstream of a woven mesh in an attempt to improve its distributive mixing.

Comparing the flows through these mixers was based on the pressure drop, velocity fields in addition to quantifying both the dispersive and distributive mixing efficiencies. The latter was accomplished by computing the dispersive mixing efficiency coefficient (i.e., extensional efficiency) and the intensity of segregation (i.e., coefficient of variation) at the outlet of the mixing chambers. Pressure drop was found larger in the new mixer geometry which generated values that are 1.2 and 3 times larger than those in the Kenics and SMV mixers, respectively. In addition, the Kenics and SMV mixers exhibited better distributive mixing than the newly proposed design since they were able to achieve the desired, commonly acceptable, homogeneity level. However, dispersive mixing was found to be improved in the new mixer where an average extensional efficiency of 0.68 was obtained compared to values of 0.57 and 0.53 in the Kenics and SMV mixers, respectively. The results suggest that the new mixer geometry can be further optimized to meet the desired mixing and power consumption criteria by optimizing various geometric parameters such as the geometry of the woven mesh, as well as the length, width, and location of the downstream inserts.

TABLE OF CONTENTS

ACKNOWLEDGEMENTS	1
ABSTRACT	2
TABLE OF CONTENTS	3
ILLUSTRATIONS	7
TABLES	11
NOMENCLATURE	12
1 INTRODUCTION	14
2 LITERATURE REVIEW	20
2.1 Evaluation of the Performance of Static Mixers.....	20
2.1.1 Pressure Drop.....	20
2.1.2 Mixing and Flow Characterization	27
2.1.3 Mixing Parameters.....	30
2.2 Mixing and Flow Characterization of Kenics, SMV and STSM.....	34
2.2.1 Kenics	34
2.2.2 SMV.....	37
2.2.3 STSM.....	39
2.3 Comparative Studies	42
2.4 Conclusions.....	45
3 SOLUTION METHODS.....	47

3.1	Geometric and Computational Domains.....	47
3.2	Working Fluid and Operating Conditions	51
3.3	Computational Domain Discretization	52
3.4	Numerical Model	53
3.4.1	Governing Equations and Assumptions.....	55
3.5	Computational Methods and Boundary Conditions.....	56
3.5.1	Model Validation	57
3.6	Hydrodynamic and Mixing Assessment	58
4	MESH SENSITIVITY ANALYSIS	59
5	KENIC STATIC MIXER: HYDRODYNAMICS AND MIXING EFFICIENCY	66
5.1	Hydrodynamics and Model Validation.....	66
5.1.1	Pressure Drop and Model Validation.....	66
5.1.2	Pressure and Velocity Distributions	71
5.2	Mixing Efficiency	77
5.2.1	Dispersive Mixing: Extensional Efficiency	78
5.2.2	Distributive Mixing.....	82
5.2.3	M-Number	88
6	SMV STATC MIXER: HYDRODYNAMICS AND MIXING EFFICIENCY	91
6.1	Hydrodynamics and Model Validation.....	91
6.1.1	Pressure Drop and Model Validation.....	91
6.1.2	Pressure and Velocity Distributions	94

6.2	Mixing Efficiency	100
6.2.1	Dispersive Mixing: Extensional Efficiency	100
6.2.2	Distributive Mixing: Coefficient of Variation and Aerial Distribution....	103
6.2.3	M-Number	105
7 NEW VARIANT OF SCREEN-TYPE STATIC MIXER: HYDRODYNAMICS AND MIXING EFFICIENCY		107
7.1	Hydrodynamics and Model Validation.....	107
7.1.1	Pressure Drop and Model Validation.....	107
7.1.2	Pressure and Velocity Distributions	110
7.2	Mixing Efficiency	113
7.2.1	Dispersive Mixing: Extensional Efficiency	113
7.2.2	Distributive Mixing: Coefficient of Variation and Aerial Distribution....	116
7.2.3	M-Number	118
8 COMPARISON BETWEEN THE THREE STATIC MIXERS INVESTIGATED IN THIS STUDY		120
8.1	Pressure Drop.....	120
8.2	Mixing Performance	123
8.2.1	Extensional Efficiency.....	123
8.2.2	CoV.....	129
8.2.3	Global Comparison.....	131
9 CONCLUSIONS AND RECOMMENDATIONS		135
APPENDIX 1 KENICS MIXER.....		139
APPENDIX 2 SMV MIXER.....		143

REFERENCES146

ILLUSTRATIONS

Figure

1. Types of static mixers: (a) Kenics, (b) LPD, (c) LLPD, (d) HEV, (e) SMV, (f) SMX, (g) SMX ⁺ and (h) ISG.....	16
2. Kenics flow pattern.....	17
3. SMV flow pattern	18
4. The flow domain of the three mixers from left to right: SMV, new mixer and Kenics.	48
5. One SMV unit.....	48
6. Geometric properties of a screen	49
7. Geometric properties of the new mixer	50
8. Mesh of 2-mixing units of Kenics over the yz plane.....	62
9. Schematic of the SMV mesh over the yz plane of 2 elements.....	64
10. Local Mesh refinement of the new mixer.....	64
11. Comparison of Kenics Fanning friction factor obtained in this study to the literature data	67
12. a) Pressure drop and b) Pressure drop per 1 element for 2, 4, and 6- Kenics mixer versus Re_{pipe}	70
13. Axial distribution of static pressure in a Kenics mixer (red curves) and rate of pressure variation per unit length (blue curves) at $Re_{pipe}=5,000$ (left column) and 30,000 (right column).	71
14. The resultants of the radial and tangential velocity components (2D streamlines) superimposed on the contour plots of the axial velocity at various axial locations within the 5 th Kenics unit at $Re=30,000$	73
15. Velocity Field through Kenics at $Re_{pipe} = 30,000$ (a) Streamlines of the flowing fluid through 6 Kenics elements and (b) vorticity contours over the central vertical plane.....	75
16. (a) Axial velocity contour plots overlaid by the tangential and radial velocity components and (b) normalized axial velocity profiles at different axial positions downstream of the last mixing element in a 6-Kenics elements mixer at $Re=30,000$ and 5,000.....	76
17. Axial variation of the extensional efficiency for 6-Kenics elements at $Re=30,000$	78

18. contour plots of extensional efficiency at different locations within the 5 th Kenics unit and downstream of the mixing section at Re=30,000	79
19. Axial variation of the area-weighted average extensional efficiency β for a Kenics mixer of 6 units.....	81
20. Axial Variation of CoV in a Kenics mixer comprising a) 2 b) 4 and c) 6 units at different Re numbers	83
21. Variation of the CoV at the outlet of the mixer chamber of Kenics as a function of Re numbers	84
22. Contour plots of the mass fraction of the secondary fluid in a Kenics comprising 6 elements for Re=5,000 and Re=30,000	85
23. Stacked bar graphs showing the discrete areal distribution of the mass fraction of the secondary fluid in Kenics at different locations for Re=5,000 (first column), Re=30,000 (second column), and for different numbers of mixing units: 2 elements (first row), 4 elements (middle row) and 6 elements (last row).....	87
24. a) M number, b) ω_{iso} (dashed lines) and ω_{max} (solid lines) for 2, 4 and 6 kenics elements.....	88
25. Comparison of SMV hydraulic Fanning friction factor obtained in this study to the literature data	92
26. Pressure drop (a) ΔP across the whole length of the mixer and (b) per 1 element (ΔPe) for 2 and 4-elements SMV mixers versus Re_{pipe}	94
27. Axial distribution of static pressure in a 4-element SMV mixer at $Re_{pipe}=30,000$	95
28. Velocity field through an SMV mixer at Re = 30,000: (a) contour plots of the radial velocity, (b) resultants of the radial and tangential velocity components (2D streamlines) superimposed on the contour plots of the axial velocity at various axial locations within the 2 nd SMV unit, and c) vorticity contour over the longitudinal plane located at $r/R = 0.4$	97
29. a) Axial velocity contour plots overlaid by the tangential and radial velocity components at Re=30,000 and b) normalized axial velocity profiles at different axial positions downstream of the last mixing element in a 2-SMV mixer at Re=5,000 and 30,000.....	98
30. Axial variation of the extensional efficiency for a 4-SMV mixer at various Re_{pipe}	100
31. Contour plots of extensional efficiency at different locations through the SMV static mixer at $Re_{pipe}=30,000$	102
32. Axial Variation of CoV in a SMV mixer comprising a) 2 b) 4 units at different Re numbers	103

33. Contour plots of the mass fraction of the secondary fluid in an SMV mixer comprising 2 elements for $Re=5,000$ and $Re=30,000$	104
34. Variation of the CoV at the exit of the mixing chamber of SMV with Re_{pipe}	105
35. SMV M-number variation with Re_{pipe}	106
36. The Fanning Friction factor of the screens alone compared to the correlation of Azizi (2019)	109
37. Axial distribution of the area-weighted average static pressure (a) along the complete new mixer length, and (b) zoomed around the 3rd screen and inserts.	112
38. Axial velocity contour plot at the central yz plane of the new mixer at $Re_{pipe}=30,000$	113
39. Axial variation of the extensional efficiency for 4 mixing elements of the new mixer a) at various Re_{pipe} , b) zoomed around the 3 rd hybrid element.....	114
40. Axial variation of CoV in 4 mixer elements of the new mixer a) along the mixer length b) at the exit of the mixing chamber at various Re_{pipe}	116
41. Discrete distribution of the aerial distribution of the mass fraction of the tracer in the new mixer at $Re_{pipe}=5,000$ and $Re_{pipe}=30,000$	117
42. Pressure losses across the investigated geometries at different Re_{pipe} (a) in terms of pressure drop ΔP across the entire volume, and (b) in terms of drag coefficient (K) for one mixing unit	122
43. Axial distribution of the area-weighted average extensional efficiency for Kenics, SMV and the novel geometry of screen-type static mixer at $Re_{pipe} = 5,000$ and $30,000$	124
44. Volumetric cumulative extensional efficiency for the different designs at (a) $Re_{pipe} = 5,000$ and (b) $Re_{pipe} = 30,000$ over the entire mixing chamber	127
45. Volumetric cumulative extensional efficiency for the different designs at (a) $Re_{pipe} = 5,000$ and (b) $Re_{pipe} = 30,000$ over the regions of the mixers occupied by the mixing units.	128
46. CoV at the exit of the mixing chamber for the various configurations versus Re_{pipe}	129
47. CoV of the various configurations versus the pressure drop they generate ..	132
48. CoV of the different mixers versus the amount of the energy input in unit time and unit volume	133
49. Axial distribution of the extensional efficiency β in kenics containing 6 elements at different Re numbers	139

50. Planar velocity streamlines colored by the axial vorticity at different planes a) within the 2nd SMV element and b) downstream of the mixing section at Re=30,000.....	143
51. Axial variation of the extensional efficiency β in a 4-SMV mixer at different Re numbers	144
52. Stacked bar graphs showing the discrete areal distribution of the mass fraction of the secondary fluid in SMV at different locations for Re=5,000 (first column), Re=30,000 (second column), and for different numbers of mixing units: 2 elements (first row) and 4 elements (second row).....	145

TABLES

Table

1. Pressure Drop correlations for KM, SMV, and STSM.....	25
2. Geometric properties of the three geometries investigated in this study.....	50
3. Physical properties of the working fluid (water) at 25°C	51
4. Operating conditions investigated in the current study	51
5. Kenics grid sensitivity analysis	60
6. SMV grid sensitivity analysis.....	63
7. NM grid sensitivity analysis	65
8. Geometrical aspects of Kenics used in the current and the literature studies..	69
9. ω_{max} , ω_{iso} , M number and CoV for Kenics mixer at $Re=30,000$	89
10. Average, maximum and minimum % relative error between the measured fh and the available literature data For SMV	93
11. ω_{max} , ΔP , M parameter, CoV and CoV_{pipe} at $4D$ downstream of the mixing chamber for the modified geometry of STSM.....	119
12. Table summarizing the results of ΔP , β and CoV for the various configurations investigated in the current study	134

NOMENCLATURE

<i>b</i>	Wire diameter	[<i>mm</i>]
<i>CoV</i>	Coefficient of variation	[–]
<i>D</i>	Pipe diameter	[<i>mm</i>]
<i>D_{f-f}</i>	Distance between two flaps	[<i>mm</i>]
<i>D_{SM}</i>	Diamtere of the Static mixer	[<i>mm</i>]
<i>e</i>	Screen thickness	[<i>mm</i>]
ΔP	Total pressure drop in static mixers	[<i>Pa</i>]
ΔP_e	pressure drop per one element	[<i>Pa</i>]
ΔP_0	Pressure drop in empty pipes	[<i>Pa</i>]
<i>Eu</i>	Euler number	[–]
<i>f</i>	Fanning friction factor	[–]
<i>k</i>	Turbulent kinetic energy	[<i>m²/s²</i>]
<i>K</i>	Drag coefficient	[–]
<i>K_s</i>	Screen Drag coefficient	[–]
<i>L_e</i>	Length of one static mixer unit	[<i>mm</i>]
<i>L_f</i>	Length of the flap	[<i>mm</i>]
<i>M</i>	Mesh size	[<i>mm</i>]
<i>Mn</i>	Mesh number	[–]
<i>M</i>	M number	[–]
<i>Ne</i>	Newton Number	[–]
<i>P_i</i>	Pressure at the inlet	[<i>Pa</i>]
<i>P_o</i>	Pressure at the outlet	[<i>Pa</i>]
<i>R</i>	radius	[<i>mm</i>]
<i>u</i>	instantaneous velocity	[<i>m/s</i>]
\bar{u}	Average velocity	[<i>m/s</i>]
<i>t</i>	Time	[<i>s</i>]
<i>t_p</i>	Thickness of a plate	[<i>mm</i>]
<i>y⁺</i>	Non-dimensional wall distance	[–]

Greek letters

α	Fractional open area	[%]
β	Extensional Efficiency	[–]
ε	Rate of energy dissipation per unit mass	[<i>m²/s³</i>]
ϕ	Porosity	[–]
γ	Deformation tensor	[<i>1/s</i>]
μ	Dynamic viscosity	[<i>Pa. s</i>]
ω	Vorticity tensor	[<i>1/s</i>]
ρ	Density	[<i>kg/m³</i>]

Dimensionless Group

Re_{pipe}	Pipe Reynolds Number	[-]
Re_h	Hydraulic Reynolds Number	[-]
Re_b	Wire Reynolds Number	[-]

Abbreviations

CoV	Coefficient of variation
DNS	Direct Numerical Simulation
FVM	Finite Volume Method
HEV	High Efficiency Vortex
ISG	Interfacial Surface Generator
KM	Kenics Mixer
LIF	Laser-Induced Fluorescence
LPD	Low Pressure Drop
MSM	M-type
NM	New Mixer
PI	Process Intensification
PNN	Point to The Nearest Neighbor
RANS	Reynolds-Average Navier-Stocks
RSM	Right- twist type
RSM	Reynolds Stress Model
RTD	Residence Time Distribution
SSM	Spiral-type
STSM	Screen-Type Static Mixer

CHAPTER 1

INTRODUCTION

The emergence of the concept of process intensification (PI) in the 1970s was followed by an increased interest in safer, more energy-efficient, cleaner and more compact technologies (Cremaschi, 2014). In the process industry, attention shifted toward multipurpose apparatuses, which can handle different operations at lower capital and operating costs. One example is the increased interest in the use of static elements to perform mixing operations.

Mixing is a complex operation that is omnipresent in most industries, including, but not limited to, chemical, pharmaceutical, polymer, petroleum, water, and wastewater. It aims at reducing the concentration non-uniformities while enhancing chemical reactions, heat, and mass transfer operations. A broad spectrum of mixers exists to satisfy these diverse needs and applications. Hence, making the right selection becomes crucial for the success of the operation because inconsistent results would have major consequences on the safety, economy, and feasibility of the process.

Static mixers are motionless equipment consisting of a tube or duct equipped with stationary elements. They are responsible for splitting the flow into substreams that are then twisted, accelerated, stretched, or rotated before being recombined. The purpose behind this is to foster the chaotic behavior of the flow, enhance the distributive and diffusive mixing mechanisms, and induce radial mixing (Regner et al., 2006; Theron & Le Sauze, 2011). In such conditions, near plug flow conditions are achievable, and narrower residence time distributions can be obtained (Haddadi et al.,

2020). These mixers provide high mixing intensities in shorter residence time and at lower energy consumption.

The use of static mixers gained momentum in the last few decades because they present many advantages over conventional designs. In general, static mixers outperform stirred tanks when dealing with fast competitive reactions and with materials that degrade over time (Bourne et al., 1992; Myers et al., 2018). Moreover, they are safer, compacter, almost maintenance-free, and durable. They also provide a quasi-uniform energy dissipation rate. Static mixers can serve in batch and continuous processes where they can be used in a once-through or recycle loop (Thakur et al., 2003).

These aforementioned properties make them suitable for different applications, such as mixing of miscible fluids and reacting systems, interface generation in multiphase systems, heat transfer, and thermal homogenization (Thakur et al., 2003). They can also handle fluids of different rheological properties (Jegatheeswaran et al., 2020) and they are appropriate for both laminar and turbulent flow regimes. Ghanem et al. (2014) classified them into five main categories based on their designs: Open designs with helices (cf. Figure 1a), open designs with blades or vortex generators (cf. Figure 1b, Figure 1c, Figure 1d), corrugated plates (cf. Figure 1e), multilayer designs (cf. Figure 1f, Figure 1g), and closed designs with channels or holes (cf. Figure 1h).

A plethora of experimental and numerical studies tackling different aspects of static mixing can be found in the literature. These studies focused on their design and optimization, hydrodynamics, and mixing performance, and even heat transfer capabilities and applications. However, the majority assessed their performance under

laminar flow conditions while little attention has been devoted to investigating static mixers in turbulent regimes even though such conditions are important for operations such as coagulation and disinfection in water and wastewater treatment industries, emulsification, heat transfer operations, oxygen mass transfer in aerobic bioreactors, synthesis of pharmaceuticals and gas-liquid dispersion (Montante et al., 2016).

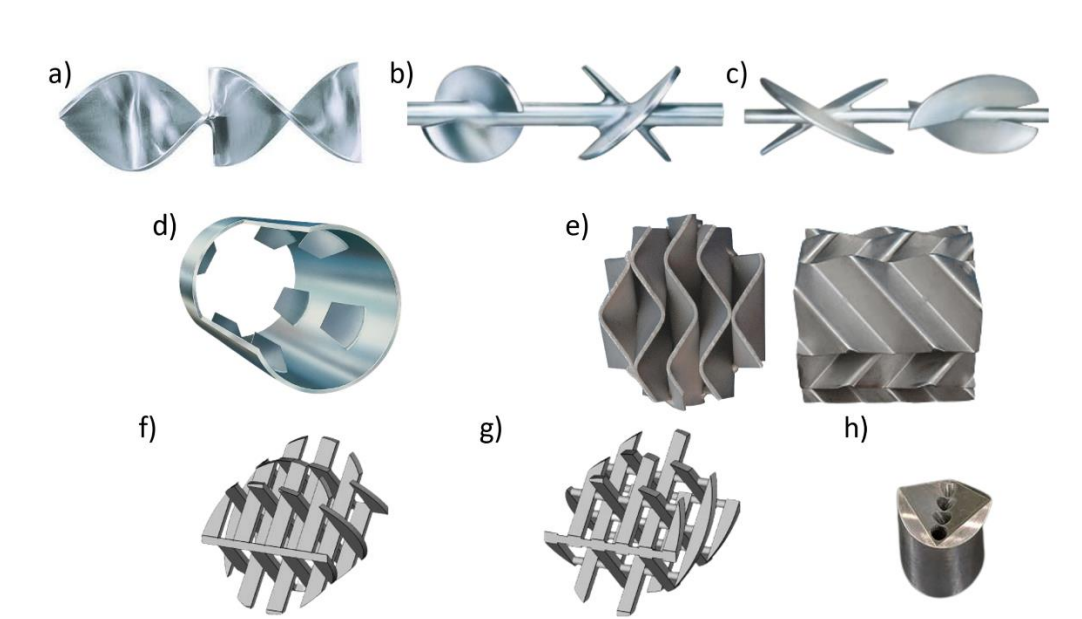


Figure 1 Types of static mixers: (a) Kenics, (b) LPD, (c) LLPD, (d) HEV, (e) SMV, (f) SMX, (g) SMX⁺ and (h) ISG

A literature search shows that the available studies that compared the performance of various static mixers mostly deals with their performance in laminar regimes. To the best of our knowledge, the number of comparative studies undertaken under turbulent flow conditions is only six and are reviewed in Section 2.3. Moreover, these studies focused on assessing their hydrodynamic performance only while less effort was invested in comparing compare their mixing efficiency.

Kenics, SMV, and screen-type static mixers are attractive choices for mixing in turbulent applications. The helical Kenics is one of the most widely studied static mixers. It consists of a series of alternating twisted plates that divide the flow and allow the fluid to move back and forth between the center of the tube and its walls (cf. Figure 1a and Figure 2). This configuration aims at stretching and folding the fluid elements to reduce non-uniformities (Song & Han, 2005). Kenics has been employed for a variety of applications including liquid-liquid dispersion (Hideo Tajima et al., 2010), gas separation (H. Tajima et al., 2010), polymer mixing (Bigg, 1975) and wastewater treatment (Krstić et al., 2007).



Figure 2 Kenics flow pattern

SMV is another variant that has been investigated in applications involving large-diameter pipes constrained by short lengths (Etchells & Meyer, 2004). The Sulzer SMV consists of several corrugated sheets stacked on top of each other to form open channels (cf. Figure 1e). These channels divide the flow into many substreams as depicted in Figure 3. The geometry of SMV allows the flow to rotate to the right and left periodically as it is diverted towards the plates' folded edges that typically form an angle of 45° to the flow axis (Lang et al., 1995). In this kind of mixers, it was shown that turbulence can be reached at pipe Reynolds numbers of approximately 1,130 (Theron & Le Sauze, 2011) which makes them suitable for a variety of applications

including single and multi-phase applications, heat transfer, and chemical reactions (Coroneo et al., 2012).

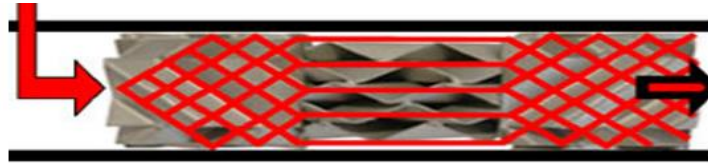


Figure 3 SMV flow pattern

Woven wire screens have been investigated in the last few decades as static mixers in reactive systems and multiphase applications. Inserting a grid normal to the flow direction is one of the simplest ways to generate, promote or reduce turbulence (Roache, 1986). Screen-type static mixers consist of a series of wire matrices whose function is to “repetitively superimpose an adjustable radially-uniform and highly turbulent field in high-velocity pipe flows” (Abou-Hweij & Azizi, 2020a; Azizi & Al Taweel, 2011; Azizi & Taweel, 2011; Habchi & Azizi, 2018). Plug flow conditions can also be attained in these types of mixers because of the low axial and radial dispersion (Abou Hweij & Azizi, 2015; Azizi & Abou Hweij, 2017). These attributes make STSM suitable for processing multiphase flow systems. The high-energy dissipation prevalent in the proximity of the screens favors the formation of finely dispersed phase entities (i.e. bubble/drop) that coalesce when further traveling downstream of the screen to the low energy dissipation region. In an attempt to improve the distributive behavior of these mixers, Abou-Hweij (2022) suggested the addition of divergent inserts downstream of the screens to continuously divert the flow.

Therefore, this study aims at conducting numerical investigations to compare the hydrodynamics and the mixing efficiencies of Kenics, SMV, and the modified geometry

of STSM under turbulent flow regimes for a pipe Re range of 5,000 to 30,000. This will be accomplished using several parameters, mainly the pressure drop, the extensional efficiency, β , and the coefficient of variation, CoV , in addition to analyzing the velocity fields. This study will be the first to compare the hydrodynamics, the distributive, and the dispersive behavior of the aforementioned mixers under the same operating conditions. Consequently, it will help better decision-making in choosing an appropriate static mixer for turbulent applications.

Thesis structure:

The thesis consists of nine chapters. Chapter 1 provides a background about static mixer and a statement of the research aims. In Chapter 2, the studies tackling topics about pressure drop, flow, and mixing characterization in static mixers are reviewed. Chapter 3 describes the fluid domain and discusses the solution methods adopted in the current research study. The results of the current study are then reported and discussed in Chapter 4 through Chapter 8, where Chapter 4 reports on the results of the grid sensitivity analysis. Chapters 5, 6 and 7 present the results and discussion of the hydrodynamics and mixing simulations of Kenics, SMV and the new mixer, respectively. In Chapter 8, the performance of the three mixers is compared based on the previous observations. This is then followed by Chapter 09 which presents the conclusions and recommendations of the current study.

CHAPTER 2

LITERATURE REVIEW

2.1 Evaluation of the Performance of Static Mixers

Assessing the performance of static mixers is of utmost importance for the success of the processes where these mixers are being employed. Basically, a mixer is assessed based on three criteria: the level of mixedness, the power consumption directly related to the pressure drop across a mixer and the mixing time (Rahmani et al., 2007). In the current study, only the first two criteria were taken into account as the third one is more critical for systems involving chemical reactions. In the following, the characterization techniques, tools and parameters used to assess the performance of static mixers are reviewed.

2.1.1 Pressure Drop

Pressure drop is a measure of flow resistance, and it defines the cost of energy input, i.e. pumping power (Jegatheeswaran et al., 2020). Static mixers generate pronounced pressure drop values compared to empty tubes due to their complex structures that impede the flow of the fluid. This makes pressure drop a decisive criterion for the selection and optimization of a design. In fact, it is always desired to achieve high degrees of homogeneity at low operating expenditures.

In the literature, data for pressure drop is basically reported following one of two approaches. The first approach consists of comparing the pressure drop across a static mixer (ΔP) to that across an empty pipe (ΔP_0) of the same length and diameter through

a dimensionless number known as Z factor (Eq.(1)). This approach is usually adopted in laminar regimes for Newtonian fluids (Theron & Le Sauze, 2011). However, some authors used the Z factor to report their pressure drop data in turbulent regimes (Kumar et al., 2008).

$$Z = \frac{\Delta P}{\Delta P_0} \quad (1)$$

The second approach consists of expressing the pressure drop in terms of a friction factor f or Newton number Ne as follows :

$$Ne = 2f = \frac{\Delta P D}{\rho \bar{u}^2 L} \quad (2)$$

In Eq. (2), f is the fanning friction factor, D is the pipe diameter, ρ is the fluid density, \bar{u} is the mean superficial velocity and L is the total mixer length. Some researchers relied on a modified form of Eq.(2) where the superficial velocity \bar{u} is replaced by the interstitial velocity (\bar{u}/ϕ) such that ϕ is the porosity of the mixer (Theron & Le Sauze, 2011). Consequently, the interstitial friction factor, f_i represented in Eq. (3) could be used instead. Joshi et al. (1995) and Theron and Le Sauze (2011) used the hydraulic friction factor f_h shown in Eq.(4) where the pipe diameter D in Eq.(3) is replaced by the hydraulic diameter D_h .

$$f_i = \frac{\Delta P \phi^2 D}{2\rho \bar{u}^2 L} \quad (3)$$

$$f_h = \frac{\Delta P \phi^2 D_h}{2\rho \bar{u}^2 L} \quad (4)$$

The hydraulic diameter of a static mixer can be calculated based on Eq.(5) where a is the specific surface area of the mixer, i.e. the ratio of the surface area to the

unit volume of the mixer (Lebaz & Sheibat-Othman, 2019). For woven wire meshes, ϕ and a can be calculated following the set of Eq.(6) where W is the length of a wire segment, and e is the screen thickness, b is the wire diameter and M is the mesh size (Azizi, 2019).

$$D_h = \frac{4\phi}{a} \quad (5)$$

$$\begin{cases} \phi = 1 - \left[\frac{\pi}{2e} \left(\frac{b}{M} \right)^2 W \right] \\ e = 2b \\ W = \sqrt{b^2 + M^2} \\ a = \pi \frac{W}{M^2} \end{cases} \quad (6)$$

Since different geometries and sizes of static mixers exist, there is no one universal correlation for pressure drop that applies to all static mixers (Azizi, 2019; Paglianti & Montante, 2013). Therefore, different forms of correlations are found in the literature. Expressions similar to Eq. (7) have been used to correlate the pressure drop data over a wide range of Re spanning laminar and turbulent flow conditions. The contribution of laminar flow is expressed by the first term on the right-hand side of the equation, whereas the second term represents the contribution of the turbulent flow in such a way that at high Re, the friction factor becomes independent of the fluid velocity. Sir and Lecjaks (1982) correlated their experimental pressure drop data across a Kenics mixer using this type of equation over a Re ranging between 0.01 and 10,000 with \pm 11% mean square error. Correlations in the form of Eq. (8) (Azizi, 2019) and Eq. (9) (Hosseini et al., 2019) were also employed in both laminar and turbulent regimes.

$$f = \frac{c_1}{Re} + c_2 \quad (7)$$

$$f = \frac{c_3}{Re^\gamma} + c_4 \quad (8)$$

$$f = \frac{c_5}{Re} + \frac{c_6}{Re^\gamma} \quad (9)$$

Other studies dealt with pressure drop in laminar and turbulent regimes separately relying on expressions similar to Eq. (10) and Eq. (11) respectively. Theron and Le Sauze (2011) adopted a Blasius type equation similar to that shown in Eq. (11) with $\gamma = 0.25$ to correlate their pressure drop data in SMV, SMX and SMX⁺.

$$f = \frac{c_7}{Re} \quad (10)$$

$$f = \frac{c_8}{Re^\gamma} \quad (11)$$

In Eq. (7), (8), (9), (10) and (11), $c_1, c_2, c_3, c_4, c_5, c_6, c_7, c_8$ and γ are constants. γ is a function of Re that decreases when Re increases, however this constant is usually smaller than 1 (Azizi, 2019).

Most of the available studies about pressure drop in static mixers are conducted under laminar flow conditions and few studies have tackled this subject in turbulent regimes. Among these studies, Song and Han (2005) conducted a CFD study to predict the pressure drop across Kenics design. The authors tested various fluid and flow conditions and different geometric properties and proposed a pressure drop correlation for a Kenics mixer covering a wide range of Re that may go beyond 10^6 by conducting a numerical study using CFD. Their results fall within 25% of the experimental data found in the literature. The latter correlation accounts for the aspect ratio which is a factor that was neglected in most of the previous studies. In fact, the previous correlations summarized in the work of Rauline et al. (1998) and Theron et Le Sauze

(2011) are limited to laminar regimes and most of them are derived at a constant aspect ratio. The authors found that the pressure drop depends on the aspect ratio since lower aspect ratios generate higher pressure drop. This was already proven in the study of Szalai et al. (2004) who conducted their investigation in laminar regimes and found that the dependency between the aspect ratio and the pressure drop at relatively higher Re values ($Re > 100$) is strong. However, it is important to note that Song and Han (2005) neglected the effect of the blade thickness and assumed a thin wall. Moreover, their comparison with the literature data was limited to $0.01 < Re < 1,500$. Thus, their correlation could not be applied with confidence out of the tested range nor for realistic problems where the wall thickness contributes to pressure losses.

Kumar et al. (2008) carried out a numerical and experimental study to investigate the hydrodynamics in Kenics mixer over a wide range of Re going to 25,000. In this study, two new pressure drop correlations were derived and found to be in good agreement with the experimental results. However, these correlations do not consider the geometric aspects of mixers and consider a constant aspect ratio of 1.5. For $Re > 1,000$, discrepancies between the simulated results and the experimental data of Berkman and Calabrese (1988) were noticed. These discrepancies can be attributed to the different dimensions used in the two studies. This, therefore, highlights the limitation of applying the available correlations to different geometries. The authors also noticed that the pressure drop per unit length is independent of the number of elements. Similar results were obtained in the study of Song and Han (2005).

Stec and Synowiec (2017a) also developed a model for pressure drop prediction in Kenics static mixers operating under turbulent flow conditions ($Re = 1000-5000$). Their correlations fitted well with their experimental and CFD data. However, it was

noticed that their data overpredicts the pressure drop in Kenics compared with the available data in the literature.

Table 1 Pressure Drop correlations for KM, SMV, and STSM

Mixer	Pressure drop correlations	Re Range	Reference
Kenics	$f = \frac{85.5}{Re} + 0.3375$	0.01-10,000	(Sir & Lecjaks, 1982)
	${}^a f AR^{2.04} = \frac{k \left(\frac{Re}{AR^{2.15}} \right)^n}{4}$	Re may go beyond 10^6	(Song & Han, 2005)
	$Z = 0.0031Re + 14.69$	1,000-10,000	(Kumar et al., 2008)
	$Z = 0.023Re - 4 \times 10^{-8} Re^2 + 25.36$	10,000-25,000	
	$Eu = 12.35Re^{-0.043} \left(\frac{L}{D} \right)$	200-14,000	(Stec & Synowiec, 2017a)
SMV	$\frac{f_h}{2} = 0.6Re_h^{-0.2}$	2,300-60,000	(Karoui & Costes, 1998) from (Theron & Le Sauze, 2011)
	$\frac{f_h}{2} = Re_h^{-0.25}$	66-14,786	(Theron & Le Sauze, 2011)
	$f = 0.0112 + \frac{2.7}{Re}$	Laminar-turbulent	(Paglianti & Montante, 2013)
STSM	$f = \frac{22.97}{Re_h^{0.8011}} + 0.3079$ (flow-through approach)	$Re_b = 2-14,000$	(Azizi, 2019)
	$K_s = \left(\frac{1 - \alpha^2}{\alpha^2} \right) \left(\frac{10.76}{Re_b^{0.8213}} + 0.4537 \right)$ (flow around approach)		

^a for $0 < \frac{Re}{AR^{2.15}} < 100$ $k=320$, $n=-0.86$; $100 < \frac{Re}{AR^{2.15}} < 1000$ $k=32$, $n=-0.36$; for $\frac{Re}{AR^{2.15}} > 1000$ $k=2.66$, $n=0$.

Panglianti and Montante (2013) proposed a new model for pressure drop prediction across SMV in turbulent regimes. Unlike the other correlations and besides accounting for different geometric aspects such as the element length and the relative position of two consecutive mixing elements, this new correlation takes into account the contribution of the distributed and the concentrated pressure drop. The former is generated due to the friction of the fluid against the mixer wall and the latter is due to pressure loss at the inlet and outlet of the mixer and at the interface of two adjacent elements. The pressure drop results were found to be in good agreement with the experimental data of Theron and Le Sauze (2011) and Karoui and Costes (1998).

Azizi (2019) conducted a series of experiments to measure the pressure drop generated by a plain-weave mesh of different geometries under a wide range of wire Reynolds numbers Re_b and under real conditions in an attempt to develop universal correlations for pressure drop through STSM. In this work, the obtained results along with data from the literature were analyzed and compared following two different approaches: a fluid dynamic approach and a chemical engineering one. The former, aka the flow around approach, is commonly employed in studies dealing with pressure drop through screens, and it treats the flow through woven mesh screen type in accordance to flow around a cylinder. In this case, the pressure drop is expressed in terms of a pressure loss coefficient K_s that is a function of Re and the fractional open area. However, in the chemical engineering approach or the flow-through approach, the flow is treated similarly to a flow through a porous medium, and in this case, the pressure drop is expressed in terms of a friction factor f similar to Equation (4). The author concluded that both approaches render similar results.

Some of the various correlations found in the literature for pressure drop in Kenics, SMV and screen-type static mixers in turbulent regimes are listed in Table 1. These correlations along with other experimental and numerical data found in the literature (Berkman & Calabrese, 1988; Hearn, 1995) will be used in this study to validate the accuracy of the numerical model in predicting the flow behavior.

The following elaborates on the main characterization techniques and mixing parameters used in evaluating the efficiency of static mixers in mixing applications.

2.1.2 Mixing and Flow Characterization

The efficiency of mixing operations does not only affect the quality of the final product, but also the process cost, operating time and safety (Aubin et al., 2010). Consequently, characterizing and evaluating the mixing efficiency inside static mixers is of tremendous importance for the success of the process and an efficient equipment design. For this reason, several quantitative and qualitative experimental techniques were employed in the literature.

Many studies relied on optical techniques to investigate the flow field inside static mixers. Among these techniques, the Particle Image Velocimetry (PIV) (Lehwald et al., 2012; Zhuang et al., 2020) and Laser Doppler Anemometry (LDA) (Halina Murasiewicz & Jaworski, 2013) have been extensively employed. These techniques consist of tracking the trajectories of illuminated injected particles (seedings) in order to determine the instantaneous velocity field. Other techniques include Laser Doppler Velocimetry (LDV) and hot wire/film anemometry (Halina Murasiewicz & Jaworski, 2013). The Positron-Emitting Particle Tracking (PEPT) is another visualization

technique that, unlike the previous methods, could be applied to opaque apparatus since it uses buoyant radioactive particles. PEPT has been used to characterize SMX and Kenics (Mihailova et al., 2015; Rafiee et al., 2013).

To assess the mixing efficiency in static mixers, researchers and industries also relied on optical tools and imaging techniques (Ghanem et al., 2014). These techniques allow tracking the dispersion of one fluid in another by monitoring the difference in fluid properties (Jegatheeswaran et al., 2020). Among these, the Planar Laser-Induced Fluorescence (PLIF), the magnetic resonance imaging (MRI), and the electrical resistance tomography (ERT) are listed. These techniques are non-invasive and provide either qualitative or quantitative information about mixing. PLIF consists of tracking the dispersion of injected fluorescent dye. The captured images of the cross-section at a certain location give insights into the striation thickness. These images could be further processed to determine the concentration of the used dye at any point of a selected cross-section (Alberini et al., 2014; Hirschberg et al., 2009; Karoui et al., 1998). MRI follows the same concept as PLIF, but it employs a contrast MRI agent instead (Lim et al., 2015; Mihailova et al., 2015). ERT consists of adding an electrolyte to one of the fluid streams to make it more conductive. Based on the distribution of the electrical conductivity the mixing homogeneity can be assessed (Yenjaichon et al., 2011).

The aforementioned techniques have many limitations. High-quality images with fine resolution are required for an accurate evaluation. However, such conditions could not be easily attained (Yenjaichon et al., 2011) as they necessitate the use of expensive tools such as sensors and digital cameras. Furthermore, additional time-consuming step of image processing is needed in some cases. Other problems could be faced when selecting the seedings and particles that, first and foremost, should not alter

the properties of the fluids nor be toxic or corrosive, not to mention their high cost (Lehwald et al., 2012). In addition, these techniques are not flexible where in some cases the sensors cannot be moved from one location to another once installed (e.g. ERT sensor) and some of the techniques are invasive which may affect the flow pattern.

It is worth mentioning that due to the complex geometries of static mixers, a deep understanding of mixing phenomena cannot be provided based on experimental data. In reality, experiments might not reveal all the hydrodynamics or predict the flow behavior inside these mixers (Joaquim et al., 2011; Kumar et al., 2008). This is why manufacturers and researchers may extensively rely in the design and scale-up phase on trial and error procedures, rule of thumb, and empiricism (Godfrey, 1997). Empirical correlations might be developed based on assumptions and simplifications. Therefore, their application involves the implementation of large safety margins leading to inefficient designs, i.e. over-designed or under-designed equipment (Azizi & Taweel, 2011; Godfrey, 1997; Wadley & Dawson, 2005). Moreover, in most cases, these correlations cannot be deemed accountable over a range of operating conditions or geometries that is out of the validated range.

Numerical tools such as Computational Fluid Dynamics (CFD) have emerged as dynamic solutions for flow modeling and characterization and as good alternatives to overcome the limitations imposed by empiricism and the costly and time-consuming experiments. These tools provide an in-depth understanding of fluid dynamics and transport phenomena at lower costs and reduced time. They also provide useful information about the three-dimensional flow domain in mixers (Aubin et al., 2010). Recently, CFD has been tremendously used to optimize the geometry of static mixers (Coroneo et al., 2012) and to assess their performance (Hobbs & Muzzio, 1997b;

Kumar et al., 2008; H. Murasiewicz & Zakrzewska, 2019; Pianko-Oprych & Jaworski, 2009; Rahmani et al., 2008; Song & Han, 2005). In general, good agreement between the CFD and experimental results was found.

2.1.3 Mixing Parameters

Predicting the mixing efficiency inside static mixers is assessed by evaluating the distributive and dispersive mixing. The former reflects the spatial distribution of fluids inside the mixer, while the latter corresponds to the reduction of the size of particles (i.e. bubble breakup or coalescence). The characterization techniques follow either qualitative routes (e.g. Poincaré sections, extensional efficiency and PNN) serving as tools for visualizing the mixing, or quantitative ones that allow direct quantification of the level of mixedness (e.g. CoV and intensity of segregation). It is important to note that a full characterization cannot be accomplished based on a single criterion. Consequently, several quantitative and qualitative techniques should be combined (Jegatheeswaran et al., 2020; Rauline et al., 1998). In what follows, the most common parameters with two new approaches will be discussed.

One of the most widely used parameters to quantify the effectiveness of distributive mixing is the coefficient of variance (CoV) or the mixing index as reported by Jegatheeswaran et al. (2020). It is a measure of the intensity of segregation, the first dimension of mixing as defined by Kukukova et al. (2009). It represents the deviation from the mean mixture composition (Eq. (12)) and acquires a value of 1 if the mixture is completely segregated and 0 if the system is perfectly mixed. Systems with $CoV < 5\%$ are deemed well mixed (Stec & Synowiec, 2019; Wadley & Dawson, 2005).

$$CoV = \frac{1}{\bar{X}} \sqrt{\sum_{i=1}^{n_p} \frac{(X_i - \bar{X})^2}{n_p - 1}} \quad (12)$$

The CoV is calculated according to Eq. (12), where X_i is the concentration or the mass fraction of the secondary stream at the i^{th} point of a given plane, \bar{X} is the average concentration or mass fraction over this plane, and n_p is the number of measurement points. The number of measurement points in numerical methods corresponds to the number of computational cells of a given plane.

The intensity of segregation or index of dispersion I is an alternative to the coefficient of variance. This parameter (Eq. (13)) compares the variance at a given cross-section to the variance at the inlet.

$$I = \frac{\sigma^2}{\sigma_0^2} \quad (13)$$

The residence time distribution (RTD) developed by Danckwerts in the early 1950s is another characterization technique that could be used to reflect the macromixing behavior inside a reactor and to assess the deviation from ideal models (Fogler, 2016). Many experimental studies (Abou Hweij & Azizi, 2015; Azizi & Abou Hweij, 2017; Li et al., 2007; Mohammadi et al., 2014) and numerical studies (Hobbs & Muzzio, 1997b; Rahmani et al., 2008; Stec & Synowiec, 2017b) used this parameter to quantify the distributive mixing in static mixers under laminar or turbulent flow conditions. The sharper the RTD of a static mixer, the closer to plug flow the behavior of this static mixer is.

The extensional efficiency β expressed in Eq. (14) is used to characterize the dispersive mixing. In Eq. (14), (15), and (16) $|\gamma|$ is the magnitude of the rate of

deformation tensor, $|\omega|$ is the magnitude rate of spin or vorticity tensor and $\nabla\mathbf{v}$ is the gradient of the velocity vector. Values of zero, 1 and 0.5 corresponds to pure rotational, extensional or elongational flow and simple shear flows, respectively (H.-B. Meng et al., 2016). In general; high values of β are desired for better mixing, and values of 0.5-1 were observed in static mixers. However, it is worth noting that this value may vary along the length of the insert as different mixing behavior (stretching, folding, rotation...) could be observed. However, high extensional efficiency is not necessarily an indication of good mixing as a region with high β may be segregated and hence the fluid under investigation will not pass through it (Haddadi et al., 2020; Rauline et al., 1998).

$$\beta = \frac{|\gamma|}{|\gamma| + |\omega|} \quad (14)$$

$$|\gamma| = \frac{1}{2} [\nabla\mathbf{v} + (\nabla\mathbf{v})^T] \quad (15)$$

$$|\omega| = \frac{1}{2} [\nabla\mathbf{v} - (\nabla\mathbf{v})^T] \quad (16)$$

According to Kukukova et al. (2009), conventional parameters, such as *CoV*, when used separately describe one dimension of mixing which is a complex operation, and therefore, could not be fully understood without considering a multi-dimensional approach to mixing problems. For this reason, Alberini et al. (2014) followed this definition and proposed the aerial distribution method to assess the mixing performance in KM under laminar flow conditions. In this method, the authors considered the effect of both the intensity and scale of segregation by examining the distribution of a cross-section with respect to different mixing intensities.

Medina et al. (2019) followed a different approach and proposed a new parameter called the M -Number (Eq. (17)) that, unlike the other parameters, accounts for both the mixing and the energy efficiency of a mixer. This parameter was derived based on the entropy of mixing of two miscible ideal gases 1 and 2. The M - number carries information about the capacity of a mixer to improve mixing, the thing that most of the conventional parameters fail to do.

$$M\text{-Number} = \frac{\omega_{iso}}{\omega_{max}} = \frac{\frac{(\zeta_{M_2} - \zeta_{M_2,nat})}{(1 - \zeta_{M_2})}}{\frac{P_1}{P_1 - P_{2,nat} + P_2}} \quad (17)$$

In Eq. (17), P is the area-weighted static pressure and ζ_M (Eq. (18)) is the mixing effectiveness which is equal to zero in case of complete segregation and unity if the system is perfectly mixed. The subscripts 1 and 2 refer to the positions where ζ_M and P are computed, i.e. at the inlet and outlet of the mixing section, respectively, while the subscript *nat* stands for natural, and it is used to refer to an empty tube with similar geometric characteristics as the investigated mix.

$$\zeta_M = \frac{\sum_{j=1}^N \frac{a_j}{A} [x_{2j} \ln x_{2j} + (1 - x_{2j}) \ln(1 - x_{2j})]}{z_2 \ln z_2 + (1 - z_2) \ln(1 - z_2)} \quad (18)$$

Where, a_j represents the area of the j^{th} cell within a cross-sectional area A that consists of a total number of N cells, x_{2j} is the mass fraction of component 2 at cell j and z_2 is the area-weighted average concentration or mass fraction of the secondary fluid over the plane of interest.

It is worth noting that the concept of M -number stemmed from the Second Law of Efficiency (SLE) which compares the efficiency of an engine or a power cycle to that of an ideal one. By analogy to SLE, the actual efficiency of an isolated static mixer

expressed in terms of ω_{iso} (Eq. (20)) is compared to the efficiency ω_{max} (Eq. (21)) of this same mixer but under ideal conditions, i.e. when the pressure drop generated by this mixer is equal to that generated by an empty tube ($P_2 = P_{2,nat}$), and the mixing effectiveness at the outlet is optimal $\zeta_{M_2} = 1$. The general expression of ω is shown in Eq. (19) and it accounts for the mixing efficiency $\Delta\zeta_M$ and the portion of the pressure that remains at the outlet of the tube ($\frac{P_2}{P_1} = \frac{P_1 - (P_1 - P_2)}{P_1}$).

$$\omega = \Delta\zeta_M \frac{P_2}{P_1} \quad (19)$$

$$\omega_{iso} = (\zeta_{M_2} - \zeta_{M_2,nat}) \frac{P_1 - P_{2,nat} + P_2}{P_1} \quad (20)$$

$$\omega_{max} = 1 - \zeta_{M_2} \quad (21)$$

2.2 Mixing and Flow Characterization of Kenics, SMV and STSM

2.2.1 Kenics

The helical mixers are among the most widely studied static mixers. They are usually used for low to moderate Reynolds numbers, but they have been recently used for turbulent applications since it was found that turbulence could be reached at low pipe $Re \cong 1000$ in this type of mixers (Rahmani et al., 2008; Stec & Synowiec, 2017b).

Most of the experimental and numerical studies focused on investigating the effect of the flow conditions and geometric parameters on the mixing efficiency of these mixers under laminar flow conditions.

Hobbs and Muzzio (1997a) investigated the effect of the injection location, flowrate ratio, and mixer geometry on the mixing effectiveness in Kenics static mixer under creeping flow conditions. The authors showed that the effect of the injection

location becomes negligible as the mixer length increases. They also highlighted the importance of alternating the twist direction in adjacent mixing elements.

Unidirectionally twisted plates induce poorly mixed region “islands” where no exchange with the surrounding can occur. This study also showed that a twist angle of 120° ends up with a 40% reduction in energy consumption compared with the standard configuration where the elements are twisted by 180° . In addition to the previous observations, Szalai and Muzzio (2003) showed that Kenics with large aspect ratios result in segregated regions for $1 < Re < 1000$.

Recently, Jiang et al. (2021) found that the aspect ratio has a major effect on the level of mixedness and number of elements at very low Re . By examining the computed CoV values they noticed that for $Re < 25$, a better homogeneity could be achieved with high aspect ratios, but this dependency becomes negligible as Re increases. Similarly, the same degree of mixedness could be obtained with a smaller number of elements with higher aspect ratios at Reynolds number $Re < 400$ beyond which the required number of elements to achieve homogeneity becomes independent of the flow velocity. Their study was limited to Reynolds numbers ranging between 1 and 500.

However, less attention was made to investigating the mixing efficiency of Kenics static mixers in turbulent regimes. Sir and Lecjaks (1982) carried out an experimental investigation to study the effect of the hydrodynamic properties, Schmidt number (Sc), flow rate ratio, and the viscosity ratio on the mixing efficiency of a Kenics mixer equipped with 24 elements of aspect ratio 2 for $10^{-2} < Re < 10,000$. Their assessment was limited to pressure drop measurements and the examination of the number of elements required to achieve full homogenization. They concluded that the number of elements increases with Re up to 50, then this number drops until reaching

Re=2000 beyond which the required number of mixing units becomes independent of the hydrodynamic conditions. This observation contradicts the finding of Jiang et al. (2021) who observed this phenomenon at a higher Re. A distinct increase in the number of elements is observed for a viscosity ratio >100 and high Sc. However, it was found that the volumetric flow rate ratio does not affect the mixing efficiency.

Rahmani et al. (2005) followed a Lagrangian approach to fully characterize the 3D flow in a Kenics static mixer for Re=0.01-5000. Unlike the available studies, a non-simplified mixer geometry where an element of an aspect ratio of 0.846 and thickness equivalent to 22% of the element length was tested. In this study, two different turbulence models, namely the $k - \omega$ and RSM were tested, and it was found that the $k - \omega$, which is computationally less demanding than RSM, is accurate enough to predict the flow behavior. In 2008, the same research group found that the one-Equation Spalart-Allmaras model is as accurate as the $k - \omega$ model with the advantage of being computationally less expensive. Similarly to the finding of Hobbs and Muzzio (1997) in laminar regimes, Rahmani et al. (2008) found that the injection location just affects the flow over the first few elements in turbulent regimes. The research team relied in their study on different qualitative and quantitative techniques to assess the mixing efficiency, namely, the G-value, the RTD, the structure radius, the CoV and the particle distribution uniformity (PDU).

Kumar et al. (2008) carried out a numerical and experimental study to investigate the hydrodynamics and the flow behavior of a Kenics mixer of aspect ratio 1.5 over a wide range of Re going up to 25,000. The analysis of the circumferential velocity results revealed two important features of Kenics: i) the effect of the transition from one element to another lasts for up to 30% of the element length beyond which the

flow becomes well developed and less cross-sectional mixing takes place and ii) forced vortices are generated in the center of the tube whereas free vortices are generated near the wall. The first observation is in line with previous findings that show that smaller aspect ratios are more efficient than larger ones (Szalai & Muzzio, 2003).

2.2.2 SMV

SMV is another type of static mixers that despite the fact of being widely used in industrial turbulent applications, has been rarely investigated in the literature either on the computational side or experimental side. The available studies focused on assessing the efficiency of SMV in multiphase applications since these designs are efficient in gas-liquid, liquid-liquid contacting, dispersion and emulsification. For instance, Lobry et al. (2011) studied the behavior of liquid-liquid dispersions under turbulent conditions in an SMV mixer. They evaluated the effect of the dispersed phase concentration on the droplet size and the hydrodynamic properties using two analytical techniques. Another example is the study of Dong et al. (2010) who showed that 6 elements of SMV are sufficient for antisolvent precipitation of nanoparticles of poorly water-soluble drugs.

Other studies tested the efficiency of SMV in reactive systems. Frascari et al. (2008) used SMV for the esterification of sunflower oil. They found that a mixer equipped with one SMV element leads to the same conversion obtained with an agitated tank with 50% energy reduction.

A limited number of numerical and experimental studies have been carried out to unravel the mixing mechanism in SMV. Lang et al. (1995) studied numerically the mixing induced by SMV that was then tested in a simulated denitrification facility. The

authors considered two cases, an ideal case where the walls do not interfere, and the second where the elements are inserted in a rectangular duct. It was found that when the fluid travels through the mixer, the intensity of segregation is reduced, and the mixing quality is improved. This improvement is due to the swirling flow induced by the vortices generated at the intersection of two adjacent plates. The generated vortices are retained further downstream of the mixer.

The latter observation was later confirmed by the PLIF experiments of Karoui et al. (1998) who tested the effect of the geometric properties and flow rates on the mixing quality in a SMV unit. Karoui and her coworkers found that for optimal results, the consecutive elements should be placed side by side and at 90° to each other. This position enhances the axial and radial mixing and improves the rate of energy dissipation. Their evaluation was done by means of CoV , the intensity of segregation and the root square mean of concentration.

Coroneo et al. (2012) performed fully predictive 3D numerical investigations to study the mixing efficiency in a laboratory and a large-scale mixer equipped with one and two SMV elements. three different turbulence models, namely the standard $k - \varepsilon$, the realizable $k - \varepsilon$ and the RSM models were tested in this study. The $k - \varepsilon$ models were found to be more accurate than the RSM model in predicting the turbulent kinetic energy, but the three variants of the $k - \varepsilon$ showed similar performance in predicting the velocity fields. This study also showed that spacing the elements worsen the quality of mixing as already stated by Karoui et al. (1998) but does not affect the pressure drop. In this study, the authors relied on the concentration contour and CoV to test the efficiency of the mixer. Panglianti and Montante (2013) conducted a numerical and experimental study to predict the pressure drop across SMV. This study reported

that the minimum aspect ratio L/D for SMV should be greater than 0.56 to prevent the fluid from bypassing the mixing elements.

Montante et al. (2016) extended the study of Coroneo et al. (2012) to investigate numerically the effect of combining different physical properties of two miscible liquids with different geometric features on the mixing quality in a tube equipped with a single SMV element. The authors used the CoV with two additional parameters, namely the scale of segregation and the exposure, to evaluate the mixing efficiency following the definition of Kukukova et al. (2009) for the mixing problem. For this purpose, the concept of aerial distribution already adopted by Alberini et al. (2014) was modified to suit turbulent applications where the striation boundaries are quickly smeared. The scale of segregation was presented through a new parameter, namely, the equivalent diameter d_{eq} which is proportional to the ratio of the area of the well-mixed region to the length of the boundary separating the well-mixed and the poor mixed regions on a cross-sectional area perpendicular to the flow direction. The exposure which is the potential of a mixer to reduce segregation was then calculated as the variation of the d_{eq} along the centerline.

2.2.3 STSM

Woven mesh screens have been successfully used as one variant of static mixers in multiphase reactors/contactors (Azizi, 2019; Azizi & Al Taweel, 2011; Azizi & Taweel, 2011; Habchi & Azizi, 2018). They have been attractive for such applications due to their ability to enhance mass transfer operations at relatively low energy consumption (Habchi & Azizi, 2018). Investigations tackling fluid flow through screen

wire mesh mainly focused on measuring or correlating the pressure drop through screens, characterizing the downstream turbulence, and studying the effect of grids on the mean-time velocity profiles (Azizi, 2019; Roache, 1986).

Accurately predicting the spatial variation of the rate of energy dissipation is of primary importance for the design of contactors/reactors since the rate of energy dissipation controls the distribution of the drop/bubble size of the flowing dispersion as well as governs the rate of heat and mass transfer between the phases (Azizi & Al Taweel, 2011). Azizi and Al Taweel (2011) proposed a one-dimensional approach that can accurately predict the spatial variation of the energy dissipation rate ε behind the screen for a wide range of operating conditions and designs. In their study, they divided the turbulence decay profile into a region of constant high energy dissipation rate prevalent over a distance governed by the mesh size and a region of fast decay that could be described by the homogeneous isotropic turbulence decay equation. Other studies tackling the same topic are those of Roache (1986) and Kurian and Fransson (2009).

One example of a study tackling the hydrodynamics in STSM is the investigation of Okolo et al. (2019). The authors carried out three-dimensional CFD simulations of low turbulence fluid to study the flow behavior through woven wire screens employed for noise reduction. For this reason, they tested two numerical grids, one with extended domain sides to replicate the behavior of the flow through the screens in external flow circumstances, while the second is tightly fitted within the flow channel. The author tested different turbulence models, namely the standard $k - \varepsilon$, the realizable $k - \varepsilon$, the RNG $k - \varepsilon$, the standard $k - \omega$, the (SST) $k - \omega$, $k - kl - \omega$, and the transition SST model. They found that the standard $k - \varepsilon$ and its variants

outperform the other models in predicting the pressure loss through the screens. The predicted pressure loss coefficient agrees well with experimental data and other correlations found in the literature. They also studied the velocity in three regions, namely the upstream region, the region in the vicinity of the screen and the downstream region. The maximum velocity is encountered within the screen apertures and is inversely correlated to the screen porosity in the case of the second grid. A fully developed velocity profile is obtained after $60M$. The first grid reveals different behavior, but since the current research is limited to bounded flows, the external flow case will not be listed here. The downstream turbulence decay obtained in this study does not compare well with the turbulent decay model of Roache (1986).

Other investigations attempted to study the effect of the geometric characteristics of the screen on the mixer hydrodynamics and mixing efficiency under turbulent regimes. Habchi and Azizi (2018) carried out a 2D CFD study to investigate the effect of the screen geometry and the operating conditions on the flow behavior and heat transfer. The results showed that better micromixing and heat transfer could be achieved by lowering the fraction open area of the screen.

Abou Hweij and Azizi (2015) and Azizi and Abou Hweij (2017) studied the hydrodynamics and residence time distribution of single-phase and multiphase flow in a contactor/reactor mounted with screen-type static mixers. Their first study showed that screens with smaller mesh openings end up with higher pressure drop and that screens are two order of magnitude more energy-efficient than other commercial static mixers. In addition, the axial dispersion coefficient was found to increase with the increase of the Re . Overall, the screens are more efficient than empty tubes since their axial dispersion coefficient was found to be smaller than those of an empty tube, except for

the case of highly dispersed phase volume fractions at low flow rates (Azizi & Abou Hweij, 2017).

Recently Abou-Hweij and Azizi (2020a, 2020b), fully characterized the three-dimensional bounded flow in screen-type static mixers by investigating the hydrodynamics and the mixing efficiency of these mixers. The authors relied on numerous qualitative and quantitative techniques to assess the distributive and dispersive mixing. They used the Point to the Nearest Neighbor (PNN) and its filtered variance, the M number, and the extensional efficiency. However, their study was limited to laminar flow conditions and they noted that the screens are not ideal for such conditions.

2.3 Comparative Studies

Few studies compared the mixing performance and the hydrodynamic properties of different static. Most of these studies tackled this subject in laminar regimes. Rauline et al. (1998) compared numerically the performance of 6 static mixers (i.e. Kenics, Inliner, LPD, Cleveland, ISG and SMX) by evaluating the extensional efficiency, the stretching, mean shear rate, intensity of segregation and pressure drop. The extensional efficiency showed that the flow is elongational at the edges of Kenics and distributive within the mixer. This trend was also observed in Cleveland, Inliner and ISG. Thus, the authors deduced that the mixing quality in Kenics, Inliner, Cleveland and ISG can be improved if a spacing was left between the elements. All in all, they found that SMX is the most efficient.

Regner et al. (2006) characterized numerically the flow in Kenics and Lightnin by evaluating the pressure drop, the helicity and the rate of striation thickness. They showed that the mixing efficiency in Kenics and Lightnin is better at low flow rates than at high flow rates.

H. Meng et al. (2015) characterized the flow in 4 different twisted tape inserts, namely, the standard helical mixer KM, the right-twist type RSM, the M-type MSM, and the spiral type SSM static mixers at $Re=0.1-100$. By evaluating the Poincaré section, the stretching history, the extensional efficiency and the CoV , they found that KM performs better than its counterparts.

Recently, Haddadi et al. (2020) also compared the performance of Kenics to SMX, Komax and a new model under laminar regimes ($Re=20-160$) relying on the results of pressure drop, extensional efficiency and CoV .

However, a few studies dealt with comparing the performance of static mixers under turbulent flow conditions. Barrue et al. (2001) compared the aerodynamic and mixing performance of a new gas-gas mixer, namely Oxynator, to Kenics and SMI static mixers in turbulent regimes. Their study was limited to pressure drop, velocity and RSM velocity measurements at the outlet relying on the LDA technique, and their mixing efficiency evaluation was based on a qualitative technique, namely the laser sheets visualization technique.

Wadley and Dawson (2005) relied on Laser-induced Fluorescence data, to evaluate the mixing performance of SMV, standard Kenics and HEV mixers in turbulent and transitional regimes. Their comparison was based upon one parameter which is the CoV . The authors focused in this study on testing the effect of the flowrate

ratio, the number of elements, and the initial injection position on the mixing efficiency. The experimental results of CoV contradict the correlations of the manufacturer.

In another study, Theron et Le Sauze (2011) also compared experimentally the performance of SMV to two other Sulzer mixers, namely SMX and SMX⁺ in both single-phase and two-phase flow in turbulent regimes. This comparison was done based on the hydrodynamic and emulsification properties. Pressure drop correlations based on the hydraulic diameter and the interstitial velocity were developed. This study showed that both SMV and the improved version of SMX, i.e. SMX⁺ are 50% more energy-efficient than the SMX design in single and two-phase flow. The analysis of the Sauter mean diameter distribution as a function of the mean energy dissipation rate per fluid mass showed that SMV is the best compared to the two other mixers.

Recently Stec and Synowiec compared the performance of Koflo to Kenics under turbulent conditions ($Re=1000-5000$) based on pressure drop (Stec & Synowiec, 2017a), RTD (Stec & Synowiec, 2017b), and CoV (Stec & Synowiec, 2019). Their results show that Koflo is 30% more energy-efficient than Kenics. This was attributed to the compact geometry of Koflo. It was also found that Koflo presents lower values of CoV (Stec & Synowiec, 2019) but Kenics has the narrowest RTD with the highest maximum and the smallest residence time.

Meng et al. (2020) also compared the hydrodynamics, the thermal, and the mixing performance of Kenics to another SM, i.e. Lightning under the turbulent flow conditions. They tested different turbulent models ($k - \varepsilon$ and $k - \omega$ families) and found that the SST $k - \omega$ yields the most accurate. They found that for $AR > 1.5$ the

Lightnin is more energy-efficient than the Kenics but its ability to enhance the dispersion mixing becomes less important.

2.4 Conclusions

The review of the available literature shows that:

1. The majority of the investigations about Kenics assessed their performance under laminar flow conditions, while little emphasis was placed on their efficiency under turbulent flow regimes.
2. The investigations tackling the mixing efficiency of SMV considered one or two elements only even though a larger number of elements is needed to achieve nearly full homogeneity.
3. Most of the studies tackling the fluid flow through woven wire meshes focused on modeling the downstream turbulence decay, assessing the hydrodynamics inside these mixers, and characterizing two-phase flows.
4. Few of the available studies about the hydrodynamics of STSM were conducted for bounded flow cases.
5. The mixing efficiency of STSM for single-phase turbulent flows was assessed from a macromixing point of view using RTD. However, none of these studies assessed the dispersive mixing behavior of the screens
6. Few studies fully characterized the mixing efficiency of the three mixers at hand.
7. Only five studies compared the performance of static mixers.
8. STSM has never been compared to any other commercial static mixer from a hydrodynamic and mixing point of view.

9. The aerial distribution method and the M number approach have never been applied to the three mixers at hand under turbulent flow conditions.
10. The available studies do not allow for a direct comparison of the three mixers at hand since they were conducted under different operating conditions and applied to various dimensions.

CHAPTER 3

SOLUTION METHODS

In this study, 3D CFD simulations were carried out using Ansys Fluent® to investigate the flow hydrodynamics and compare the mixing efficiency of three static mixers, namely Kenics, Sulzer SMV, and a modified geometry of screen-type static mixer denoted by NM, i.e. New Mixer, at different flow conditions under turbulent regimes.

3.1 Geometric and Computational Domains

The computational domain of the three mixers consists of a horizontal pipeline of roughly the same internal diameter D equipped with an arrangement of two, four or six mixing units of either Kenics, SMV or the new mixer with $1D$ and $5D$ empty tube sections placed upstream of the 1st mixing unit and downstream of the last mixing unit, respectively. The adjacent units are arranged at 90° with respect to each other. Figure 4 represents the geometric domain equipped with two units of each geometry and $1D$ upstream and downstream of the mixing sections.

Kenics geometry was generated in Ansys DesignModeler, and it consists of a series of rectangular plates of length $L_e = 24.56 \text{ mm}$, diameter $D_{SM} = D = 16.37 \text{ mm}$ and thickness $t_p = 1 \text{ mm}$ twisted by an angle of 180° clockwise and counterclockwise alternately.

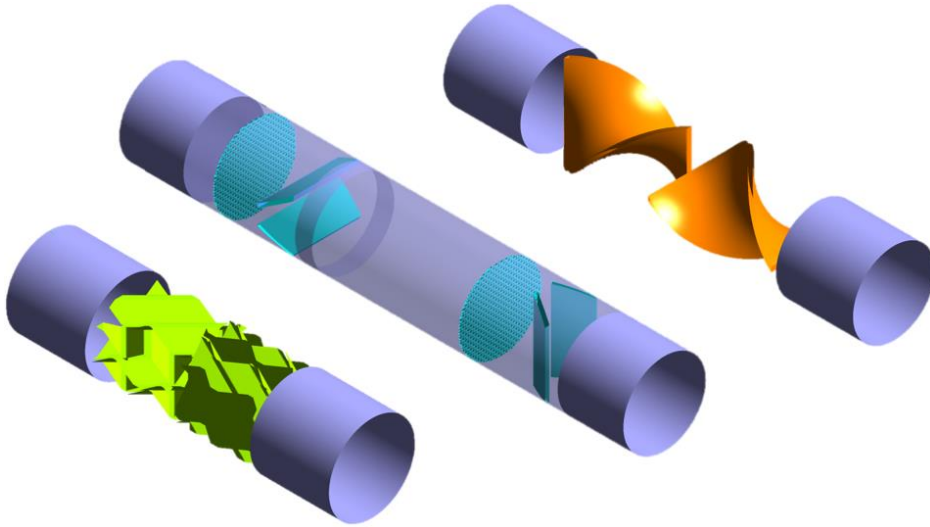


Figure 4 The flow domain of the three mixers from left to right: SMV, new mixer and Kenics.

SMV was modeled in AutoCAD due to its complexity (Figure 5). Each SMV unit comprises five intersecting corrugated plates of $D_{SM} = 16.37 \text{ mm}$, width equals 13.75 mm and $L_e = 15 \text{ mm}$. The axis of the corrugations forms an angle of 45° to the flow axis, i.e. the z-axis. It is worth noting that the SMV elements were placed in a pipeline of a diameter D that is 2% larger than D_{SM} due to meshing complications.

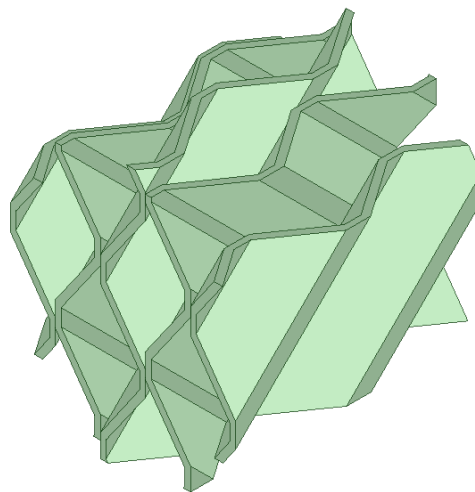


Figure 5 One SMV unit

The modified geometry of STSM used here was proposed and obtained from Abou-Hweij (2022). Each hybrid unit consists of a combination of a woven wire mesh that is tightly fitting into a pipeline of $D = 16.51 \text{ mm}$ and 2 divergent inserts or flaps of length $L_f = 2D_{pipe}/5$ and thickness $t_p = 0.635 \text{ mm}$ placed at $D/2$ downstream of the screen. The flaps are separated by a distance $D_{f-f} = 2D/5$ and rotated in opposite directions by 30° around their top faces. The screens are characterized by the center-to-center distance that separates two adjacent wires, i.e. mesh size M , the wire diameter b , the fractional open area α and the mesh number, Mn , that represents the number of openings per unit length (Figure 6). The consecutive screens were separated by a distance of $4D$ in the proposed design and each hybrid element extends from the screen inlet down to the trailing edge of the inserts and hence has a length $L_e = 2b + D/2 + (2D/5)\cos(30^\circ)$.

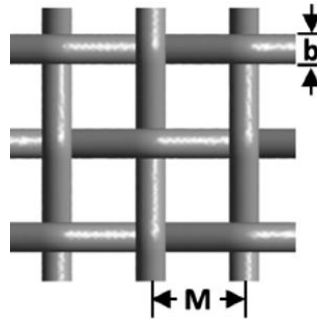


Figure 6 Geometric properties of a screen

The geometric properties of the designs investigated in this study are summarized in Table 2 and those of the new mixer are illustrated in Figure 7 . In the table, ϕ represents the void fraction or porosity of the mixer and is calculated as the ratio of the mixer volume to the empty pipeline volume and D_h is the hydraulic diameter and is estimated based on Eq.(5) for Kenics and SMV and Eq. (5) and (6) for STSM.

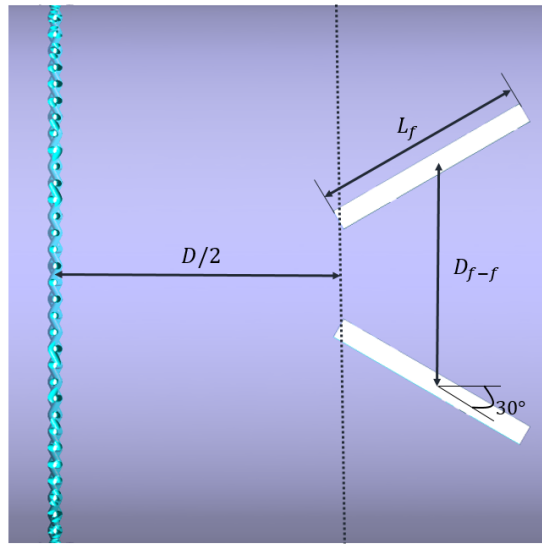


Figure 7 Geometric properties of the new mixer

It is worth noting that the differences between the diameters of the pipelines are negligible since the deviation between the smallest and largest diameters is estimated at 2%.

Table 2 Geometric properties of the three geometries investigated in this study

	Kenics	SMV	New Mixer
D (mm)	16.37	16.7	16.51
D_{SM} (mm)	16.37	16.37	16.51
D_h (mm)	8.56	3.24	–
L_e (mm)	24.56	15	14.43
L_e/D_{SM} (mm)	1.5	0.92	0.87
t_p (mm)	1	0.43	–
ϕ (–)	0.95	0.86	–
# tested elements	2,4,6	2,4	4

Geometric properties of the screen $Mn = 50$ alone

b (mm)	M (mm)	α (%)	D_h (mm)	ϕ (–)
0.2286	0.508	30.06	0.3612	0.61

Geometric properties of the inserts

t_f (mm)	L_{f-f} (mm)	L_f (mm)	L_{s-f} (mm)	angle
0.635	6.604	6.604	8.25	30°

3.2 Working Fluid and Operating Conditions

Water whose physical properties at 25°C are listed in Table 3, was used as the working fluid for both hydrodynamics and mixing assessments. It was employed as a primary and a secondary fluid to avoid disturbing the flow pattern by using fluids of different properties (González-Juárez et al., 2017). The 2 fluids were fed separately at the inlet cross-section divided into two semi-circles.

Table 3 Physical properties of the working fluid (water) at 25°C

Density, ρ (kg/m^3)	998.2
Viscosity, μ ($Pa \cdot s$)	0.001003
Thermal conductivity, K_t ($W/m \cdot K$)	0.6
Specific heat, C_p ($J/kg \cdot K$)	4182
Water self-diffusion coefficient, D_{w-w} (m^2/s)	1×10^{-9}

Table 4 Operating conditions investigated in the current study

Re_{pipe}	<u>Kenics</u>		<u>SMV</u>		<u>New Mixer</u>	
	Re_h	\bar{u} (ms^{-1})	Re_h	\bar{u} (ms^{-1})	Re_h	\bar{u} (ms^{-1})
5,000	2,776	0.307	1,153	0.301	179	0.304
10,000	5,512	0.614	2,306	0.602	357	0.609
15,000	8,268	0.921	3,460	0.903	N/A	N/A
20,000	11,024	1.228	4,613	1.203	715	1.217
25,000	13,780	1.535	5,766	1.504	N/A	N/A
30,000	16,535	1.841	6,919	1.805	1,072	1.826

The simulations were undertaken in turbulent regimes for 6 pipe Reynolds numbers (Re_{pipe}) spanning a range between 5,000 and 30,000. The investigated

operating conditions are listed in Table 4 where Re_h is the hydraulic Re number and is equal to $Re_h = \frac{\rho D_h \bar{u}}{\mu}$ and \bar{u} represents the average superficial velocity of the fluid.

3.3 Computational Domain Discretization

Unstructured meshes with tetrahedral elements were generated first in ANSYS automatic meshing tool and then converted to polyhedral meshes in Ansys Fluent[®]. The main advantage of polyhedral meshes over tetrahedral ones is their capability to produce more accurate solutions at lower cell count and reduced computational time in general (Dančová et al., 2018; H. Meng et al., 2020).

Special care was taken to generate a fine enough boundary layer mesh near the wall in such a way that the values of the dimensionless y^+ at the wall of all the mixers and the tube maintains an average value near 1 and a maximum value less than 5 as recommended by (Ansys, 2013). This step is essential to resolve the viscous sublayer where important phenomena, such as flow reversal, are expected to take place. The whole region of the mixer was well refined in order to capture the details of the turbulent flows that most probably will be retained further downstream of the mixing section.

The accuracy of the solution depends heavily upon the mesh density. Therefore, it is important to ensure that a sufficiently refined mesh is created so that the computed solution is in the asymptotic range of convergence. However, very fine meshes could result in unjustified computational costs when a grid-independent solution could be obtained for a lower grid density. For this purpose, three grids of increasing densities were generated for each geometry and a grid sensitivity analysis was conducted at the

highest Re_{pipe} to select the optimal grid that ensures a grid-independent solution at the lowest possible cost. The pressure drop across the mixers and the CoV at various locations within the mixers were selected to analyze these grids. In addition, the relative error between the predicted parameters based on two consecutive levels of refinement is selected as a criterion to select the final mesh. The results of the mesh sensitivity analysis are discussed in Chapter 4.

3.4 Numerical Model

Ansys Fluent[®], a Finite Volume Method (FVM)-based solver, was used in this study to solve the continuity and transport equations for the flow through the three investigated mixers.

Turbulent flows are characterized by irregular fluctuations around a mean value in space and time which renders the direct solution of Navier Stokes equations impractical. The Direct Numerical Simulation (DNS) in this case, requires the use of an extremely fine mesh whose elements should be smaller than the Kolmogorov length scale besides the very small time step needed (Moukalled et al., 2015). To reduce the computational efforts tied to DNS, an approach based on solving the Reynolds-Averaged Navier-Stokes (RANS) equations has emerged and was adopted for the current simulations. This approach consists of decomposing the instantaneous values of a flow variable of interest, for instance, the velocity $\mathbf{v}(x, t)$, into a mean value ($\bar{\mathbf{v}}(x, t)$) and a fluctuating component ($\mathbf{v}'(x, t)$):

$$\mathbf{v}(x, t) = \bar{\mathbf{v}}(x, t) + \mathbf{v}'(x, t) \quad (22)$$

Due to the averaging process, an additional term known as the Reynolds stress tensor ($-\overline{\mathbf{v}'\mathbf{v}'}$) appears in the momentum equation (Eq.(25)), and consequently, a problem of closure arises. To close the set of RANS equations, the Reynolds stress tensor is modeled based on the Boussinesq hypothesis that relates the Reynolds stress tensor to the mean velocity gradient by a linear function through the introduction of a new term: the turbulent viscosity or the eddy viscosity μ_t . The problem, hence, transforms into computing the eddy viscosity. To accomplish this, several turbulence models were developed over the years.

In the current study, the Two-Equation realizable $k - \varepsilon$ turbulence model with the enhanced wall treatment was employed. This model consists of solving two additional transport equations, namely the equation of the turbulent kinetic energy k (Eq.(26)), and that of the rate of dissipation of kinetic energy per unit mass ε (Eq.(27)). This selection is justified by the fact that $k - \varepsilon$ is an improved variant of the standard $k - \varepsilon$ model that was successfully employed in many similar studies and has demonstrated its ability to correctly predict the solution of similar problems (Coroneo et al., 2012; Kumar et al., 2008; Lang et al., 1995; Montante et al., 2016; Okolo et al., 2019), The realizable $k - \varepsilon$ model has the advantage of being more suitable for applications involving strong streamline curvature, vortices and rotation such as mixing applications in static mixers (Ansys, 2013).

3.4.1 Governing Equations and Assumptions

A steady, single-phase, incompressible and isothermal flow was assumed, and the effect of the gravity and external forces was ignored. The model equations are represented below in vector form.

Eddy viscosity

$$\mu_t = \rho C_\mu \frac{k^2}{\varepsilon} \quad (23)$$

Mass Conservation Equation

$$\nabla \cdot \mathbf{v} = 0 \quad (24)$$

Momentum Equation

$$\rho \nabla \cdot \{\mathbf{v}\mathbf{v}\} = -\nabla p + \mu \nabla^2 \mathbf{v} - \rho \nabla \cdot \{\overline{\mathbf{v}'\mathbf{v}'}\} \quad (25)$$

In Eq.(24) and Eq.(25), \mathbf{v} is the mean velocity vector, p is the static pressure, ρ and μ are the density and the dynamic viscosity of the working fluid which is the water in the current study.

Turbulent Kinetic Energy Equation

$$\rho \nabla \cdot (k\mathbf{v}) = \nabla \cdot \left[\left(\mu + \frac{\mu_t}{\sigma_k} \right) \nabla k \right] + G_k + G_b - \rho \varepsilon + S_k \quad (26)$$

Rate of Kinetic Energy Dissipation Equation

$$\rho \nabla \cdot (\varepsilon \mathbf{v}) = \nabla \cdot \left[\left(\mu + \frac{\mu_t}{\sigma_\varepsilon} \right) \nabla \varepsilon \right] + \rho C_1 S_\varepsilon - \rho C_2 \frac{\varepsilon^2}{k + \sqrt{\nu \varepsilon}} + C_{1\varepsilon} \frac{\varepsilon}{k} C_{3\varepsilon} G_b + S_\varepsilon \quad (27)$$

Where $C_1 = \max \left[0.43, \frac{\eta}{\eta+5} \right]$, $\eta = S \frac{k}{\varepsilon}$, $S = \sqrt{2S_{ij}S_{ij}}$, G_k is the generation of the turbulent kinetic energy due to the velocity gradient, G_b is the generation of the turbulent kinetic energy due to buoyancy. C_2 and $C_{1\varepsilon}$ are constants, σ_k and σ_ε are the turbulent Prandtl number for k and ε , S_k and S_ε are user-defined source terms. The default values of these parameters were used in the simulations.

Species transport Equation

$$\rho \nabla \cdot (Y \mathbf{v}) = -\nabla \cdot (\rho D_{w-w} \nabla Y + \frac{\mu_t}{\sigma_t} \nabla Y) \quad (28)$$

with Y being the mass fraction of the secondary stream and σ_t the turbulence Schmidt number which assigned a value of 0.7 (Coroneo et al., 2012).

3.5 Computational Methods and Boundary Conditions

All the simulations were performed in double precision and the solution methods are the following:

- Computational model: The realizable $k - \varepsilon$ model with the enhanced wall treatment (EWT)
- Pressure-velocity coupling: The coupled algorithm
- Discretization of the gradient terms: The Least-square based method
- Pressure interpolation: The second-order scheme
- Discretization of the convective and turbulence terms: The second-order upwind (SOU) scheme

- The solution was deemed convergent when the following three criteria were met:

The scaled residuals for each transport equation are reduced by at least three orders of magnitude (Celik et al., 2008),

- The solution of static pressure, the standard deviation of mass fraction of the tracer, and k and epsilon reaches a steady-state,
- The net difference between the mass flow rate at the inlet and outlet approaches zero.

To reduce the length of the computational domain, fully-developed turbulent velocity profiles were imposed at the inlet of the pipes through a user-defined function (UDF) where the axial velocity (u_z) is estimated based on the one-seventh power-law velocity profile (H. Meng et al., 2020) with $n=7$ as follows:

$$u_z = \frac{(2n + 1)(n + 1)}{2n^2} \left(1 - \frac{r}{R}\right)^{\frac{1}{n}} \bar{u} \quad (29)$$

Outflow boundary conditions were imposed at the outlet and all the walls of the empty tube and the mixers were set to no slip-boundary conditions. The non-reacting species transport model available in Fluent[®] was used to solve the species transport equation along with the continuity and momentum equations. The mass fraction of the secondary stream was set to zero and one at the first and second inlets to ensure that the two streams are initially separated.

3.5.1 Model Validation

The computed ΔP values were used for model validation. For each mixer, the Fanning factors over the tested Re range were computed and compared against the

available literature data, and the results for Kenics, SMV, and the new mixer are discussed in Sections 5.1.1, 6.1.1, and 7.1.1.

3.6 Hydrodynamic and Mixing Assessment

The velocity and pressure fields were obtained from solving the continuity and momentum equations. The pressure distribution was first used to quantify the pressure drop Δp across each mixer and to locate the regions of pressure losses. The velocity profiles were then thoroughly analyzed to provide a deep understanding of the mixing phenomena taking place inside each mixer.

The solution of the local mass fraction of the secondary fluid was used to compute the parameters used in the mixing assessment investigation. One parameter was selected to assess the dispersive efficiency of the three investigated mixers, namely, the extensional efficiency β (Eq.(14)). Whereas, three other parameters were used to quantify and qualify the distributive behavior of these mixers, namely the CoV (Eq.(12)), the M -number (Eq.(17)) and the Aerial distribution. Details about these parameters were provided in Section 2.1.3 and will be further discussed in the following chapters.

CHAPTER 4

MESH SENSITIVITY ANALYSIS

For each mixer, three tetrahedral meshes with different refinement levels were created for a two-element configuration with Grid 1 being the coarsest and Grid 3 the finest. The ratio between the average cell sizes of two consecutive levels was kept at ~ 1.3 for all the meshes. Details about these meshes are provided in Table 5 through Table 7 for the three investigated mixers. To account for the near-wall effect, a different number of inflation layers was employed with a fixed first layer thickness and a growth rate varying between 1.05 and 1.2. In all the generated meshes, a $y^+ < 4$ was satisfied (cf. Table 5, Table 6, and Table 7)

All the tests were done at the highest Re number, i.e. $Re_{\text{pipe}} = 30,000$ since under high turbulence, more fluctuations are expected. To investigate the effect of the grid on the solution accuracy, the pressure drop ΔP was calculated across the total length of the mixers for the different generated meshes and the results were reported in the tables. Similarly, the CoV values were computed at the exit of the mixing chamber and denoted by CoV_{mix} and at various locations downstream of the mixing section in the empty tube and denoted by CoV_{emp} . The value of CoV generating the maximum relative error in the downstream section was reported in the tables for each case.

Table 5 Kenics grid sensitivity analysis

Case	Grid 1	Grid 2	Grid 3
#Tetrahedral cells	1,768,232	3,131,770	6,563,175
#Polyhedral cells	745,385	1,136,088	2,440,226
Average cell size (mm)	0.19	0.13	0.10
First layer thickness	0.01	0.01	0.01
#Inflation layers	8	10	12
y_{avg}^+	3.5	3.7	3.6
y_{max}^+	1.09	1.15	1.19
ΔP	7896	7913	7871
$\left \frac{\Delta P^i - \Delta P^{i+1}}{\Delta P^i} \right $	-	0.0022	0.0053
CoV_{mix} (%)	41.88	38.86	37.95
$\left \frac{CoV_{mix}^i - CoV_{mix}^{i+1}}{CoV_{mix}^i} \right $	-	0.072	0.024
CoV_{emp} (%)	4.83	5.46	5.66
$\left \frac{CoV_{emp}^i - CoV_{emp}^{i+1}}{CoV_{emp}^i} \right $	-	0.13	0.039

The relative errors between the computed parameters at two consecutive grid refinement levels were estimated as follows and the results were reported in the tables:

$$\left| \frac{a^i - a^{i+1}}{a^i} \right| \quad (30)$$

Where a^i and a^{i+1} are the resultant parameters from the low and high grid density levels, respectively. To select the final mesh, a threshold for the relative error is set at 0.03

For Kenics simulations, the finest mesh, i.e. Grid 3, was selected. It is worth noting that Grid 2 could have been selected since the relative error between Grid 2 and Grid 3 is less than 3% for all the tested parameters, however at the early stages of this study, the *GCI* parameter (Celik et al., 2008) was employed for the grid sensitivity analysis. The *GCI* values showed that Grid 3 is the optimal mesh. Later on, this same method rendered very high values of *GCI* with the two other mixers, this is why the relative error was used as a criterion for the grid sensitivity study instead.

The same grid settings were then used to discretize the domain of a mixer comprising 4 and 6 Kenics inserts and a total of 4,738,393 and 6,975,840, respectively, elements were obtained. It is also worth noting that grids with lower densities were also tested, but they rendered unstable solutions.

A schematic of the polyhedral grid generated for the Kenics cases is depicted in Figure 8. This figure perfectly shows the refined areas at the cross-junction where high-velocity gradients are encountered because of the sudden change in the fluid direction. It also shows the inflation layers placed at the pipe and Kenics walls.

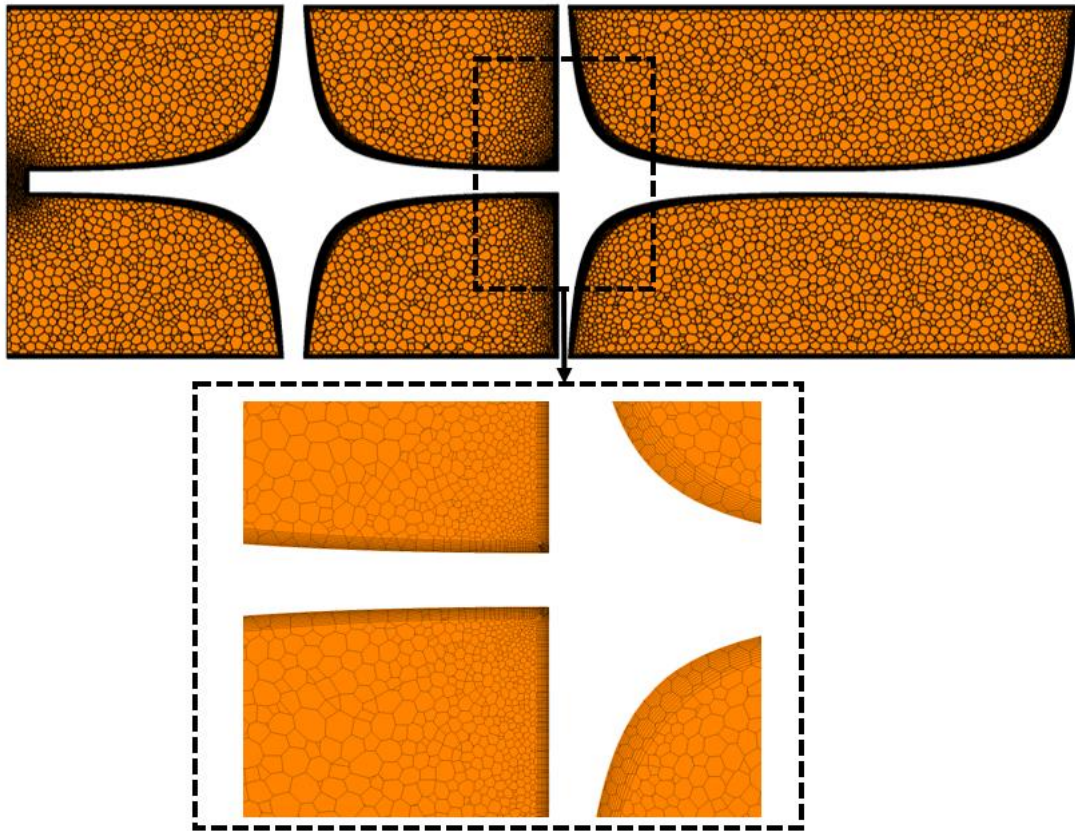


Figure 8 Mesh of 2-mixing units of Kenics over the yz plane

The results of the grid sensitivity analysis for the 2-element configuration of SMV are reported in Table 6. It can be clearly seen that the relative errors resulting from the set of Grid2 and Grid 3 are below the set threshold value of 3% except for those of the CoV downstream of the mixing section (CoV_{emp}) that are estimated at 31% and 15% between Grid 1 and Grid2, and Grid 2 and Grid 3, respectively. These errors are deemed acceptable since the values of CoV_{emp} are smaller than 5% which is desired for industrial applications (Wadley & Dawson, 2005). However Grid 2 was selected since in general, it ended up with relative errors lower than 3% for ΔP and CoV_{mix} . The number of elements obtained for the 4-element configuration of SMV using the same mesh settings is 37,892,059.

Table 6 SMV grid sensitivity analysis

Case	Grid 1	Grid 2	Grid 3
#Tetrahedral cells	25,655,738	61,849,131	129,619,678
#Polyhedral cells	9,494,290	20,395,538	36,969,083
Average cell size (mm)	0.152	0.121	0.088
First layer thickness	0.006	0.006	0.006
#Inflation layers	10	9	7
y_{avg}^+	0.67	0.65	0.6
y_{max}^+	2.92	2.84	2.66
ΔP (Pa)	15303	15192	15119
$\left \frac{\Delta P^i - \Delta P^{i+1}}{\Delta P^i} \right $	-	0.0073	0.0048
CoV_{mix} (%)	13.60	12.96	12.68
$\left \frac{CoV_{mix}^i - CoV_{mix}^{i+1}}{CoV_{mix}^i} \right $	-	0.0467	0.0219
CoV_{emp} (%)	1.67	1.15	0.98
$\left \frac{CoV_{emp}^i - CoV_{emp}^{i+1}}{CoV_{emp}^i} \right $	-	0.31	0.15

An illustration of the polyhedral mesh of SMV is represented in Figure 9. This figure shows the inflation layers and the refinement zone that are located in the proximity region between two neighboring plates.

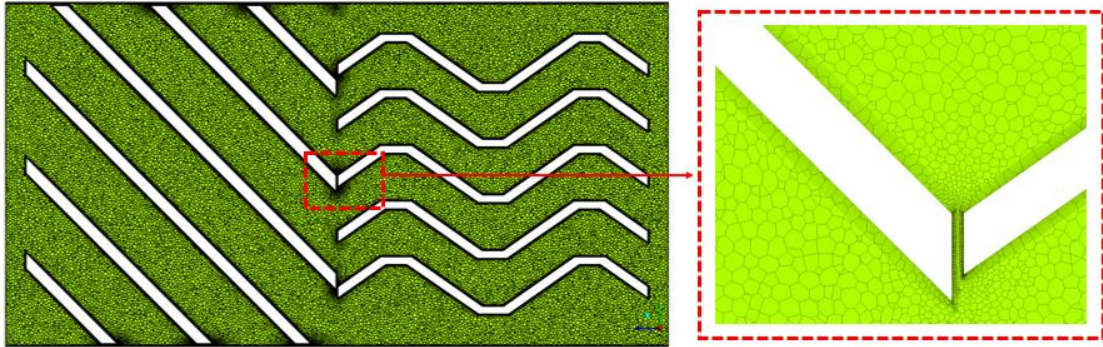


Figure 9 Schematic of the SMV mesh over the yz plane of 2 elements

Grid 2 was selected for the new geometry simulations and a total of 116M elements was obtained for a mixer consisting of 4 hybrid units. A representation of the refinement regions in the new mixer is depicted in Figure 10.

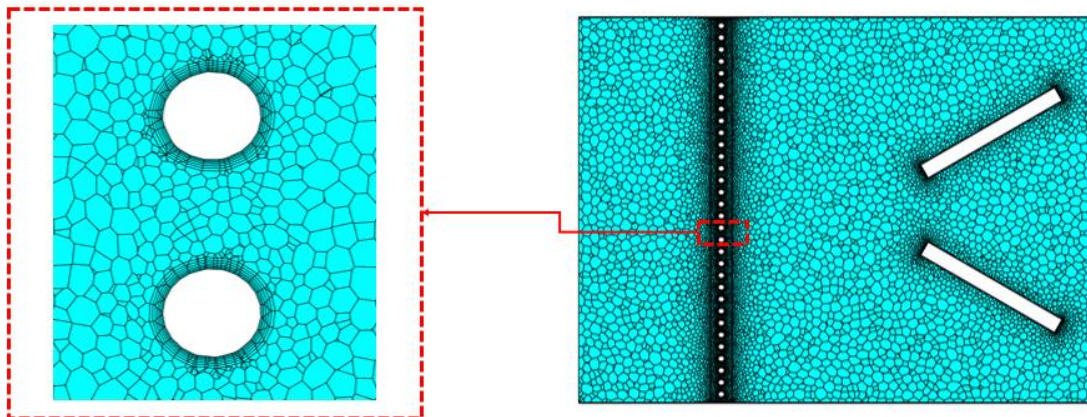


Figure 10 Local Mesh refinement of the new mixer

Table 7 NM grid sensitivity analysis

Case	Grid 1	Grid 2	Grid 3
#Tetrahedral cells	39042134	50,034,738	102,324,983
#Polyhedral cells	32,647,736	58,632,617	77,732,023
First layer thickness (mm)	0.003	0.003	0.003
# inflation layers	5	8	11
y_{avg}^+	0.62	0.5	0.62
y_{max}^+	3.23	2.56	2.52
ΔP (Pa)	33268	33859	33958
$\left \frac{\Delta P^i - \Delta P^{i+1}}{\Delta P^i} \right $	-	0.0178	0.0029
CoV_{mix} (%)	38.74	31.74	30.90
$\left \frac{CoV_{mix}^i - CoV_{mix}^{i+1}}{CoV_{mix}^i} \right $	-	0.181	0.0264
CoV_{emp} (%)	31.46	27.03	26.40
$\left \frac{CoV_{emp}^i - CoV_{emp}^{i+1}}{CoV_{emp}^i} \right $	-	0.141	0.023

CHAPTER 5

KENIC STATIC MIXER: HYDRODYNAMICS AND MIXING EFFICIENCY

5.1 Hydrodynamics and Model Validation

In this section, the hydrodynamics of the flow through Kenics mixers are investigated. The pressure was first computed and the pressure drop data was compared against the available literature data to validate the computational model. The velocity fields were then calculated as they carry information about the flow pattern that greatly affects the mixing efficiency of the mixer. Moreover, velocity fields are primordial to evaluate some parameters used for the assessment of the mixing efficiency such as the extensional efficiency.

5.1.1 Pressure Drop and Model Validation

Predicting the pressure drop across a mixer is a key variable in the early design stages. The pressure drop carries information about the cost of the energy needed to achieve the required degree of mixing, and a proper estimation of it is crucial for sizing pumps.

In the current work, pressure drop was computed as the difference between the area-weighted average static pressure on two planes placed 1 mm before the first mixing element and 1 mm downstream of the last element. These measurements were done at different empty pipe Re numbers (Re_{pipe}) ranging between 5,000 and 30,000 and equivalent to hydraulic Re numbers (Re_h) of 2,760 and 16,535, respectively. Re and Re_{pipe} are used interchangeably in this manuscript.

The predicted pressure drop values across six Kenics inserts were expressed in terms of the Fanning friction factor f and compared against the available literature data in an attempt to validate the currently used computational approach. A literature search showed that a couple of numerical and experimental studies reported pressure drop data for Kenics mixers under the studied Re range, namely (Hearn, 1995), Berkman and Calabrese (1988), Song and Han (2005), and Kumar et al. (2008). The literature values along with the predicted ones are depicted in Figure 11.

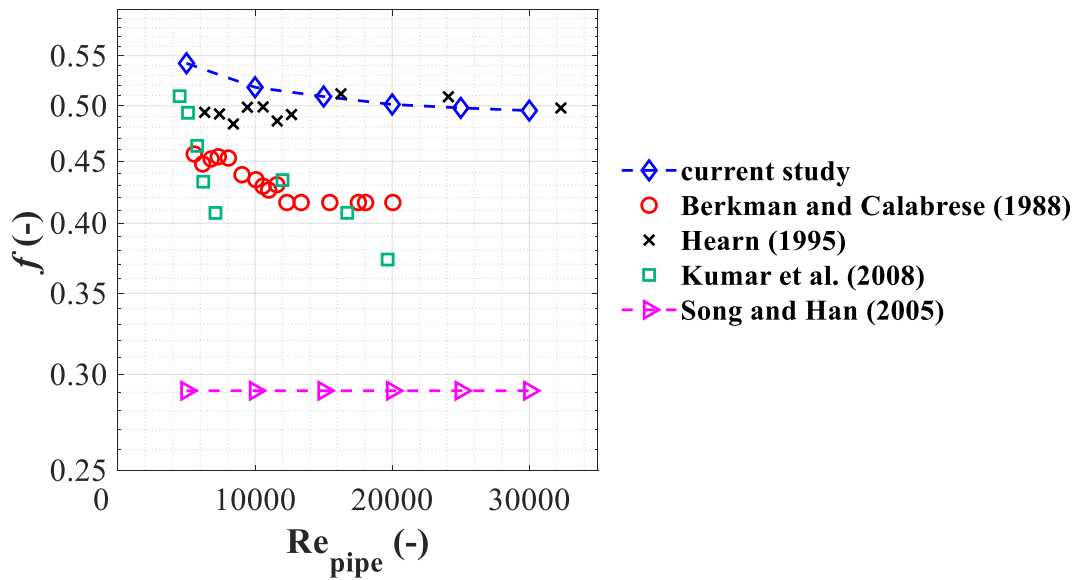


Figure 11 Comparison of Kenics Fanning friction factor obtained in this study to the literature data

One can first notice that the friction factor follows the same decreasing trend in the different studies except in those of Hearn (1995) and Song and Han (2005). In the former, random fluctuations are observed over low Re numbers and this may be due to experimental errors, whereas in the latter f is constant over the tested Re range. Moreover, it is important to note that in the current study, f approaches an asymptotic value of roughly 0.495 at around $Re_{pipe}=15,000$ beyond which it becomes independent

of Re . This observation is in line with the findings of Berkman and Calabrese (1988). Hence, one cannot but notice the analogy between the flow in Kenics static mixer and fully developed turbulent pipe flows where the friction factor decreases until reaching a value independent of the flow rate.

The comparison presented in Figure 11 also shows good agreement between the simulated results and the literature data which validates the current approach. The average Fanning friction factor is 0.510 in the current study, while it is 0.485, 0.435, 0.450, and 0.291 in Hearn (1995), Berkman and Calabrese (1988), Kumar et al. (2008), and Song and Han (2005) studies, respectively. While the calculated values are close to literature data, the best fit was found for the data of Hearn (1995) where an average relative error of 3.1% and a maximum error of 9.36% were obtained over the tested Re range. An average relative error of 19.12%, 22.10% and 76.63% was obtained for the study of Berkman and Calabrese (1988), Kumar et al. (2008) and Song and Han(2005), respectively. The observed inconsistency between the computed Fanning friction factor and the available data could be a result of the different geometries used in the various studies. To illustrate this, Table 8 summarizes the differences in the geometries of these studies. For instance, the results obtained by Song and Han (2005) are the lowest because the authors neglected the blade thickness in their numerical simulation and only assumed a thin wall. Although this simplification is favored in easing the mesh generation process, it is prone to erroneous results. In addition, the pressure drop is highly dependent on the blade geometry, i.e. its thickness, aspect ratio, material and mode of construction (Simpson et al., 2016).

It can therefore be concluded that relying solely on the data and correlations available in the literature may not always render a good outcome for the case of Kenics mixers because of two main reasons:

- i. The available empirical correlations are usually validated over a limited Re range, and hence are not valid outside of it.
- ii. Any modification to the geometry can lead to huge discrepancies in the results.

Table 8 Geometrical aspects of Kenics used in the current and the literature studies

	$D(mm)$	L_e/D	Thickness $t_p (mm)$	t_p/D
Current Study	16.37	1.5	1	0.061
Hearn (1995)	40	1.5	N/A	N/A
Berkman and Calabrese (1988)	19.1	1.5	N/A	N/A
Kumar et al. (2008)	25.4	1.5	2	0.079
Song and Han (2005)	variable	>1	Thin-wall	0

The variation of pressure drop across 2, 4, and 6 elements with Re_{pipe} is represented in Figure 12a. As expected, the pressure drop increases with the number of elements and Re since it is directly proportional to the distance traveled by the fluid and its velocity inside the mixer.

To better understand the effect of the number of elements on the pressure distribution, the pressure drop per element $\Delta P_{e,n}$, with n being the number of inserts, was evaluated as the ratio of the pressure drop across the mixer to the corresponding number of mixing units and is illustrated in Figure 12b. One can notice that ΔP_e varies in the three configurations in such a way $\frac{\Delta P_{e,6}}{\Delta P_{e,4}} = 1.08$, and $\frac{\Delta P_{e,4}}{\Delta P_{e,2}} = 1.17$. This

observation contradicts the findings of Kumar et al. (2008) who reported that the number of elements does not significantly affect the pressure drop per unit element. However, our findings follow a similar trend to that observed by Hearn (1995), who reported that the pressure drop for 6 elements was larger than twice that measured for 3 elements.

To explain this, it should be observed that a 2-element mixer contains one single junction, i.e. the region between two consecutive elements, while a 4-element mixer contains 3 junctions and a 6-element mixer contains 5. While these junctions are the main contributor to pressure drop because the fluid has to change its rotation as it crosses them, it is therefore expected to observe $\Delta P_{e,6} > \Delta P_{e,4} > \Delta P_{e,2}$. In reality, the Kenics mixer is mostly effective at the transition between two consecutive elements (Simpson et al., 2016). It is also worth mentioning that $\Delta P_{e,6} - \Delta P_{e,4} \neq \Delta P_{e,4} - \Delta P_{e,2}$. This shows that the pressure is not uniformly distributed along the mixer length. The following elaborates more on the previous observations.

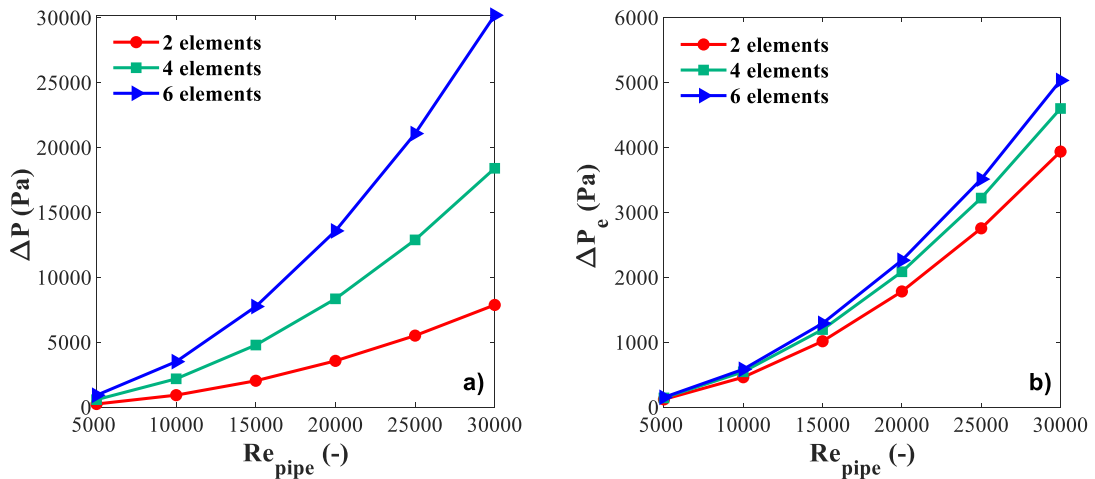


Figure 12 a) Pressure drop and b) Pressure drop per 1 element for 2, 4, and 6- Kenics mixer versus Re_{pipe}

5.1.2 Pressure and Velocity Distributions

Figure 13 represents the axial variation of the area-weighted average static pressure and its rate of variation per unit length of the mixer (dp/dz) in a Kenics mixer comprising 6 elements at Re_{pipe} equals 5,000 and 30,000. The abscissa represents the normalized axial position z/D where $z=0$ corresponds to the tube inlet. The grey dashed lines in the figures indicate the axial position of the inserts' leading and/or trailing edges.

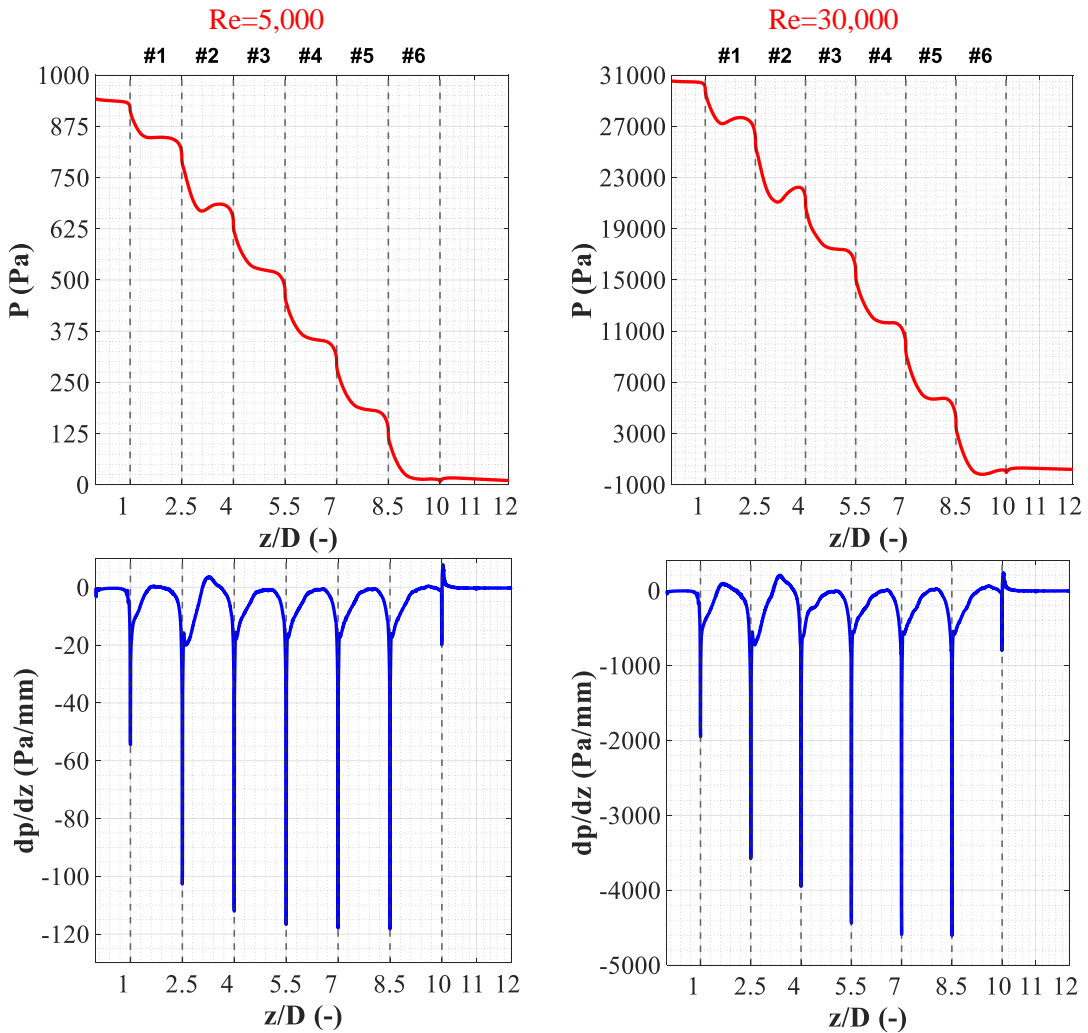


Figure 13 Axial distribution of static pressure in a Kenics mixer (red curves) and rate of pressure variation per unit length (blue curves) at $Re_{pipe}=5,000$ (left column) and 30,000 (right column).

Based on Figure 13, it can be observed that a regular repetitive pattern is obtained after the 4th element before which the distribution shows odd patterns (bumps). This indicates that the turbulent flow is not fully established until downstream of this element. This observation is in accordance with other studies (H. Murasiewicz & Zakrzewska, 2019; Simpson et al., 2016) who focused their study on the middle of the fifth Kenics element since previous LDA measurements by Adamiak and Jaworski (2001) showed that in this region the flow can be considered fully. Moreover, the previous observation suggests that pressure losses are not evenly distributed along the length of the mixer which explains the reason behind $\Delta P_{e,6} - \Delta P_{e,4} \neq \Delta P_{e,4} - \Delta P_{e,2}$. However, it is worth noting that the observed disturbances in the pressure distribution are less important at $Re_{\text{pipe}}=5,000$ than at $Re_{\text{pipe}}=30,000$ which justifies that the chaotic nature of turbulence is behind the observed irregularities.

In the following, the analysis will be restricted to the fully-developed flow and the 5th element will be used as a representative unit. The pressure profile in one Kenics insert can be divided into two main regions according to the values of dp/dz (cf. Figure 13):

- A region of high-pressure drop at exactly the transition between two consecutive elements assigned with a high negative value of the axial pressure gradient dp/dz . The effect of the transition is seen up to 30% of the length of the element.
- A region of almost constant values of pressure around the middle of the element where dp/dz approaches zero. This region extends up to 2/3 of the length of the insert after which the pressure starts decaying again under the influence of the downstream element.

To provide a better insight into the observed trend, the axial velocity profiles overlaid with the resultants of the tangential and radial velocity components over xy planes at different axial locations within the 5th element are shown in Figure 14. The represented planes are normal to the flow direction, and their axial positions are normalized and represented by L_5^* such that

$$L_n^* = \frac{z - z_n}{D} \quad (31)$$

where z_n represents the z -coordinate of the leading edge of the n^{th} element edge. The composite plots in Figure 14 reveal the formation of complex and strong secondary flows within the mixing section.

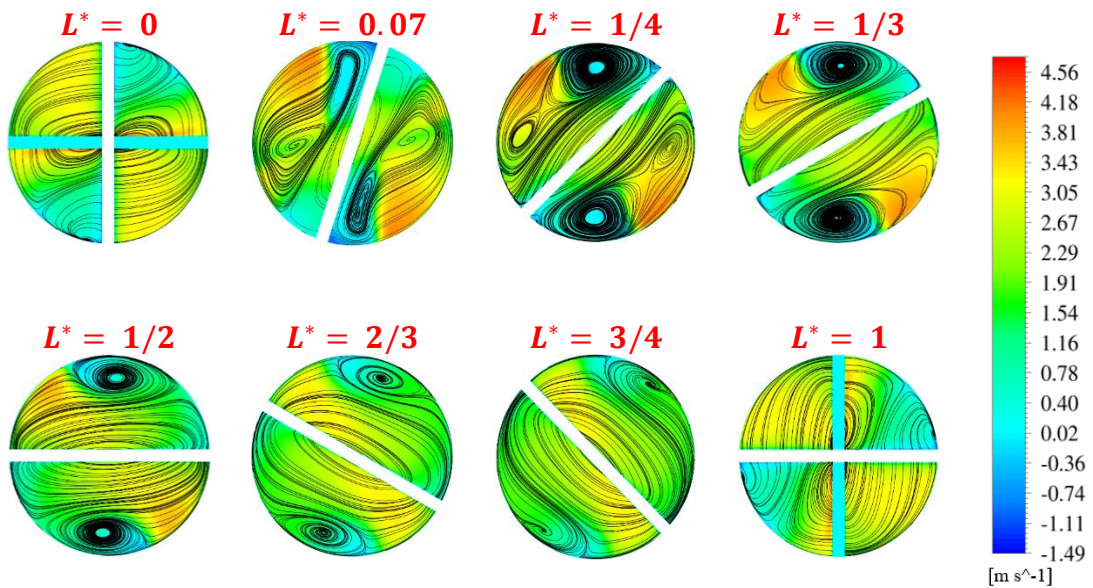


Figure 14 The resultants of the radial and tangential velocity components (2D streamlines) superimposed on the contour plots of the axial velocity at various axial locations within the 5th Kenics unit at $\text{Re}=30,000$

As the fluid enters the element ($L_5^* = 0$), it is divided into 4 regions of high momentum. In this region, the flow is redirected and is strongly reversed because of the

alternating positions of right and left-hand elements. Boundary layer separation occurs and high velocity gradients are created as indicated by the abrupt change in the color of streamlines from green to red in this region (see also the streamlines in Figure 15a). This is, therefore, the reason behind the high-pressure drop generated by the cross-junction.

One can also discern the formation of recirculation zones characterized by negative velocity values behind the intersection of the inserts with the tube wall. These low-pressure regions are suitable for the development of vortices as indicated by the swirling structures in Figure 14 and the blue spiral-like lines in Figure 15a. Two attached vortices are created directly downstream of the leading edge ($L_5^* = 0.07$) in each half of the mixer: a small one in the vicinity of the wall of the tube and a larger one near the Kenics surface (See also the high values of vorticity encountered directly behind the entrance of the element in Figure 15b). The small vortex called free vortex, and the large vortex, or forced vortex, were already observed and reported in the literature (H. Meng et al., 2020; Rahmani et al., 2008). Advected by the flow, these vortices interact with each other to form one vortex whose center starts moving toward the tube wall. This region is surrounded by areas of high axial velocity. In fact, as the fluid hits the first element, it starts accelerating, under the influence of centripetal forces, following the curvature of the plate. This effect is seen up to approximately 30% ($L_5^* = 1/3$) of the length therefore resulting in high pressure drops. Beyond this length, the flow starts decelerating following the smooth path of the Kenics curvature, the velocity gradients diminish and the vortices start dissipating. Consequently, the constant values of pressure obtained in this region are justifiable.

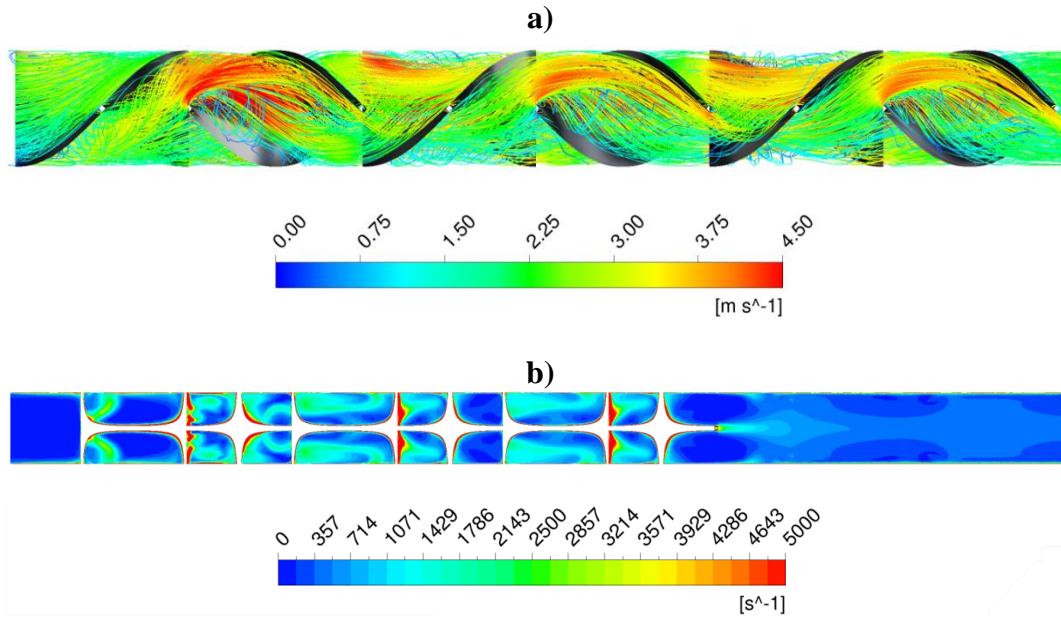


Figure 15 Velocity Field through Kenics at $Re_{\text{pipe}} = 30,000$ (a) Streamlines of the flowing fluid through 6 Kenics elements and (b) vorticity contours over the central vertical plane

The evolution of the flow downstream of the last mixing element is shown in Figure 16a at different axial locations represented by $d^* = \frac{z-z_7}{D}$ where z_7 is the axial position of the trailing edge of the 6th element, i.e. the leading edge of the 7th mixing element. The graphs in Figure 16b show the axial velocity profiles at the same axial locations and along the vertical diameters of the same planes at $Re=5,000$ and $Re=30,000$. The fully developed turbulent velocity profile extracted from the fully-developed region of an empty tube is also overlaid on these graphs for evaluation. For ease of comparison, the axial velocity was normalized by the centerline axial velocity at the inlet of the tube and is represented by U_z^* . Similarly the radial position was non-dimensionalized by dividing it by the radius of the tube R . It is worth mentioning that the representation of the fluid velocity distribution was limited to one case, i.e. for $Re=30,000$, as the obtained distributions for the other cases were qualitatively the same.

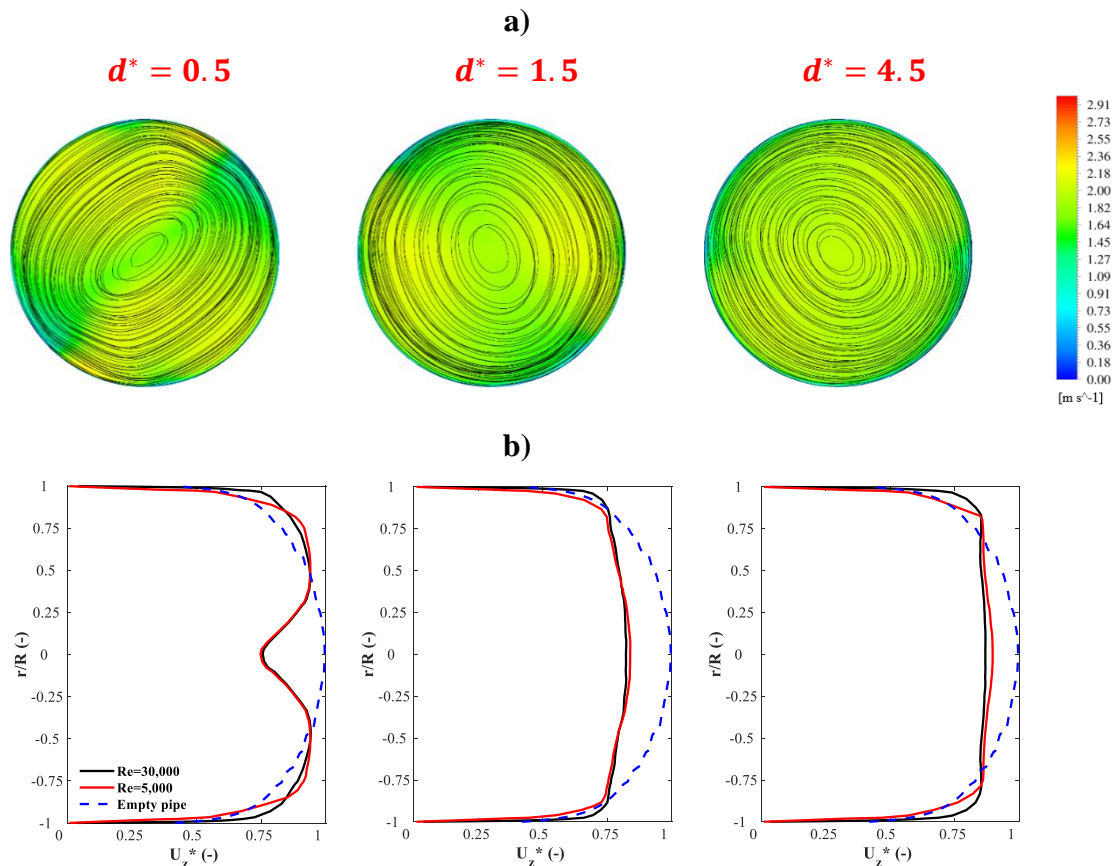


Figure 16 (a) Axial velocity contour plots overlaid by the tangential and radial velocity components and (b) normalized axial velocity profiles at different axial positions downstream of the last mixing element in a 6-Kenics elements mixer at $Re=30,000$ and $5,000$

From the velocity contours overlaid by the 2D streamlines, one can notice that the fluid core exits the mixing zone while rotating en masse. This behavior is seen even after 4 pipe diameters. The observed pattern reveals the strong effect of the last mixing element on the fluid flow. This is further justified by the dip present in the velocity profile at $d^* = 0.5$ just in the center of the tube ($r/R=0$) indicating, therefore, the formation of a wake region behind the last mixing plate. This region seems to weaken as the fluid travels further downstream as reflected by the blunt shape of the velocity profiles that starts approaching the one of a fully turbulent flow. However, it is worth mentioning that the recovery of the flow in Kenics is slow since a fully developed flow

was not established at the exit of the tube. The variation of the Re numbers seems to have a slight influence on the core region; however, it greatly affects the flow near the wall where steeper velocity gradients are obtained at higher Re values.

Based on the aforementioned observations, one can deduce that Kenics features many interesting characteristics that can be summarized as follows:

- i. The cross-junction in Kenics is a region where most of the important phenomena take place
- ii. the helical shape of Kenics and the relative position of two adjacent elements are responsible for the creation of very complex secondary flow structures and recirculation zones
- iii. The flow recovery is slow and complex

The influence of these features on the mixing efficiency will be discussed in the next section.

5.2 Mixing Efficiency

The dispersive and distributive mixing efficiency were assessed quantitatively and qualitatively in this section. For this purpose, four parameters, namely the extensional efficiency, the coefficient of variation (CoV), the M-number, and the aerial distribution of the tracer mass fraction, were used and the results are represented and discussed in the following.

5.2.1 Dispersive Mixing: Extensional Efficiency

In order to assess the dispersive mixing efficiency in Kenics, the extensional efficiency β was adopted. β measures the relative strength of the elongational flow to the rotational flow (De La Villéon et al., 1998). Elongational flows, i.e. high values of β , are desired for an effective break-up and dispersion of agglomerates throughout the volume of the mixer (De La Villéon et al., 1998; Nyande et al., 2021). Many previous studies have used this parameter to characterize the dispersive mixing in Kenics static mixers for laminar flows (Haddadi et al., 2020; H. Meng et al., 2014; Nyande et al., 2021; Rauline et al., 1998), but none were reported under turbulent regimes.

The axial variation of the area-weighted average of β in a Kenics mixer comprising 6 elements at $Re_{pipe} = 30,000$ is shown in Figure 17 and a visual representation of its distribution at different cross-sections within the 5th element and downstream of the mixing zone is represented in Figure 18.

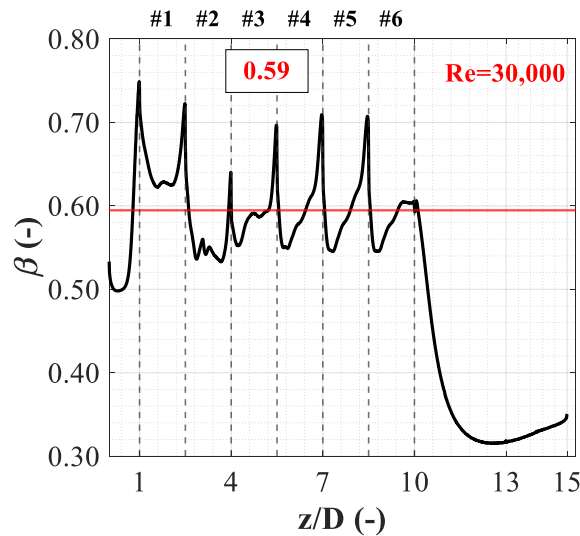


Figure 17 Axial variation of the extensional efficiency for 6-Kenics elements at $Re=30,000$

The average value of β over the entire mixing section is displayed in the rectangular box on the figure and is graphically represented by the horizontal red line. it can be easily discerned that the highest values of β are reached at the entrance of each mixing element with a repetitive pattern obtained starting from the 5th element. This observation was also noted previously when analyzing the pressure patterns, which further confirms the fact that the turbulent flow in Kenics mixers could not be considered fully turbulent until after the 4th mixing unit.

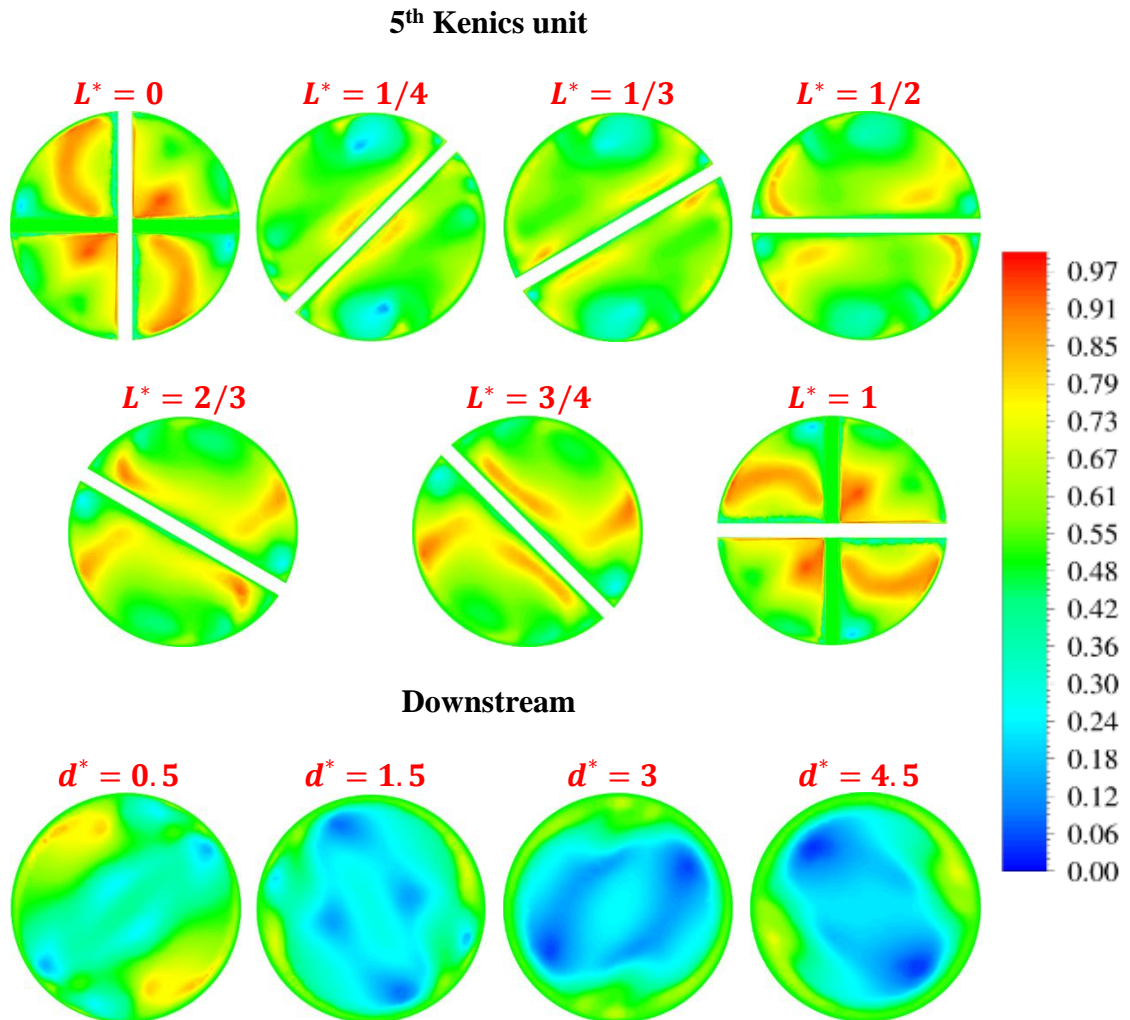


Figure 18 contour plots of extensional efficiency at different locations within the 5th Kenics unit and downstream of the mixing section at Re=30,000

β reaches a maximum of 0.75 when the fluid hits the first element. This behavior is expected since the fluid is subject to disturbances when it meets an obstacle for the first time. Slightly lower maxima of approximately 0.71 (after the 4th element) are then observed at the entrance of each subsequent element. These high values of β encountered in the transition region between consecutive elements are due to the high velocity gradients generated following the strong flow reversal at the cross-junction. This further indicates that the flow is highly dispersive at the leading edges of Kenics elements.

Just downstream of the leading edge, the extensional efficiency drops abruptly until reaching a minimum of 0.55 at approximately 30% of the mixing element length, after which it starts increasing in a relatively slower fashion until peaking again at the cross-junction of two adjacent elements. Such behavior is expected since in the region limited by 30% of the length of the element, the formation of vortices was already witnessed which might be the cause behind the drop in the value of β . Blue spots indicating highly rotational flow are discerned in Figure 18 in the same regions of formation of vortices (cf. Figure 14). The variability of β values along the length of an element suggest that the flow within the mixing element is far from being a simple shear flow. Moreover, it highlights the complexity of the mixing pattern induced by the helical mixer.

Downstream of the last mixing element, the flow becomes highly rotational as indicated by the low values of β and the blue color that covers the core region in Figure 18. This is also in line with the observations reported in Figure 16a where a rotational flow dominates downstream of the last element as well as those of Figure 16b where a flat velocity profile was recorded. In fact, β decreases immediately to reach a value of

0.32 after approximately 2D. Subsequently, a gradual increase of β is observed which indicates a slow recovery of the fully-developed turbulent velocity profile. It is worth mentioning, however, that a fully-developed pipe flow could have been re-established if a longer tube section was available.

The effect of fluid velocity on the extensional efficiency is reported in Figure 19 and Figure 49. One can at first expect that Re has a slight influence on the dispersive behavior of the mixer as reflected by the average value of β that varies between 0.56 and 0.59 for the two extreme cases, i.e. for Re=5,000 and Re=30,000. The first peak has a magnitude of 0.75 regardless of the Re number. However, Higher values of β are observed at higher Re numbers within the mixing section, whereas lower values are observed downstream this section. It can therefore be deduced that operations under higher Re numbers improve dispersive mixing.

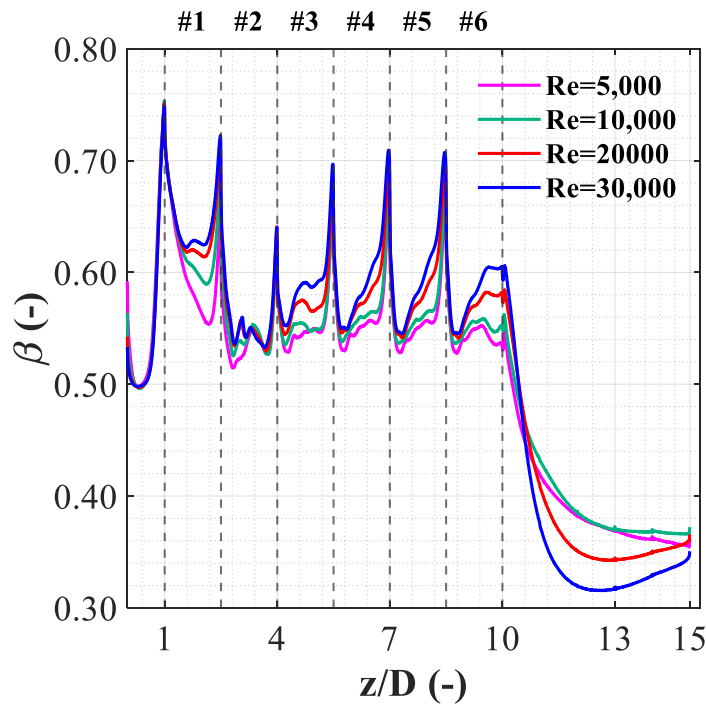


Figure 19 Axial variation of the area-weighted average extensional efficiency β for a Kenics mixer of 6 units

5.2.2 Distributive Mixing

The distributive mixing was assessed in this section by means of 2 parameters, namely the coefficient of variation (CoV) and the aerial distribution that measure the intensity and scale of segregation, respectively. The former reflects the deviation of the concentration distribution from the average, while the latter quantifies the distribution of a cross-section in terms of the intensity of mixing.

5.2.2.1 Coefficient of Variation

The *CoV* was computed in Fluent at a given plane as the ratio of the standard deviation to the area-weighted average mass fraction over this plane. To assess the effect of varying the fluid velocity and the number of elements on the distributive mixing in a Kenics mixer, the axial variation of *CoV* is shown in Figure 20 and Figure 21. The former shows the variation of *CoV* for different number of elements, while the latter reports the *CoV* at the outlet for the various configurations. A *CoV* of 1 typically reflects a completely segregated system, whereas a value of 0 denotes a fully-mixed system. A commonly accepted value of 5% or lesser indicates that the mixture could be considered as completely mixed (Stec & Synowiec, 2019; Wadley & Dawson, 2005).

It could be discerned from Figure 20 that the first element slightly improves the mixing as the *CoV* hits a value of about 78% at the outlet of this element for the three configurations regardless of the velocity of the flow. The 2nd and 3rd mixing elements have the greatest effect on the mixture homogeneity as a sharp decrease of approximately 42% and 30% in the *CoV* values is recorded at their exits. This observation was previously noted by Rahmani et al. (2008) and illustrated in Figure 22. The latter represents the contour plots of the mass fraction of the secondary fluid at

different Re numbers and clearly shows that the flow is nearly-homogeneous after the 3rd element. It also indicates that the first few elements have the greatest impact on the mixing efficiency compared with subsequent elements.

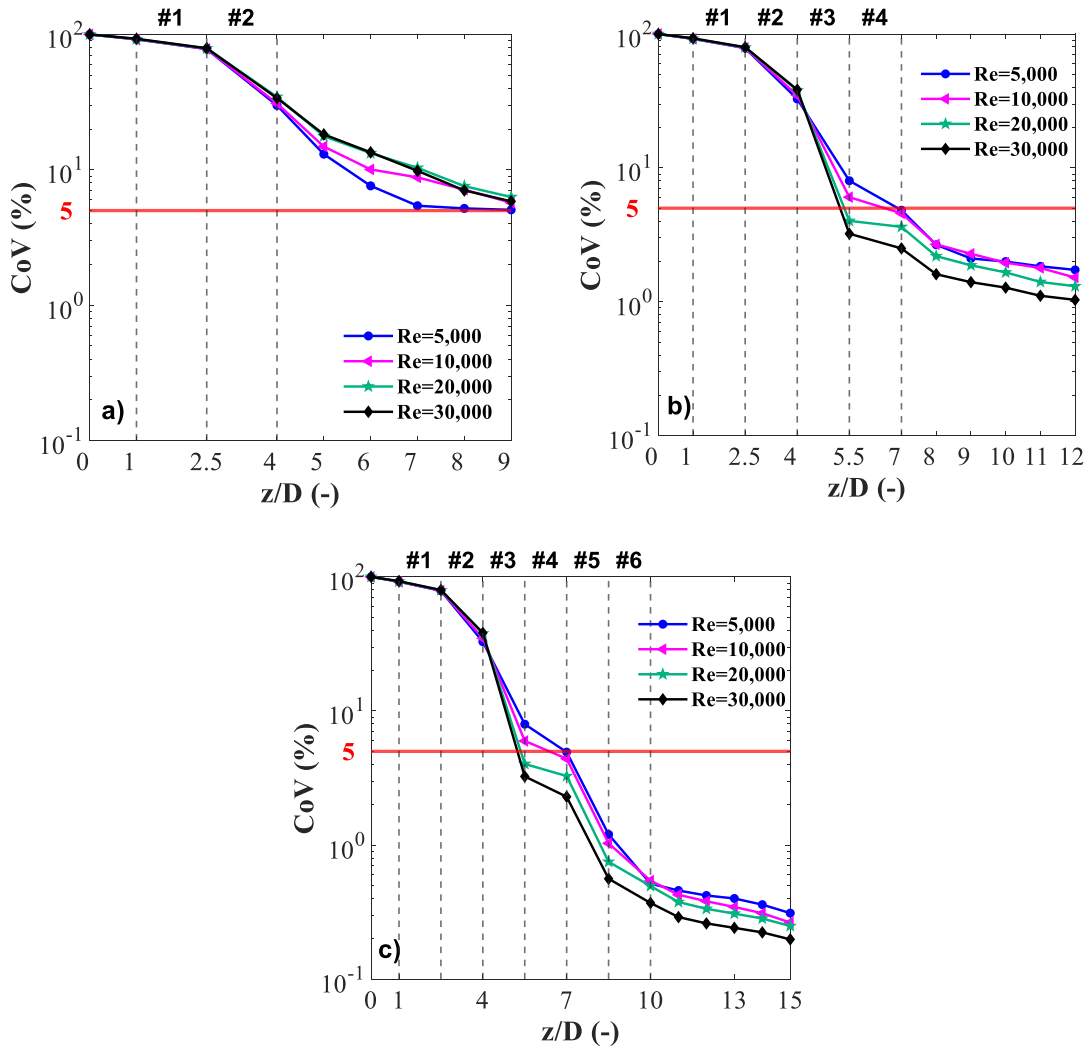


Figure 20 Axial Variation of CoV in a Kenics mixer comprising a) 2 b) 4 and c) 6 units at different Re numbers

When comparing Figure 20a, Figure 20b and Figure 20c, one cannot but notice that 2 elements were not sufficient to achieve the desired homogeneity level unlike the case of 4 and 6 elements. However, lower values of *CoV* could have been obtained, for

the 2 elements case, if a longer tube was used. This would have been achieved due to the contribution of the empty pipe and the complex flow structures transported downstream of the last mixing element.

Higher Re numbers seem to improve the distributive mixing as transverse flow is promoted at higher velocities, yet this effect becomes insignificant after the 4th mixing element where a value of $CoV=5\%$ has already been reached (Figure 20b, 10c, and Figure 21). On the other hand, the value of CoV at the exit of the pipe increases slightly with Re when considering a mixer with 2 elements (Figure 20 a) and Figure 21). Two reasons may be behind this behavior:

- i. at lower velocities, a particle has a larger residence time compared to the case of higher velocities. Consequently, the particle has more time to intermingle with other particles instead of bypassing the mixer immediately.
- ii. The boundary layer might be a great contributor to mixing, and since it becomes thinner at higher Re numbers (steep velocity gradients seen in Figure 16), then a slight decrease in mixing efficiency might be observed.

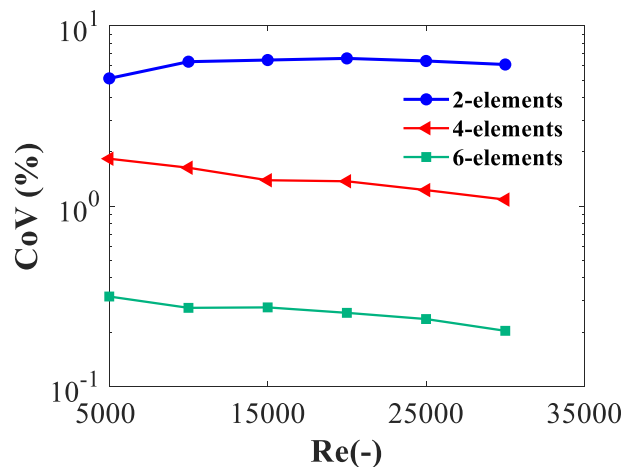


Figure 21 Variation of the CoV at the outlet of the mixer chamber of Kenics as a function of Re numbers

One can therefore conclude, that 2 Kenics elements with a sufficiently long downstream empty tube section, i.e. greater than 5D, may be enough to achieve homogeneity in applications involving fluids whose physical properties are close to those of water. This suggestion ensures the production of a well-mixed system but at a lower energy cost.

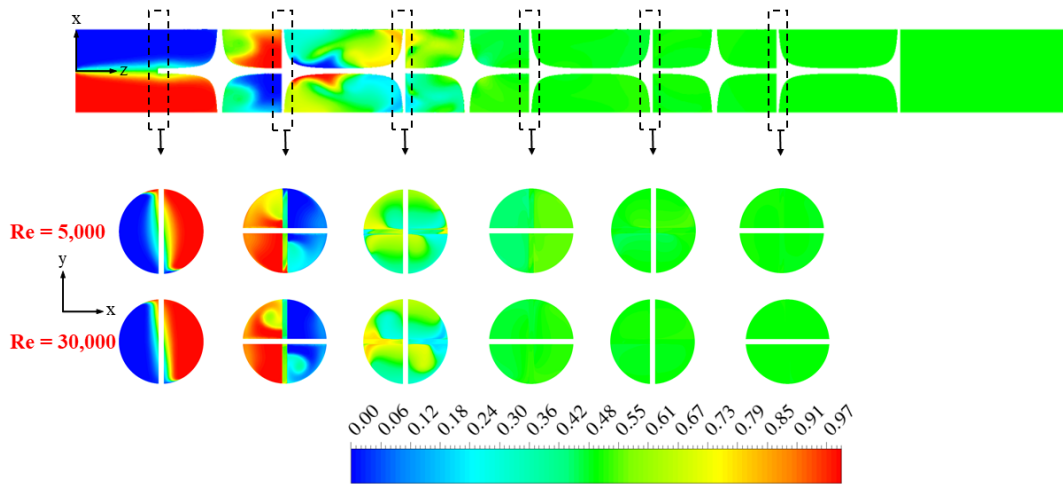


Figure 22 Contour plots of the mass fraction of the secondary fluid in a Kenics comprising 6 elements for $Re=5,000$ and $Re=30,000$

5.2.2.2 Aerial Distribution

The aerial distribution is a more rigorous way to quantify the distributive mixing inside static mixers. Proposed by Alberini et al. (2014), this method aims at sorting a cross-section in the mixer according to different levels of mixedness. In this study, 5 levels of mixedness were considered, precisely 95%, 90%, 80%, 70%, and 60%. That is, a cell on a cross-section is said to be at least 95% fully mixed if its mass fraction lies within $\pm 5\%$ of the completely mixed state, i.e. an average mass fraction of 0.5. The distributions of the mass fraction of the secondary fluid over different planes normal to the flow direction were exported from Fluent and the data was post-processed in MATLAB using the code shown in Appendix A.

The discrete distribution of area fraction in terms of intensity of mixing for 2, 4, and 6 Kenics mixing elements is depicted by the bar graphs in Figure 23 for $Re_{\text{pipe}} = 5,000$ and $30,000$. This distribution was evaluated at 7 different axial positions as indicated by the horizontal axis: the inlet of the tube, just at the exit of the last mixing element in each configuration (K2, K4, and K6), and at 5 positions further downstream of this element and whose axial positions are represented by d^* .

The two fluids enter the tube fully separated as indicated by the first bar showing an intensity of mixing lower than 60% for all the cases. For the two elements cases, the mixture leaves the mixing zone partially mixed since different levels of mixedness prevail in this region (second bar in the first row). For the two represented Re , the system at the exit of the pipe is almost fully mixed; however, a better homogeneity is achieved at lower Re , i.e. at $Re=5,000$, 90% of the mixture has an intensity of mixing $> 95\%$ while the same level of mixedness is prevailing in only 80% of the system. Increasing the number of mixing units ensures the achievement of a homogeneous mixture.

Similar results were obtained from the analysis of CoV data. Nevertheless, through the analysis of the aerial distribution of mass fraction in Kenics, one can make sure that no segregated regions are formed in the system. This makes of the aerial distribution a better tool to assess the distributive mixing efficiency. Low values of CoV mask, sometimes, the presence of such regions which may be detrimental for various critical applications.

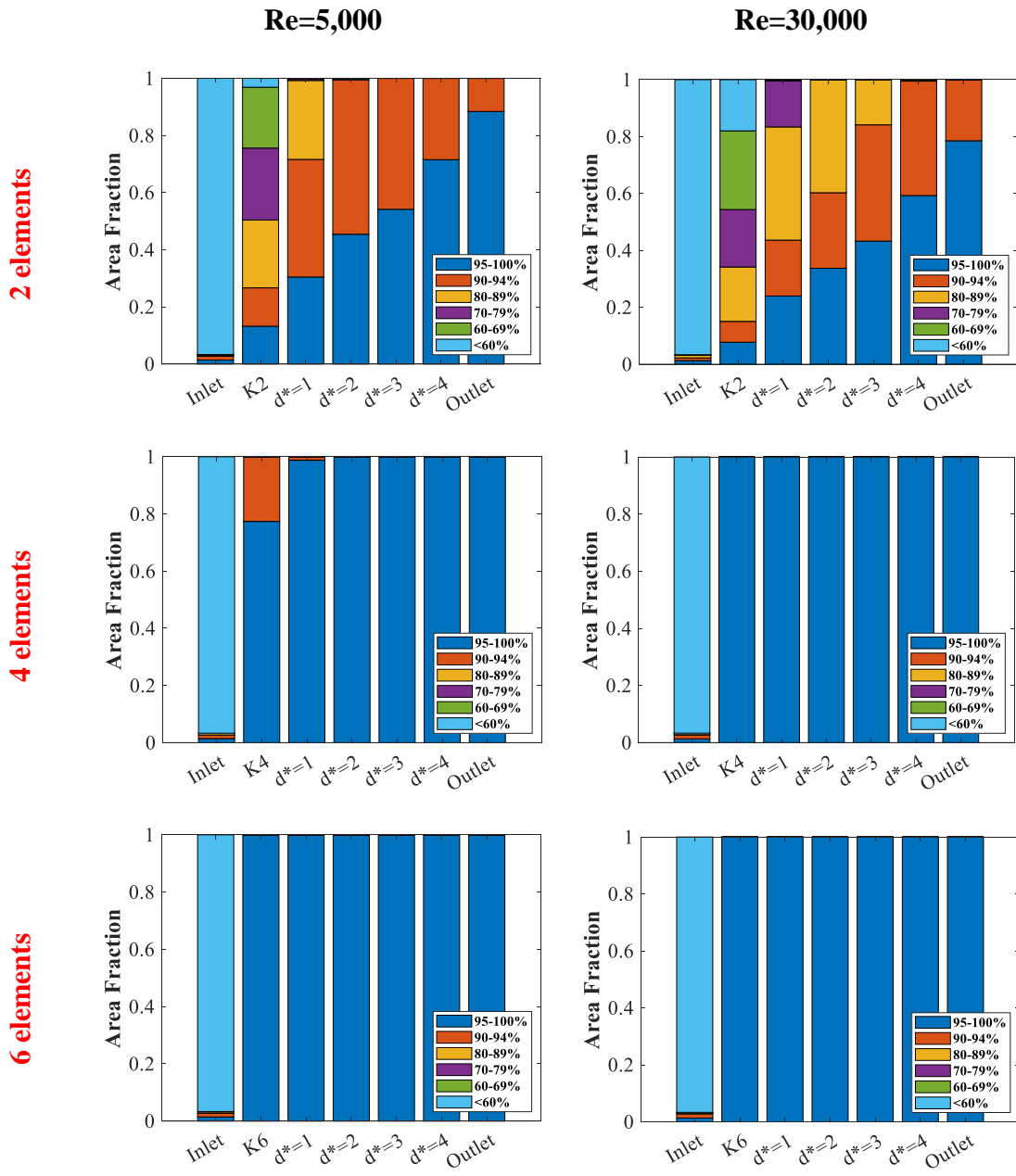


Figure 23 Stacked bar graphs showing the discrete areal distribution of the mass fraction of the secondary fluid in Kenics at different locations for $Re=5,000$ (first column), $Re=30,000$ (second column), and for different numbers of mixing units: 2 elements (first row), 4 elements (middle row) and 6 elements (last row).

5.2.3 M-Number

The M number was proposed by Medina et al. (2019), whereby the efficiency of a static mixer is approached from an economic and mixing efficiency perspectives.

Unlike the other parameters, it considers the contribution of the natural mixing induced by the empty pipe. In the following, the M parameter is computed at 4D downstream of the last mixing element in an attempt to evaluate the effect of the number of elements and flow velocity on Kenics efficiency. Its variation along with that of ω_{max} and ω_{iso} are represented in Figure 24.

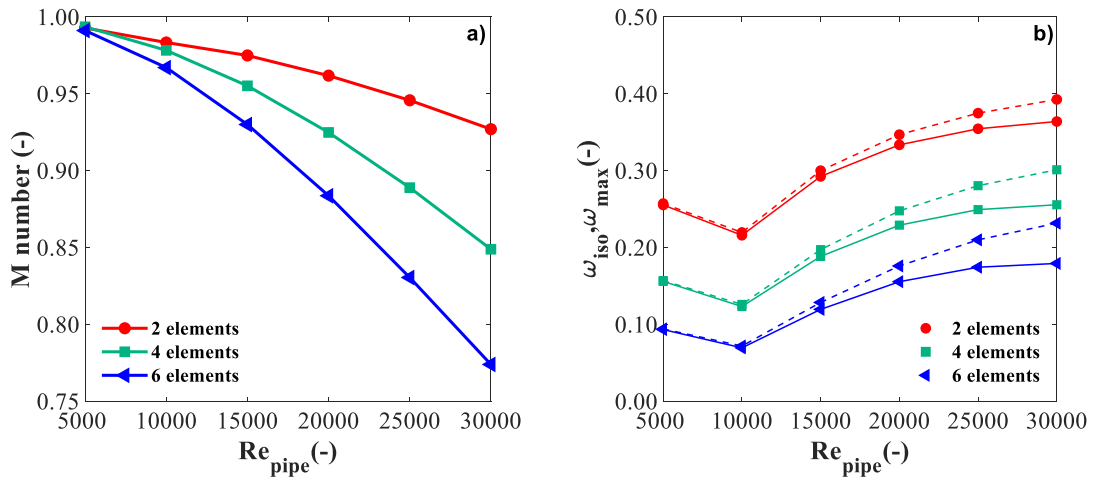


Figure 24 a) M number, b) ω_{iso} (dashed lines) and ω_{max} (solid lines) for 2, 4 and 6 Kenics elements.

Table 9 shows the results for ω_{max} , ω_{iso} , M number and CoV for 2, 4 and 6 Kenics elements at $Re=30,000$. For 6 Kenics elements, it could be noticed that in the ideal case, the mixer would perform up to $\omega_{max} = 23\%$, yet in reality it reached a performance of $\omega_{iso} = 18\%$. In this case, the mixer is 77% as effective as an ideal mixer. The same analysis would apply to the two other cases, i.e. 2 and 4 elements. According to this parameter, the additional elements do not improve the overall mixing

efficiency, yet they worsen it given that M is higher for 2 elements than for 4 and 6 elements as indicated in Table 9 and Figure 24a. This decreasing trend, therefore, contradicts that reflected by CoV (Figure 21 and the last 2 columns in Table 9).

However, one should recall that the M number accounts for the energy losses that are more significant for a higher number of elements (Figure 12 a) which explains the observed trend.

Table 9 ω_{max} , ω_{iso} , M number and CoV for Kenics mixer at $Re=30,000$

# elements	$\omega_{max}(-)$	$\omega_{iso}(-)$	M-number(-)	CoV (%)
2	0.39	0.36	0.93	6.10
4	0.30	0.26	0.85	1.09
6	0.23	0.18	0.77	0.20

The effect of Re on the M parameter is illustrated in Figure 24a. For the three configurations, higher velocities seem to exacerbate the efficiency of Kenics. A decrease of nearly 7%, 15%, and 22% is observed when Re goes from 5,000 to 30,000 for 2, 4, and 6 kenics elements respectively. On another note, the drop of M with Re becomes more significant when the number of elements increases. This decrease in performance is attributed to the additional pressure drop generated by the higher velocities and the added mixing units.

One, however, should mention that the interpretation of the M parameter alone without looking at the values of ω_{max} does not reflect the real performance of a static mixer. The latter reveals the maximum capacity of the static mixer to improve the level of mixedness after subtracting the effect of the empty pipe. The comparison of this parameter for the different configurations shows that shorter mixers have more potential

to improve the mixing efficiency than longer ones since in this case, the particles have lower residence time as mentioned previously. Moreover, the increasing trend of ω_{max} with Re indicates that mixing gets worse in empty tubes at higher velocities. The reason behind this observation could be the shear layer that becomes thinner under these conditions (Çengel & Cimbala, 2017; Dimotakis, 2005). Therefore, static mixers seem to have more work to do to improve the mixing efficiency at higher Re numbers. It is worth mentioning, however, that for all the cases the relatively low values of ω_{max} where a maximum and minimum of 39% and 9% encountered at the highest and lowest Re numbers for the 2 and 6 elements cases respectively, shows that originally little potential was left for the mixer to improve the efficiency of the system.

CHAPTER 6

SMV STATC MIXER: HYDRODYNAMICS AND MIXING EFFICIENCY

6.1 Hydrodynamics and Model Validation

The hydrodynamics of the flow through a Sulzer SMV static mixer is investigated in this chapter by adopting the same approach employed in Chapter 5. The analysis is restricted to 2 and 4 elements only since the CFD data showed that the addition of supplementary elements does not further improve the mixing efficiency. To accomplish this, the flow was tested in the Repipe range of 5,000 and 30,000, which corresponds to a hydraulic Reynolds number, Re_h , between 1,150 and 7,000.

6.1.1 Pressure Drop and Model Validation

In order to validate the adopted computational model, the hydraulic Fanning friction factor, f_h , computed from simulations was compared against the experimental data of Hearn (1995) and the correlations of Karoui and Costes (1998) and Theron and Le Sauze (2011) listed in Table 1. It should be noted that the data of Hearn (1995) was converted to f_h to get a global comparison. These results are shown in Figure 25 and the average, maximum, and minimum relative errors between CFD calculations and experimental data are listed in Table 10.

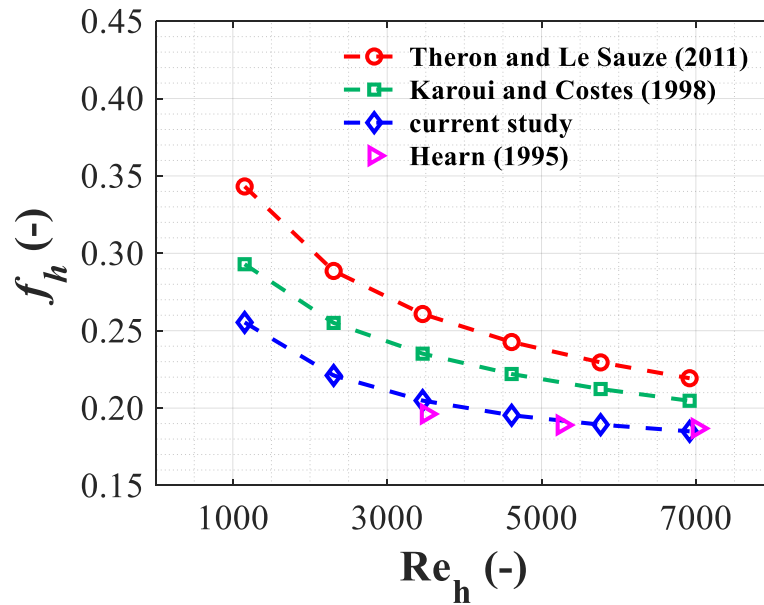


Figure 25 Comparison of SMV hydraulic Fanning friction factor obtained in this study to the literature data

It can be discerned from Figure 25 and Table 10 that the CFD results compare well with the available literature data where a maximum relative error of 25.6% was recorded at $Re_h=1150$. The best fit was obtained with the data of Hearn (1995) where the average and maximum relative errors were found to be 1 and 2%, respectively, over the complete range of Re_h (i.e., 3500-15,450) that was considered in the study of Hearn (1995). The observed discrepancies could be attributed to differences in the roughness of the material of construction used in the different studies (Theron, 2009). Theron and Le Sauze (2011), used a stainless steel mixer whereas plexiglass was employed in the work of Karoui and Costes (1998). In the current work, the roughness was neglected and this could be the reason behind the low values of f_h when compared to the work of Theron and Le Sauze (2011).

Table 10 Average, maximum and minimum % relative error between the measured f_h and the available literature data For SMV

	% relative error (f_h)		
	Average	Max	Min
Hearn (1995)	1.40	1.90	1.06
Karoui and Costes (1998)	11.92	13.83	9.64
Theron and Le Sauze (2011)	20.52	25.60	15.64

To assess the effect of the number of mixing elements on the pressure drop ΔP , and the pressure drop per unit element, ΔP_e , were plotted against Re_{pipe} for a 2 and a 4-element mixer in Figure 26a and b, respectively. It can be clearly noticed that the number of elements has almost no effect on ΔP_e in the SMV mixer. This observation is in line with the findings of Karoui and Costes (1998) who reported that ΔP_e is the same for 1, 2 and 3 elements. However, it should be mentioned that Theron and Le Sauze (2011) claimed that the number of elements affects ΔP_e up to 10 mixing units beyond which ΔP_e becomes constant. The authors calculated ΔP_e for 5 elements and found it greater than that using 10 elements and attributed this to the entrance effect that could not be ignored when a small pipe diameter of 9.45 mm was used. This effect was not observed in the current study nor in that of Karoui and Costes (1998) possibly because larger diameters of 16.7 mm and 50 mm, respectively, were investigated.

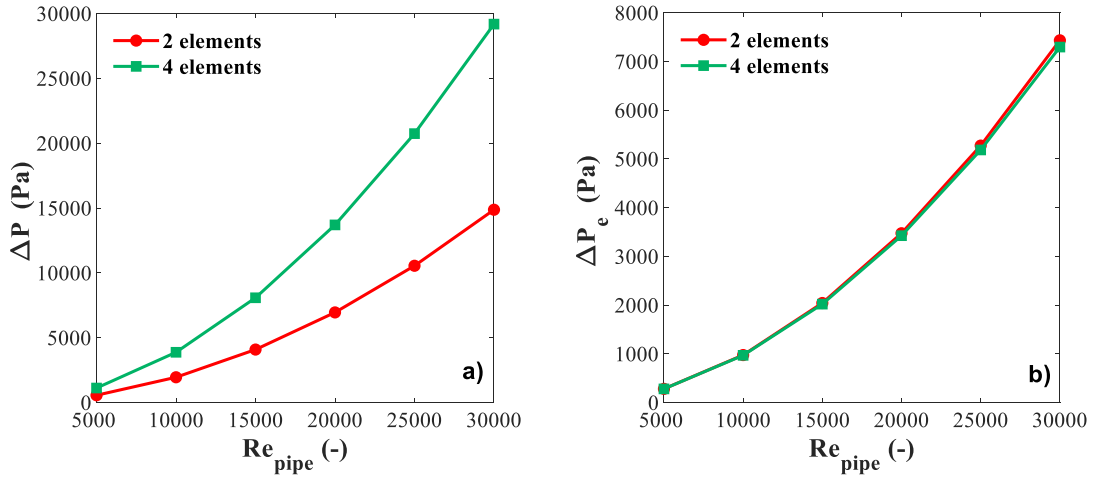


Figure 26 Pressure drop (a) ΔP across the whole length of the mixer and (b) per 1 element (ΔP_e) for 2 and 4-elements SMV mixers versus Re_{pipe}

6.1.2 Pressure and Velocity Distributions

The axial variation of pressure in a 4-element SMV mixer at $Re_{pipe}=30,000$ is depicted in Figure 27. One case is represented here since the patterns are qualitatively similar for the tested Re_{pipe} numbers. It can be noticed that, unlike the Kenics mixer, the pressure losses in SMV are not concentrated at the interface between two consecutive elements (cf. Figure 13), but rather they are evenly distributed along the length of the mixer. This could be attributed to the complex and “crowded” structure of an SMV mixer where two adjacent sheets intersect at various locations. This could further confirm the previous observation where ΔP_e was found to be independent of the number of mixing units.

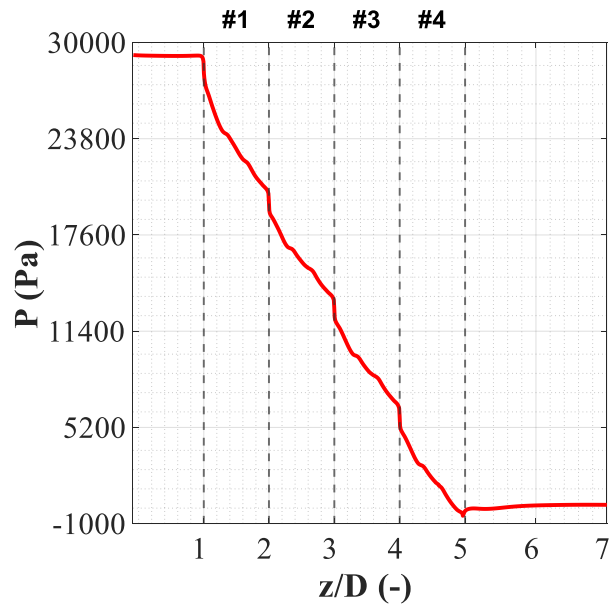


Figure 27 Axial distribution of static pressure in a 4-element SMV mixer at $Re_{pipe}=30,000$

Figure 28a, Figure 28b represent the contour plots of the radial velocity and the axial velocity overlaid with the resultants of the tangential and radial velocity components over various planes normal to the flow direction within the 2nd mixer element in a 2-element mixer. It should be mentioned that the axial positions of these planes are normalized and represented by L_2^* which is calculated based on Eq.(31) with $n = 2$.

When the fluid hits the first element, it is divided into many substreams. Each stream then crosses separately a horizontal channel. Inside these channels, the flow is diverted in opposite directions following the inclination of the folded edges in the adjacent layers as indicated by the positive and negative values of the radial velocities in Figure 28a (cf. the stratified streamlines in Figure 28b). This promotes the radial distribution of the flow and consequently affects the radial mixing within a channel.

Figure 28b also reveals the development of vortices in the wake region behind the touching points of two adjacent layers. This is further illustrated by the high vorticity values that prevail in these regions as indicated by the vorticity contours represented in Figure 28c. For example, one can notice that a set of vortices are present at $L_2^* = 1/4$ at the same locations where the sheets meet at $L_2^* = 0$. These vortices are convected along the mixer length where they either merge with the vortices generated at the subsequent touching points or dissipate. The same streamlines shown in Figure 28b were colored by the axial vorticity and depicted in Figure 50. The latter reveals the formation of clockwise vortices that are assigned with a negative value of axial vorticity and colored by blue in addition to counterclockwise ones (colored by red and assigned with positive values) which reflects the complexity of the flow inside the Sulzer SMV mixer. The formation of streamwise vortices was already reported in the literature in the study of Lang et al. (1995) which suggests that these structures are behind the enhanced performance of the Sulzer mixer.

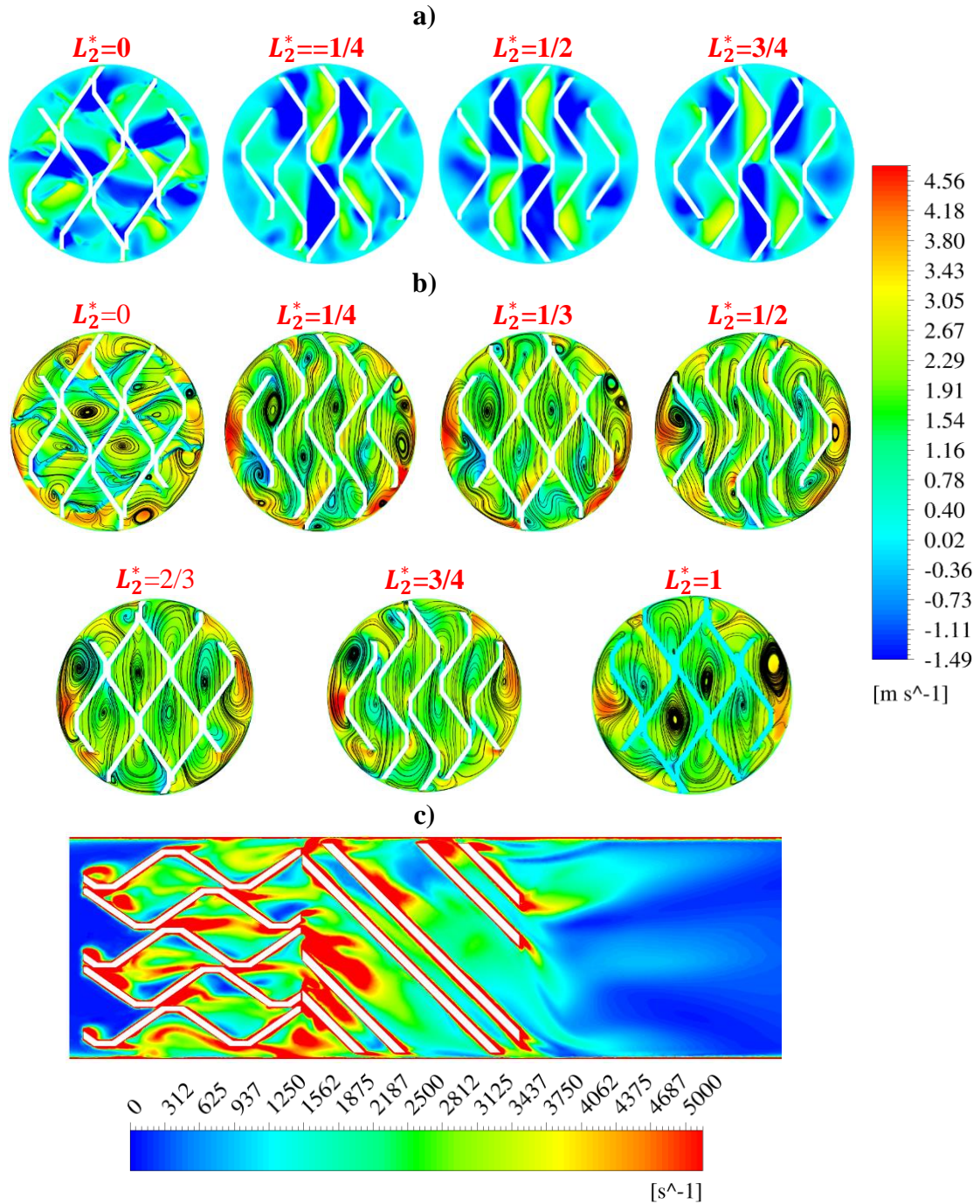


Figure 28 Velocity field through an SMV mixer at $Re = 30,000$: (a) contour plots of the radial velocity, (b) resultants of the radial and tangential velocity components (2D streamlines) superimposed on the contour plots of the axial velocity at various axial locations within the 2nd SMV unit, and c) vorticity contour over the longitudinal plane located at $r/R = 0.4$.

Figure 29a and Figure 50b describe the motion of the fluid downstream of the last mixing element. It can be noticed that the flow is highly chaotic downstream of the mixer ($d^*=0.5$) where distorted counterclockwise and clockwise vortices are present in the core region of the mixer and two other smaller clockwise vortices are found near the wall of the pipe. These vortices were either created in the mixing section and advected by the flow or developed in the wake region of the blunt body. This chaotic behavior is further revealed by the highly distorted axial velocity profile at $d^*=0.5$ and shown in Figure 29b. In this figure, high values of the axial velocity can be observed near the tube wall since a fluid bypass takes place in this region. This is due to the inherent geometry of the SMV mixer where two adjacent sheets do not have the same length.

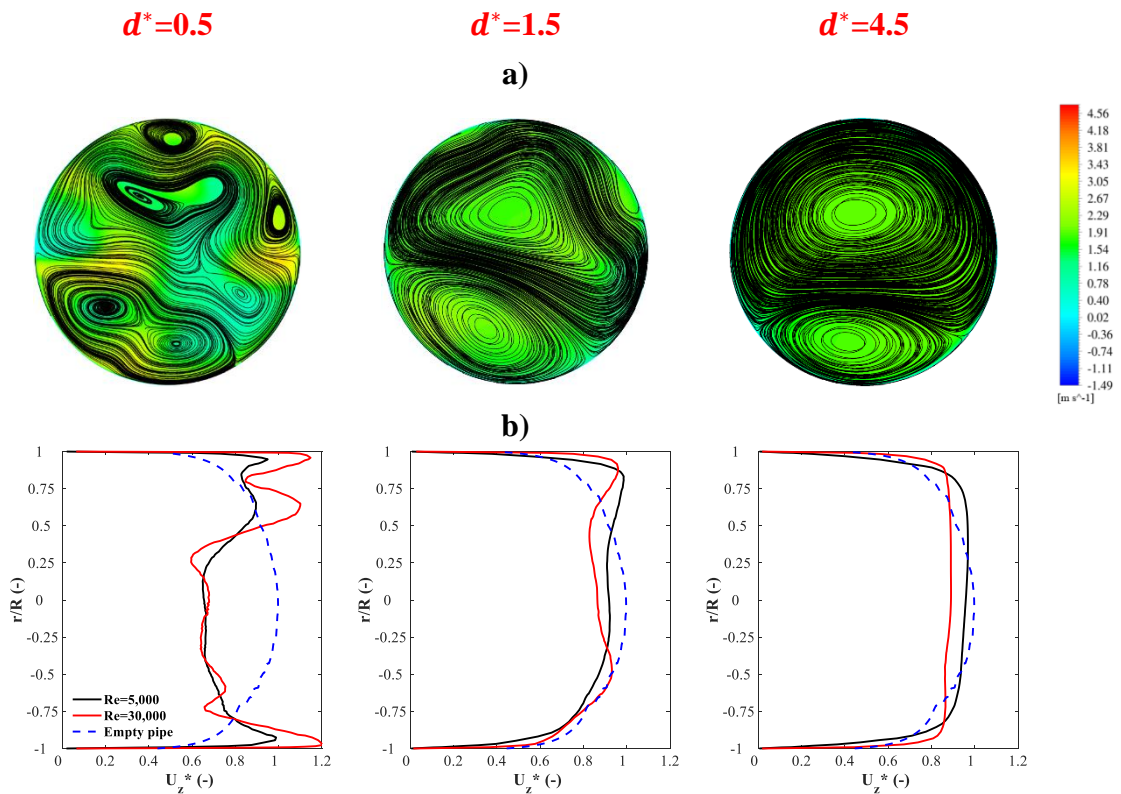


Figure 29 a) Axial velocity contour plots overlaid by the tangential and radial velocity components at $Re=30,000$ and b) normalized axial velocity profiles at different axial positions downstream of the last mixing element in a 2-SMV mixer at $Re=5,000$ and $30,000$

Further downstream, the small clockwise vortices dissipate and the larger ones coalesce to give rise to one large and one small counter-rotating structures that now cover the entire cross-section of the pipe and persist even after $4.5D$ downstream of the last mixing element. This further explains the slow recovery of the fully-developed turbulent velocity profile in the downstream pipe section, with the recovery being slower at higher velocities. It is also worth noting that these vortices are swirling in opposite directions which inhibits their coalescence and leaves them to dissipate as their magnitude decreases the further they flow (cf. Figure 50b).

The analysis of the velocity fields therefore revealed important features about the flow through an SMV mixer. These features are summarized below and their effects on the mixing performance of this unit will be discussed in Section 6.2:

- i. The flow through an SMV mixer is continuously divided due to the complex structure of the mixer where stacked sheets intersect at different locations
- ii. The radial distribution of the flow is promoted due to the relative position of two adjacent sheets that divert the flow in opposite directions
- iii. Swirling structures and vortices are created behind the touching points of two adjacent layers and in the wake of the mixing body which further promotes the radial distribution of the flow
- iv. The complex swirling structures are advected by the flow and prevail over extended distances downstream of the mixing section which delays the re-establishment of the fully-developed velocity profile.

6.2 Mixing Efficiency

In the following sections, the dispersive and distributive behavior of the Sulzer SMV mixer is qualitatively and quantitatively assessed based on different parameters namely, the extensional efficiency, CoV , the aerial distribution and the M parameter.

6.2.1 Dispersive Mixing: Extensional Efficiency

The axial variation of the area-weighted average extensional efficiency for 4 SMV elements at different Re_{pipe} is depicted in Figure 30 and an illustration of its distribution at different planes normal to the flow direction at $Re_{pipe}=30,000$ is shown in Figure 31.

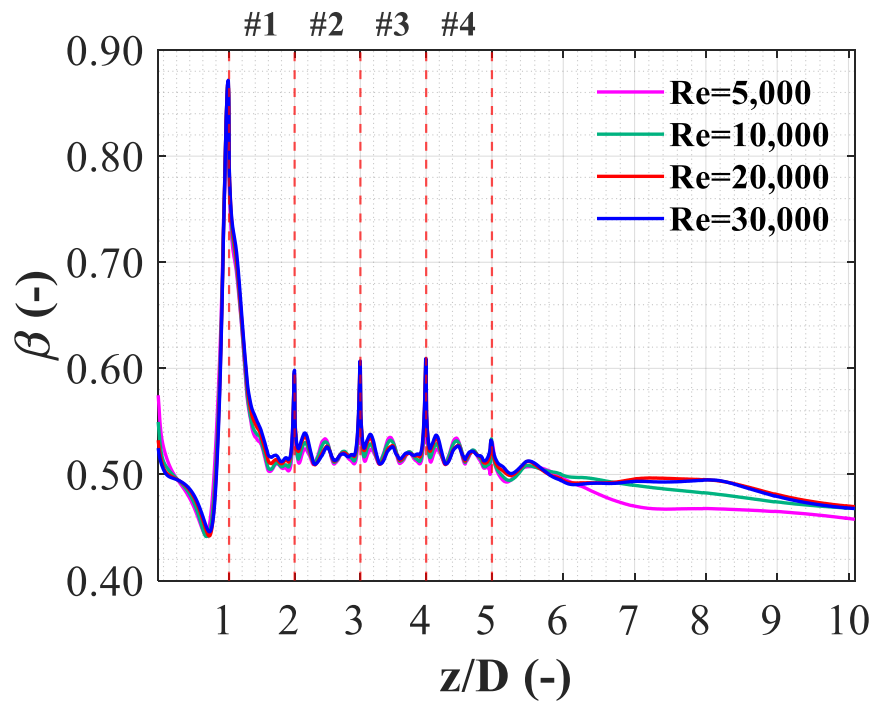


Figure 30 Axial variation of the extensional efficiency for a 4-SMV mixer at various Re_{pipe}

One cannot but notice that the velocity has almost no impact on the dispersive behavior within the mixer as reflected by Figure 30 which reflects patterns that are quantitatively and qualitatively the same. This observation is further confirmed by the average values of β displayed in the rectangular boxes in Figure 51 and that show almost no variation in the value of β . β reaches its highest value at the entrance of the 1st mixing unit since the fluid is subject to elongation as it crosses the narrow channels of SMV (cf. the contour plot at $L_1^* = 0$ in Figure 31). The value of β then starts to decrease until the flow reaches the second element beyond which the pattern becomes repetitive. At the entrance of the 2nd and subsequent elements, less pronounced peaks of magnitude 0.6 are observed and this is further illustrated in Figure 31, where at $L_2^* = 0$ the highest values of β are only seen around the sharp edges and the touching point of the plates. Within the elements, the value of β is close to that of a shear flow. This was expected since the flow within the elements undergoes simultaneous rotation and elongation under the effect of the developed vortices and as it crosses the narrow passages formed by two adjacent sheets, respectively (cf. Figure 29b).

As the fluid leaves the mixing section, a gradual decrease in the value of β (< 0.5) is observed, however, a value of 0.5 was never reached even at the exit of the investigated pipe. This further confirms the slow recovery of the fully-developed flow described in Section 6.1.2 and is due to the rotational nature of the flow downstream of the mixing elements. A purely rotational flow is characterized by a β that approaches 0.

The contour plots of the downstream region in Figure 31 show that just downstream of the last mixing element at $d^*=0.5$, regions with high values of β are present indicating that the fluid particles are still being elongated as they exit the mixer.

This is expected since, in this region, the axial velocity profiles were distorted and hence velocity gradients are large (cf. Figure 29b). It can also be noticed that further downstream, red and yellow blobs that reveal that highly dispersive regions coexist. These blobs are located at the same region between the two large swirling structures reported in Figure 29a. This indicates that the fluid is being squeezed and deformed by the two counter-rotating vortices. The presence of regions where β approaches 0 in the downstream section can also be observed notably at locations $d^* \geq 3$. These regions indicate areas where the fluid elements are being rotated.

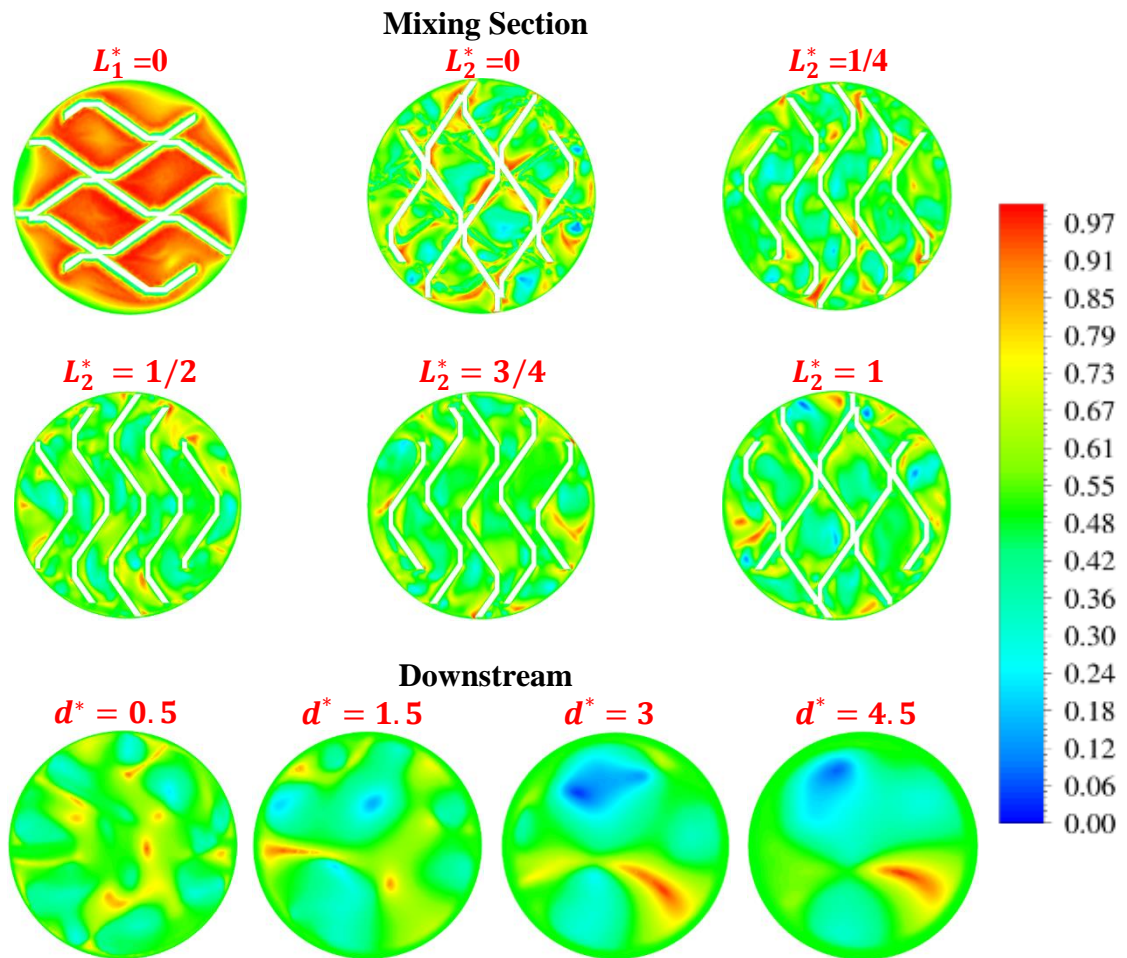


Figure 31 Contour plots of extensional efficiency at different locations through the SMV static mixer at $Re_{pipe}=30,000$

6.2.2 Distributive Mixing: Coefficient of Variation and Aerial Distribution

The axial variation of CoV for 2 and 4 elements is shown in Figure 32a,27b, and the distribution of the mass fraction of the tracer at $Re_{pipe}=5,000$ and $Re_{pipe}=30,000$ are displayed in Figure 33.

As can be seen from Figure 32, the fluid exits the first mixing element partially mixed with a CoV of approximately 55% and 47% at $Re_{pipe}=5,000$ and 30,000. This slightly enhanced efficiency at higher velocities exists because the particles inside the separate channels are mixed by convection rather than diffusion. Consequently, the mean radial velocities created by the deviation of the flow in opposite directions and the transverse flow created by the induced vortices are responsible for this behavior. The effect of radial mixing can be clearly discerned in Figure 33 at the exit of the first element where horizontal mixed layers are observed. The next element is rotated by 90° so that the homogenization occurs in the vertical direction.

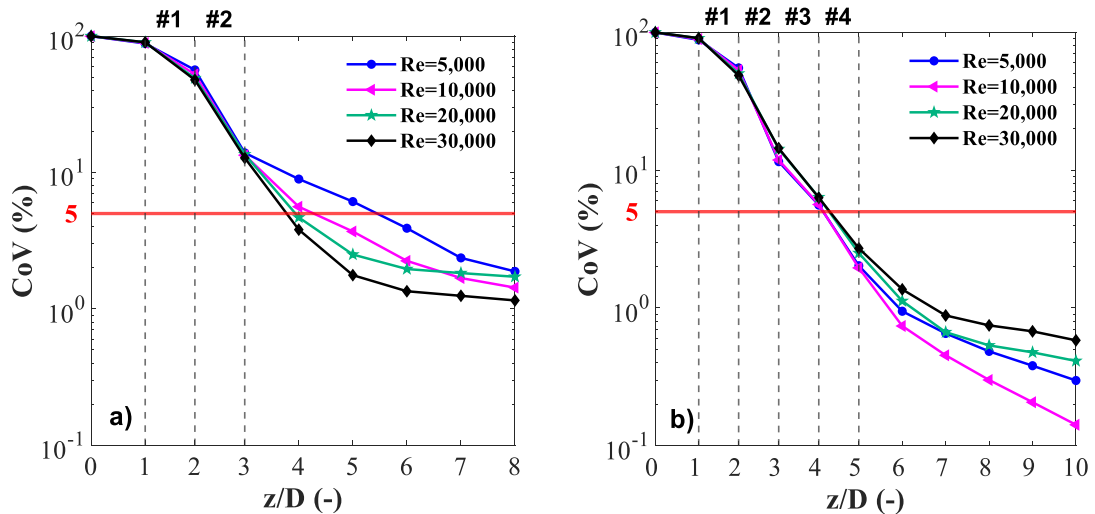


Figure 32 Axial Variation of CoV in a SMV mixer comprising a) 2 b) 4 units at different Re numbers

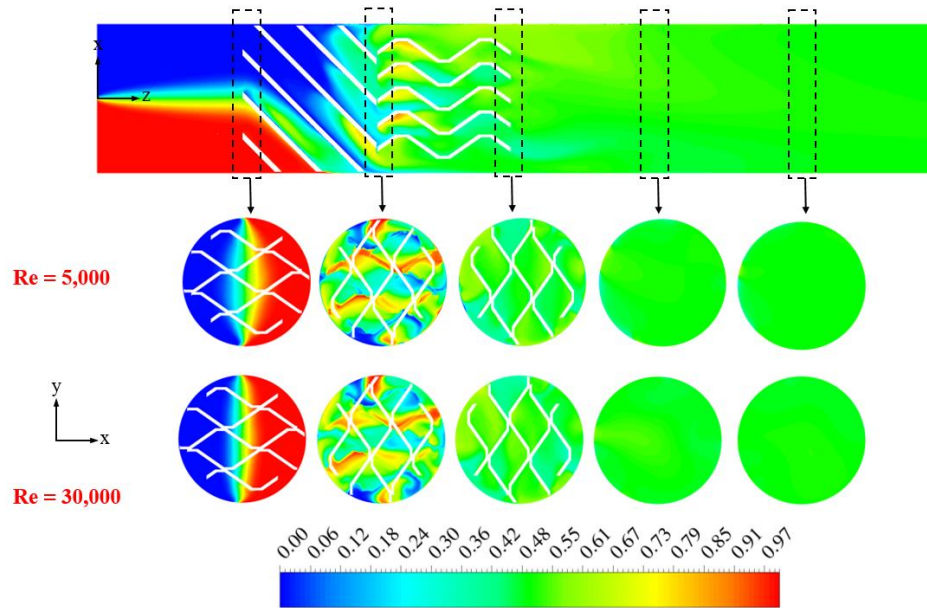


Figure 33 Contour plots of the mass fraction of the secondary fluid in an SMV mixer comprising 2 elements for $Re=5,000$ and $Re=30,000$

At the exit of the mixing section, the CoV continues to drop under the influence of the increased intensity of turbulence (Karoui et al., 1998) and the transported vortices, the desired degree of homogeneity (i.e., $CoV < 5\%$) is achieved after 1D for $Re_{pipe} > 5,000$ and after 2D otherwise when 2 elements are used. When considering the 4-element configuration, a CoV value that is slightly larger than 5% was reached at the exit of the 3rd element before it drops to $< 5\%$ after the 4th element for all the Re values. These findings can imply that the use of 2 elements (with an additional empty pipe stretch downstream) may be deemed sufficient to achieve a good degree of mixing without the need for the added operational cost that would arise by inserting additional mixing units. The results are further confirmed by the aerial distribution bar graphs represented in Figure 52 in Appendix 2. These plots clearly shows that downstream of the mixing section, the homogeneity is drastically improved after 1-2D of the mixing section for the 2-element configuration at both Re number, whereas a fully-

homogeneous system is obtained directly at the exit of the mixing section of the 4-element configuration.

The effect of the flow velocity on the CoV at the outlet of the mixing chamber for a 2- and 4-element mixer configuration is represented in Figure 34. It should be mentioned that the mixing chamber also comprises a $5D$ empty pipe section downstream of the last mixer. Figure 34 shows that the CoV values are quasi-constant and fluctuate between 1 and 2% when Re_{pipe} varies between 5,000 and 10,000 in the 2-element configuration. The CoV at the exit of the mixing chamber of the 4-element configuration seems to drop between $Re_{pipe} = 5,000$ and 10,000 before increasing again beyond $Re_{pipe} = 10,000$. However, this effect can be neglected as in this case, the CoV varies between 0.14 and 0.58% at $Re = 10,000$ and 30,000 respectively.

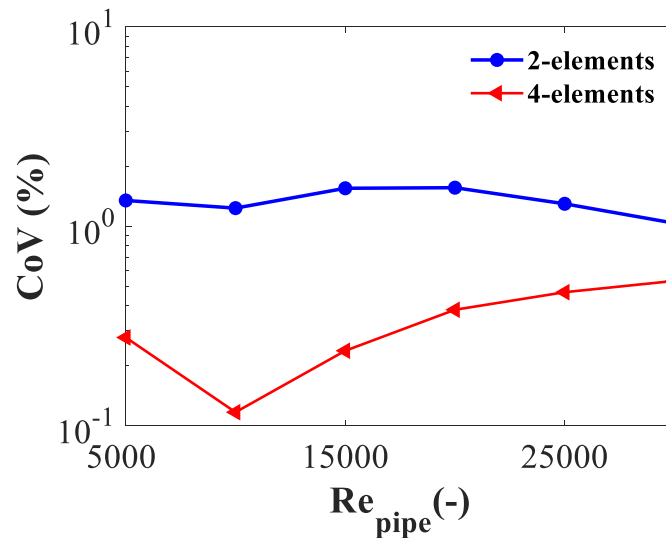


Figure 34 Variation of the CoV at the exit of the mixing chamber of SMV with Re_{pipe}

6.2.3 M-Number

To further assess the effect of the number of elements and the flow velocity on the mixing performance of an SMV static mixer, the M number was evaluated at a plane

located at 4D downstream of the last mixing element and its variation with Re_{pipe} is represented in Figure 35.

It can be easily discerned from Figure 35 that a 2-element configuration is more efficient than a 4-element configuration since higher M numbers are obtained. This is due to the fact that the former configuration can achieve a fully-mixed system at lower energy losses.

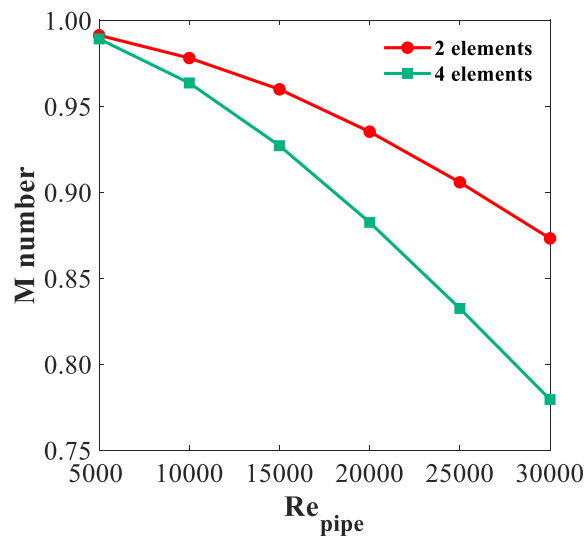


Figure 35 SMV M-number variation with Re_{pipe}

CHAPTER 7

NEW VARIANT OF SCREEN-TYPE STATIC MIXER: HYDRODYNAMICS AND MIXING EFFICIENCY

7.1 Hydrodynamics and Model Validation

In this Chapter, the hydrodynamics of the single-phase flow through a novel hybrid static mixer that consists of an arrangement of alternating screen-type static mixers and inserts is characterized, and its impact on the mixing efficiency is investigated in Section 7.2. Due to the large computational cost imposed by the presence of plain woven meshes that requires high levels of refinement, the analysis was restricted to 4 elements. For this purpose, the simulations were carried out at 4 different Re_{pipe} numbers spanning a range between 5,000 and 30,000 and corresponding to Re_h of 179 and 1,072.

7.1.1 Pressure Drop and Model Validation

Because of the lack of experimental data for the newly proposed geometry, the pressure drop values across the screens alone were used to validate the ability of the model to correctly predict the flow behavior through the novel mixer. For this reason, the hydraulic Fanning friction factor was computed according to Eq (32) and compared against the available literature data:

$$f_h = \frac{\Delta P_s \phi^2 D_h}{2\rho \bar{u}^2 L} \quad (32)$$

In the above equation, L is the screen thickness and is equal to $2b$ (Azizi, 2019), and $D_h = 0.36124 \text{ mm}$. The overall pressure drop across a tubular reactor/contactor equipped with STSM results from the frictional losses induced by the fluid as it crosses the screens besides the losses generated at the tube wall (Habchi & Azizi, 2018). Therefore, the pressure drop, ΔP_s , across one screen can be calculated as follows:

$$\Delta P_s = (P_i - P_o) - \Delta P_{empty} \quad (33)$$

Typically, in mixers that only comprise STSM, P_i and P_o are the area-weighted average static pressures at the inlet and outlet of the mixing section, respectively, and ΔP_{empty} is the pressure drop across an empty pipe of the same length as the static mixer. However, in the current study, since the mixer comprises additional inserts that are placed at a distance of $0.5D$ downstream from the center of the screens, P_i and P_o were evaluated at two planes located at $0.25D$ upstream and downstream of the center of the screen, respectively.

Quantifying the pressure drop across STSM has been one of the main aspects tackled in the studies related to flow through screens. Hence, pressure drop measurements and a couple of correlations can be found in the literature. However, the values of the hydraulic Fanning friction factor computed in the current study were compared against only the correlation of Azizi (2019) represented in Eq (34), and the results are shown in Figure 36:

$$f_h = \frac{22.97}{Re_h^{0.8011}} + 0.3079 \quad (34)$$

The latter correlation was used solely because it allows a ‘universal’ comparison with the literature data. The author derived it using data that covers 60 different screen geometries and a wide range of flow conditions ($Re_h = 27-7600$) and tested it against a

total of ~700 experimental data points that were either obtained in his study or extracted from the literature. However, the author claimed that a deviation of $\pm 30\%$ should be always expected when employing this correlation. To account for this, two dashed lines representing these limits were plotted on Figure 36.

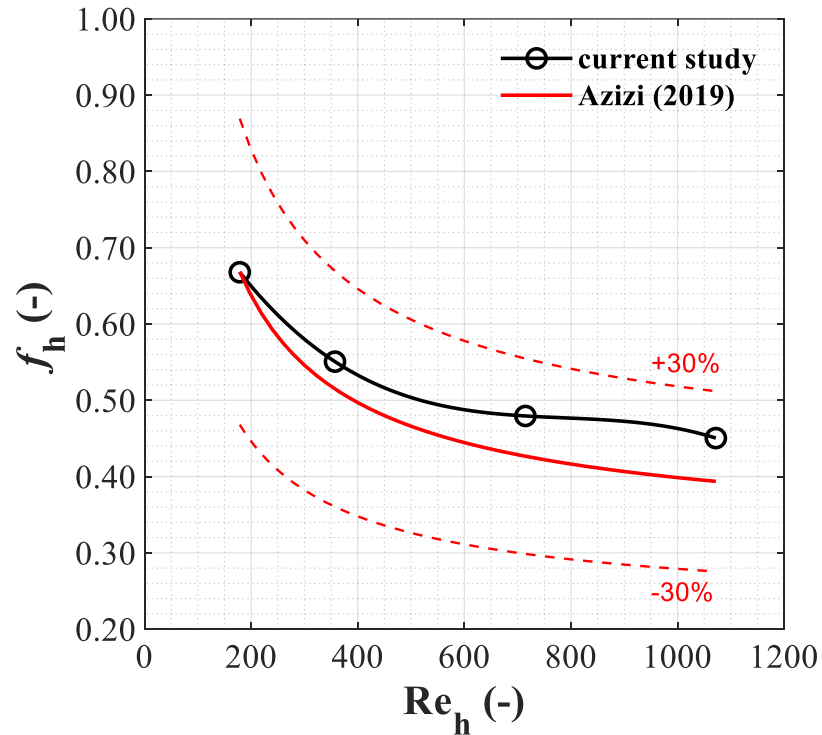


Figure 36 The Fanning Friction factor of the screens alone compared to the correlation of Azizi (2019)

It can be clearly discerned from Figure 36 that simulated data compare well with the correlation of Azizi (2019) with the average and maximum relative errors being 8.5 and 14.4%, respectively.

7.1.2 Pressure and Velocity Distributions

The axial distribution of the area-weighted average static pressure along the mixer length is plotted in Figure 37a. The axial position was rendered non-dimensional by dividing by the tube diameter such that $L^* = (Z - 1)/D$. The grey dashed lines indicate the axial position of the screens centers whereas the red dash-dotted lines point to the positions of the leading and trailing edges of the inserts. From this figure, the repeatability of the pressure profile along the mixer length can be clearly discerned and one can conclude that the pressure losses are “uniformly” distributed across the mixer. A close-up on the region around the 3rd mixing unit limited by the green dashed rectangle is shown in Figure 37b. This figure clearly shows the major pressure losses and recovery regions as the fluid passes through the screen and/or inserts.

Accordingly, the pressure profile in Figure 37 can be divided into 4 main regions:

1. A region of pressure loss around the screens: The pressure drops significantly in this region. This drop is a result of the flow accelerating as it enters the apertures of the screens because of the sudden reduction in the effective flow area. This is further illustrated by the high-velocity jets that emerge in this region as represented by the contour plots of the axial velocity in Figure 38.
2. A region of pressure recovery downstream of the screens: As the fluid exits the screens, it starts to gradually decelerate as the individual jets start to coalesce. However, this is not sufficient to fully recover the lost pressure as is obvious in Figure 37b and commonly agreed upon in the literature. The pressure starts

plateauing after a very short distance from the center of the screens and extends up to the entrance of the flaps.

3. A region of pressure loss along the length of the flaps: Again as the fluid passes through the narrow throat of the flaps or the constricted regions between the flaps and the wall of the pipe, the pressure steadily decreases until reaching their trailing edges. The same explanation adopted in region 1 applies here.
4. A region of pressure recovery downstream of the flaps: At the exit of the flaps, the pressure starts to increase but in a slower fashion compared to that observed in region 2. This slow recovery is due to the behavior of the jets leaving the flaps. This could be perfectly discerned in Figure 38, where the flow downstream of the flaps is not entirely decelerating unlike the jets leaving the screens in a parallel and similar fashion. While the part of the fluid that is leaving the throat of the flow starts decelerating, the parts confined between the wall of the pipe and the trailing edges of the inserts start accelerating which slows down the pressure recovery. The pressure recovery is further hindered by the presence of the screens downstream of the flaps.

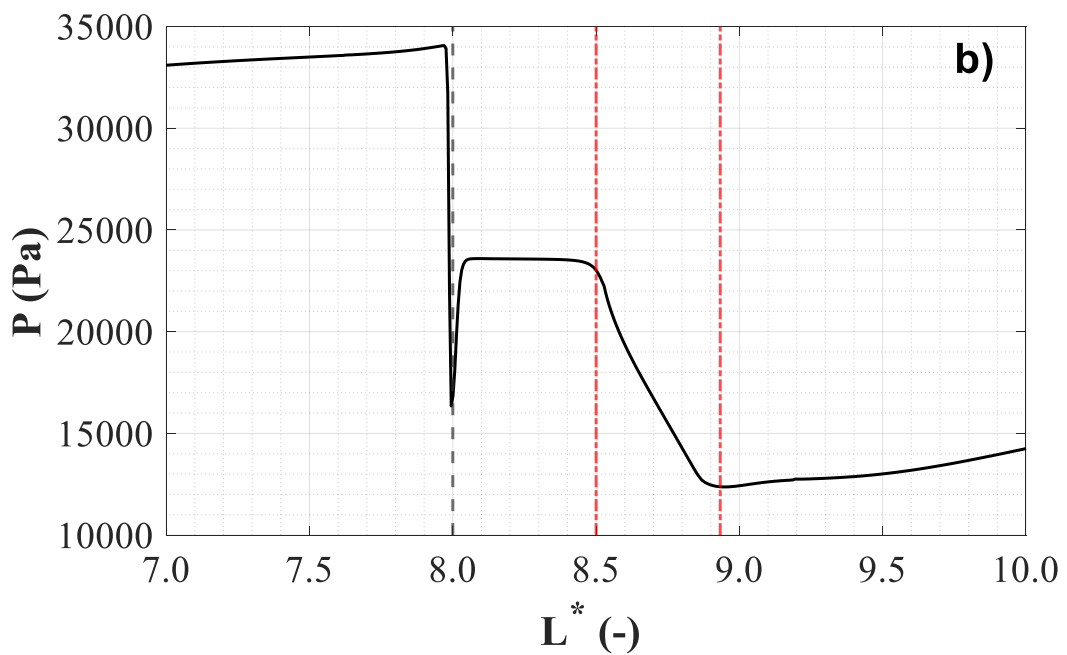
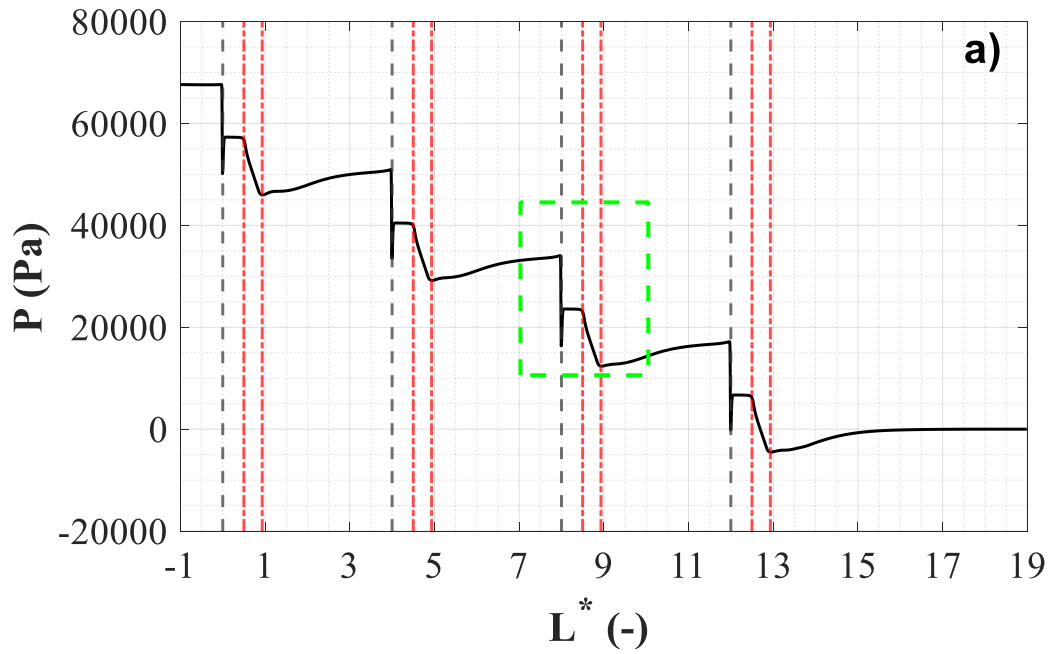


Figure 37 Axial distribution of the area-weighted average static pressure (a) along the complete new mixer length, and (b) zoomed around the 3rd screen and inserts.

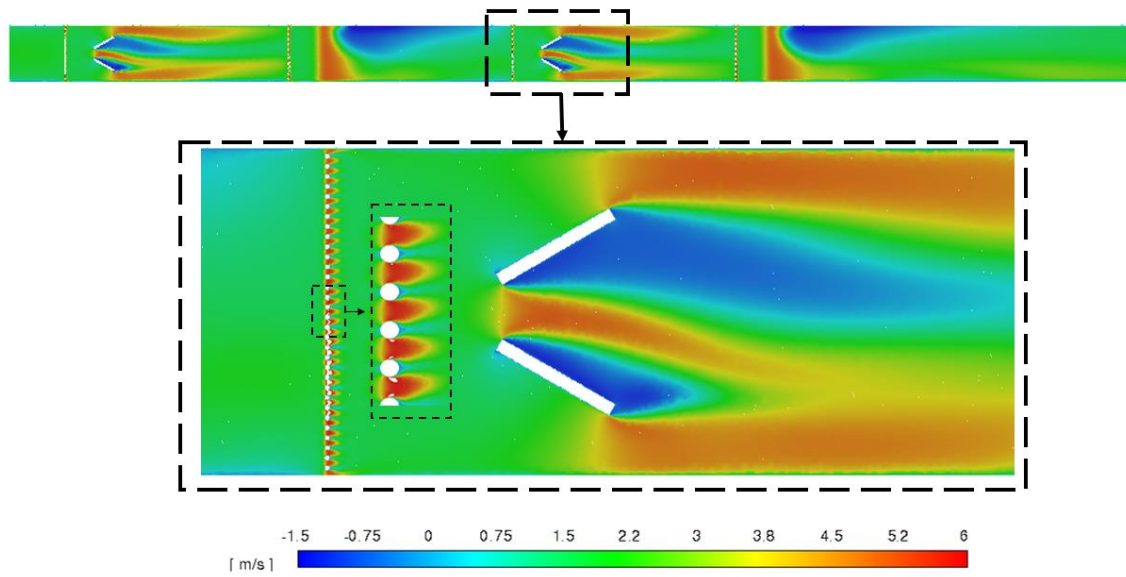


Figure 38 Axial velocity contour plot at the central yz plane of the new mixer at $Re_{pipe}=30,000$

7.2 Mixing Efficiency

7.2.1 Dispersive Mixing: Extensional Efficiency

Figure 39a represents the axial variation of the area-weighted average extensional efficiency for the novel geometry of STSM at various Re_{pipe} values. One cannot but notice that repeatable patterns are obtained for the 4 tested cases which suggests that the dispersive behavior within the mixer is “uniform”. Moreover, it can be clearly seen that these patterns are quantitatively and qualitatively the same for all the tested Re numbers except for $Re_{pipe}=5,000$.

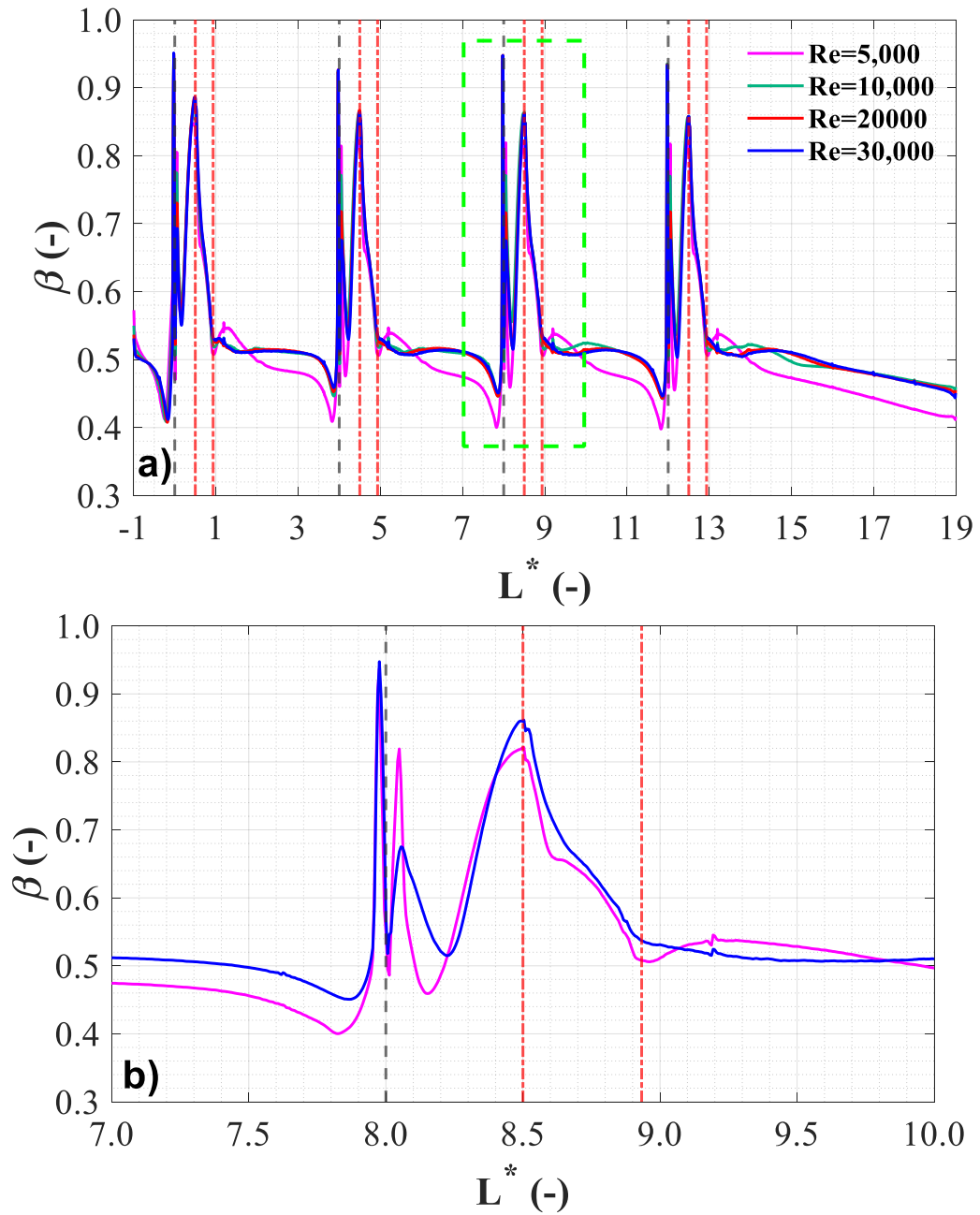


Figure 39 Axial variation of the extensional efficiency for 4 mixing elements of the new mixer a) at various Re_{pipe} , b) zoomed around the 3rd hybrid element

To better analyze these profiles, a close-up view of the region near the 3rd mixing element as well as the 3rd screen alone are depicted in Figure 39b. The plots for $Re_{\text{pipe}} = 10,000$ and $20,000$ were omitted from the figure since no considerable

difference was noticed at these 2 Re numbers and the 3rd screen was used as a representative unit.

Three major peaks can be clearly discerned from Figure 39b: two sharp ones around the screen and a broader one spanning the region occupied by the flaps. It can be clearly discerned that β decreases before it hits its highest value ($\beta \cong 0.95$) just upstream of the screen center for both Re numbers. This is due to the rotation of the fluid elements before being elongated as they enter the screen apertures (Azizi et al., 2022). The rotation is more pronounced at $Re_{\text{pipe}} = 5,000$ than $Re_{\text{pipe}} = 30,000$, probably because at lower velocities, the flow has more time to rotate.

As the fluid crosses the screen, the flow attempts to revert back to a simple shear flow (i.e., $\beta = 0.5$) before peaking again downstream of the screen. This new elongation/stretching region most probably coincides with the location of coalescing jets as they exit the woven mesh. One can clearly observe that the location of this downstream peak shifts to the right as Re increases, which might further explain the fact that at larger velocities, the individual jets exiting the screen require a longer distance before they coalesce again. The value of β then decreases again to ~ 0.5 before increasing again as the fluid prepares to enter the constricted space between the inserts downstream of the screen. The extensional efficiency reaches a new maximum value of $\beta = 0.85$ at the leading edge of the inserts beyond which it starts to gradually decrease towards its 0.5 value at the trailing edge. Due to the fact that fluid elements accelerate to pass through the narrow space between the leading edges of the inserts, and this acceleration continues in the near-wall regions where the available flow area diminishes as the fluid nears the trailing edges of the inserts, the high β value are maintained over the complete length of these inserts.

Downstream of the trailing edge of the flaps, the value of β drops gradually to reach 0.5 and maintains this quasi-constant value until it approaches the following mixing element and a similar trend restarts.

These results clearly show that the dispersive behavior of the woven meshes is further enhanced by the use of these inserts.

7.2.2 Distributive Mixing: Coefficient of Variation and Aerial Distribution

Distributive mixing was studied by analyzing the evolution of both the coefficient of variation and aerial distributions in the current mixer. The axial variation of the CoV along the mixer length as well as the effect of changing Re_{pipe} on its value at the outlet of the pipe are depicted in Figure 40a, Figure 40b, respectively. The dotted red lines are placed at $2D$ downstream of the center of each screen, i.e. $\sim 0.85D$ from the trailing edges of the flaps and midway between two consecutive screens.

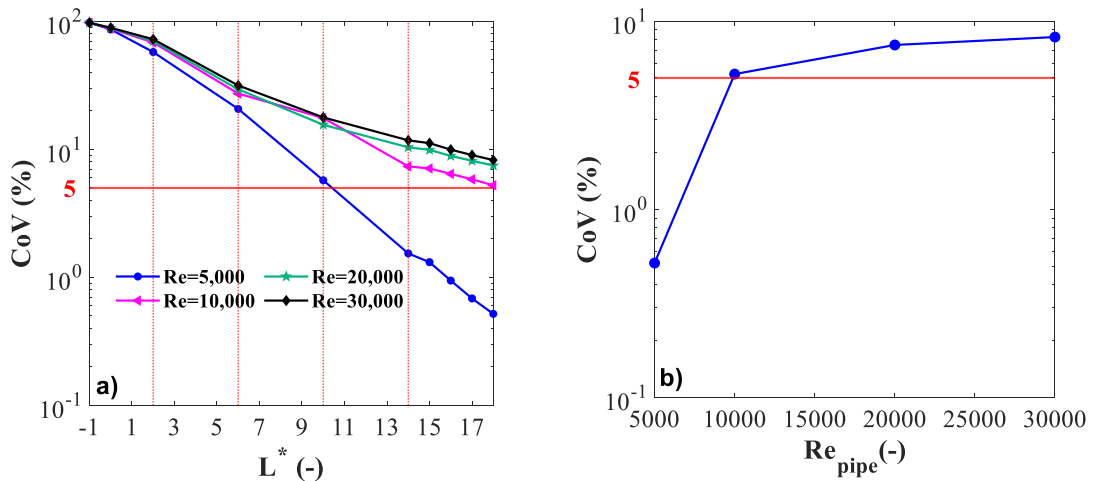


Figure 40 Axial variation of CoV in 4 mixer elements of the new mixer a) along the mixer length b) at the exit of the mixing chamber at various Re_{pipe}

The evolution of the aerial distributions are also shown in Figure 41 at different axial locations for $Re_{pipe} = 5,000$ and $30,000$. In these plots, SF_x stands for the axial position of a plane that is similar to that of the red dotted lines placed on Figure 40a, i.e. SF1 stands for the midway plane between the 1st and 2nd screens, etc.

As can be discerned from Figure 40a, the flow velocity has a great impact on the distributive mixing in the novel geometry. However, this impact weakens at $Re_{pipe} > 10,000$. In fact, at lower velocities, the fluid particles reside for a longer period inside the mixer and therefore have more time to interact with each other. This effect could be further illustrated in Figure 40b, where an increase from ~ 0.35 to 7.5% in the CoV value at the outlet of the mixing chamber is noticed when Re_{pipe} increases from $5,000$ to $30,000$.

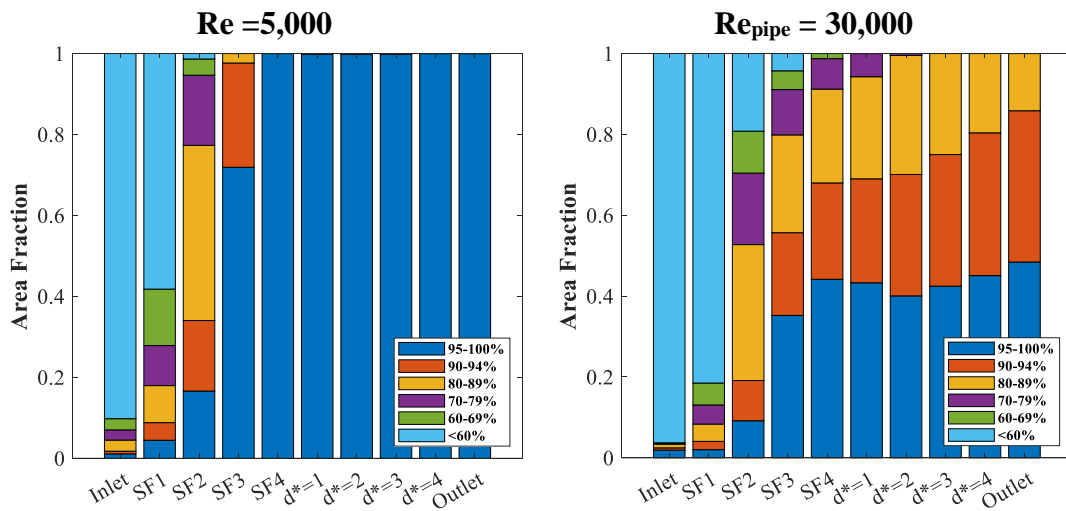


Figure 41 Discrete distribution of the aerial distribution of the mass fraction of the tracer in the new mixer at $Re_{pipe}=5,000$ and $Re_{pipe}=30,000$

From the current data, it can be deduced that the first element does not significantly improve the homogeneity of the mixture as indicated by the high values of

CoV. This is also reflected by the aerial distribution of the mass fraction at SF1, where less than 5% of the entire cross-section is fully-mixed, i.e. has an intensity of mixing $\geq 95\%$ at the reported Re_{pipe} . As the fluid travels further downstream in the pipe, the *CoV* keeps on dropping until reaching a value of $\sim 6\%$ and the homogeneity improves dramatically after $3D$ at $Re_{\text{pipe}} = 5,000$ (cf. Figure 41, SF3 at $Re_{\text{pipe}} = 5,000$). This is expected since the flaps, in two adjacent elements are rotated by 90° to each other so that the flow is alternately diverted in the horizontal and vertical directions. Consequently, the radial distribution of the tracer elements is improved. This effect, however, diminishes at higher Re numbers where lower *CoV* values are obtained at the exit of the mixing section.

Downstream of the last mixing element and at $Re_{\text{pipe}} = 30,000$, the *CoV* continues to drop but in a slower fashion as indicated by the aerial distribution where a slight variation in the mixing efficiency after SF₃ is observed. In general, the distributive mixing is improved because of the presence of the flaps and not the screens. Since these flaps are spaced, one therefore can expect their effect to be concentrated in their vicinities. This observation clearly indicates the need for optimizing and matching the geometry of the mixer to the flow conditions. For example, a longer insert and/or longer inter-mixer spacing might be required at higher Re values to obtain more efficient distributive mixing.

7.2.3 M-Number

The *CoV* results analyzed in the previous section are further confirmed in Table 11 where the M parameter, along with ω_{max} , ΔP , *CoV* and the *CoV* in an empty pipe, CoV_{pipe} , of the same geometrical aspects as the mixer are listed.

As can be seen, the M -number decreases as Re_{pipe} increases similarly to CoV . For instance, the novel mixer is $\sim 98\%$ as efficient as an ideal mixer at $Re_{\text{pipe}}=5,000$, whereas this efficiency drops to 59% at $Re_{\text{pipe}}=30,000$. This is expected since a better homogeneity is achieved at lower energy cost at lower Re numbers (cf. columns 3 and 5 in Table 11). However, as suggested by the authors (Medina et al. (2019)), one should also take the value of ω_{max} into account as it reflects how much potential is left for the mixer to improve the efficiency of the system. In the current study, the values of the latter parameter are extremely low even at the highest Re number and show that most of the work is actually done by the empty pipe instead of the static mixer, even though the values of CoV_{pipe} show the opposite, especially for the highest flow conditions. It is worth mentioning that these results are obtained for a pipe length of $19D$ and according to the literature an empty pipe of $100\text{-}200D$ length is required to achieve a fully-mixed system (Karoui et al., 1998; Lang et al., 1995; Paglianti & Montante, 2013). Therefore a $\omega_{\text{max}}= 4.7\%$ seems to be not reasonable and the M -number cannot be relied on for an accurate evaluation of the mixing efficiency. Therefore, this parameter will not be used later to compare the performance of the three mixers.

Table 11 ω_{max} , ΔP , M parameter, CoV and CoV_{pipe} at $4D$ downstream of the mixing chamber for the modified geometry of STSM

Re_{pipe}	ω_{max}	ΔP (Pa)	\mathcal{M} number	CoV (%)	CoV_{pipe} (%)
5,000	0.047	2,438	0.976	0.68	25
10,000	0.034	8,473	0.889	5.84	22
20,000	0.115	30,886	0.742	8.15	39
30,000	0.254	66,846	0.593	9.04	56

CHAPTER 8

COMPARISON BETWEEN THE THREE STATIC MIXERS INVESTIGATED IN THIS STUDY

In this chapter, the performance of Kenics, SMV, and the modified screen-type static mixer is compared from both a mixing and energy efficiency perspectives. For this purpose, all the configurations studied in the previous chapters were considered and compared based on pressure drop, CoV , and extensional efficiency. To reduce the clutter, the various mixer configurations were renamed based on their geometry and the number of elements. For example, 6-Kenics stands for a Kenics mixer that consists of 6 elements, etc... All the configurations have a diameter $D \sim 16.5 \text{ mm}$ and comprise a $5D$ empty pipe stretch downstream of their mixing sections.

8.1 Pressure Drop

The pressure drop across the various geometries is plotted in Figure 42a at different pipe Reynolds numbers. Accordingly, the following observations can be deduced accordingly:

1. When the performance of the 4-element configurations (i.e. 4-Kenics, 4-SMV and 4-Screens) is compared, it can be clearly discerned that for all the tested Re values, the pressure losses across the novel geometry are the highest and those generated by Kenics are the lowest. The pressure drop values across the 4-STSM mixer are ~ 1 and 3 times higher than those generated by the mixers comprising the same number of units of SMV and Kenics, respectively. One may at first attribute these huge discrepancies to differences in the lengths of the three

geometries, i.e. $L_{4-Kenics} = 197$ mm, $L_{4-SMV} = 158$ mm and $L_{4-NM} = 330$ mm.

However, it is not the case because the novel hybrid geometry, unlike the two others, does occupy a small fraction of the total length of the housing and the losses generated across the empty pipe, in this case, are negligible compared to those induced by the static mixer itself.

2. The pressure drop across the new mixer geometry is substantially impacted by the geometry of the screens. Accordingly, the use of a lower solidity woven mesh would therefore positively impact the pressure losses across this mixer.
3. The pressure drop values across SMV are greater than those generated by Kenics even though the former geometry is more compact in size, where an SMV element is ~ 1.5 times shorter than a Kenics one. In fact, the pressure losses across any SMV configuration, are on average one time higher than those across a configuration containing the same number of Kenics mixers over the tested Re range. One is also referred to Table 12 that summarizes the main results of this investigation.

These observed differences could be attributed to differences in the void fractions of the various geometries. The screens alone have the lowest void fraction ($\phi = 0.61\%$) compared to SMV ($\phi = 0.86\%$) and Kenics ($\phi = 95\%$). Flows are more hindered in volumes with high solidity, i.e., low ε , and result therefore in higher pressure drops which explains the observed trends.

For a fairer comparison, the pressure drop across a static mixer could be expressed in terms of a dimensionless quantity such as the drag coefficient, K . The latter coefficient is equivalent to the ratio of total pressure drop across a static mixer to the

dynamic pressure of the fluid flowing through the mixer (Azizi, 2019; Habchi & Azizi, 2018):

$$K = \frac{\Delta P}{\frac{1}{2}\rho u^2} \quad (35)$$

In other words, it is the ratio of the pressure forces to the inertial forces and it measures the resistance of the flow. The drag coefficient was calculated based on the pressure drop for one mixing unit and plotted for the different designs in Figure 42b. It can be clearly discerned that Figure 42b confirms the previous observations where the novel geometry seems to generate the highest pressure losses among all the designs followed by the screens, then SMV and finally Kenics.

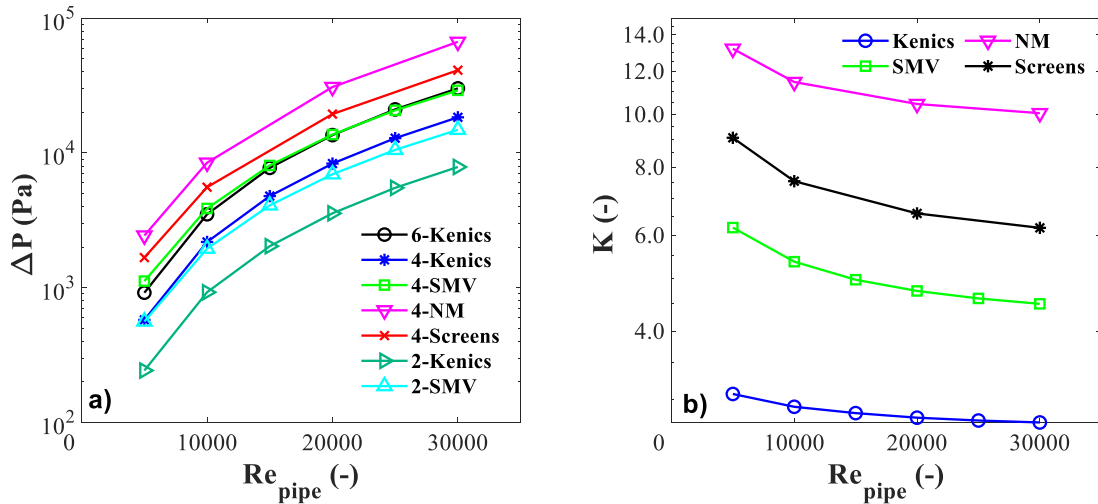


Figure 42 Pressure losses across the investigated geometries at different Re_{pipe} (a) in terms of pressure drop ΔP across the entire volume, and (b) in terms of drag coefficient (K) for one mixing unit

8.2 Mixing Performance

In chapters 4, 5 and 6 four parameters, namely the extensional efficiency, the coefficient of variation, the aerial distribution and the M -number, were employed to characterize the mixing efficiency of each design. Since the aerial distribution rendered results that are similar to CoV while the M -parameter proved to be not reliable, the comparison of the mixing efficiency was based here on only the extensional efficiency and the coefficient of variation.

8.2.1 Extensional Efficiency

In order to compare the dispersive behavior of the three investigated geometries, the axial variations of the area-weighted average extensional efficiency of the 4-unit configurations were overlaid on the same plots in Figure 43 for the two extreme Re values. To accomplish this, the axial position for each mixer was rendered non-dimensional by dividing by the length of one mixing element such that $Z^* = \frac{z-D}{L_e}$ where $Z^* = 0$ coincides with the axial position of the leading edges of the 1st elements in Kenics and SMV and the center of the 1st screen in the novel mixer geometry. The element length, L_e , is taken as the inter-screen spacing in the novel geometry to account for the downstream effect of the screens and the inserts. Grey dotted lines pointing to the entrance and exit of the mixing units and green solid lines indicating the value of a shear flow (*i. e.* $\beta = 0.5$) are also plotted on the same figure.

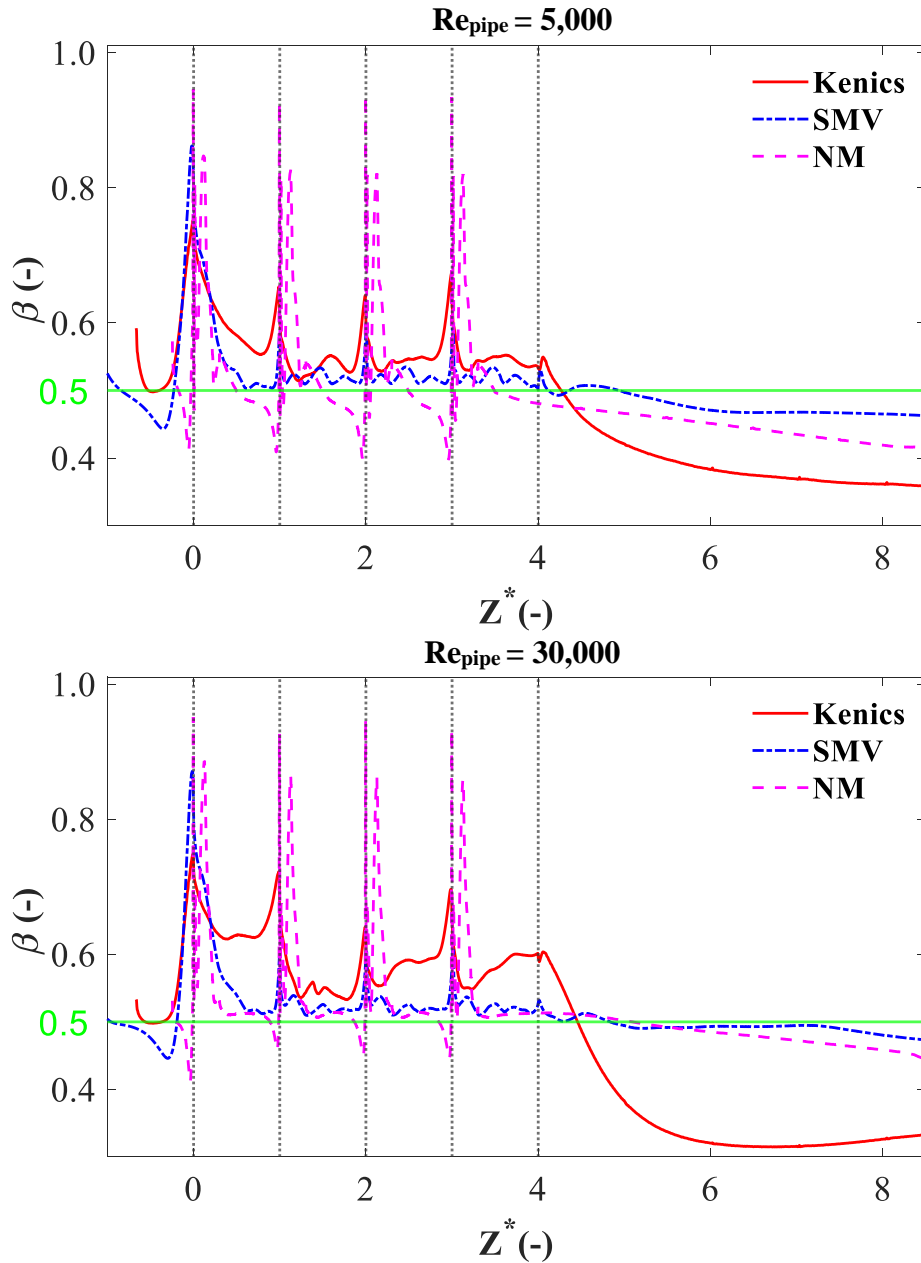


Figure 43 Axial distribution of the area-weighted average extensional efficiency for Kenics, SMV and the novel geometry of screen-type static mixer at $Re_{\text{pipe}} = 5,000$ and $30,000$

These plots show that both Kenics and SMV feature a major peak of magnitudes of 0.75 and 0.88, respectively, at the inlet of the mixing sections and less pronounced ones at the entrance of the subsequent elements and whose magnitudes are slightly higher for Kenics ($\beta \sim 0.7$ and 0.6 for Kenics and SMV, respectively). Nevertheless, the

novel mixer shows a different trend since repetitive patterns with three major peaks prevailing around the screen-inserts regions can be observed (cf. Figure 39 for a close-up view around the peaks). The highest peak of magnitude ~ 0.95 is encountered just before the entrance of the screens and the two slightly less important ones are found at a very short distance downstream of the woven meshes and at exactly the leading edges of the inserts ($\beta \sim 0.8$ and 0.85 , respectively).

Elsewhere within the mixing units, the extensional efficiency values are the highest for Kenics and this observation is more pronounced at higher Re values as indicated by the profile at $Re_{\text{pipe}} = 30,000$ compared to that at $Re_{\text{pipe}} = 5,000$. However, for SMV these values slightly fluctuate and approach the value of a shear flow with almost no noticeable variations at the various displayed Re cases. As for the novel geometry, the flow within the mixing unit downstream of the trailing edges of the inserts is highly dependent on the fluid velocity as it becomes highly rotational at lower velocities upstream of the wire meshes. This is due to the fact that the flow is not continuously within the mixer boundaries but it flows in an empty pipe and needs to rotate before it flows through the approaching screen (cf. Section 7.2.1). Downstream of the mixing sections, the values of β drop in all the configurations but in a more pronounced fashion in Kenics especially at the highest Re number.

One can therefore conclude that the three configurations exhibit excellent dispersive behavior at their leading edges while the best results are being achieved by the novel geometry followed by Kenics and then SMV even though SMV shows better performance than Kenics at the entrance of the mixing section. The addition of the inserts in the hybrid geometry rendered the mixer more dispersive as revealed by the enhanced values of β that are no longer limited to the near screen regions, however they

now prevail over a larger region that extends up to the trailing edges of the inserts. Similarly, the fluid particles in Kenics, precisely at high Re values, are subject to continuous deformation and elongation as they flow over the twisted tapes as indicated by the relatively high values of β covering larger regions of the mixer compared to SMV. In the latter mixer, the highly dispersive regions are limited to the entrance and transition zones between consecutive elements. However, one should always recall that the average values of β may mask sometimes the presence of highly-dispersive regions. This is for example highlighted by the contour plots of the extensional efficiency revealing regions with high values of β at the interface between the counter-rotating pair of vortices downstream of the mixing section of SMV (cf. Figure 31).

The observed distinct patterns of β are attributed to the different flow patterns induced in these three geometries. In short, the highly dispersive regions corresponding to high values of β in Kenics are mainly encountered in the regions of flow reversal and high velocities prevailing in approximately the first 1/3 length of the element, however they prevail in the confined and high-velocity regions of the screens and SMV.

The extensional efficiency results were further quantified in Figure 44a and 44b that depict the volumetric cumulative distribution of the extensional efficiency for the different geometries at $Re_{\text{pipe}}= 5,000$ and $30,000$, respectively. This representation allows a more comprehensive comparison of the dispersive efficiency of the various geometry (Haddadi et al. (2020)). The ordinate values represent the percent of the entire mixer volume that has an extensional efficiency greater than or equal to the values indicated by the corresponding abscissa.

It can be clearly noticed from the above graphs that the extensional efficiency is higher than 0.4 in the entire volume of the novel geometry and SMV but in only ~ 70% of the Kenics mixer for both Re values. This shows that the flow is more rotational in Kenics than in the two other geometries. For $\beta \geq 0.5$, the percent cumulative volume of SMV is always lower than that of the two other geometries at both Re values which suggests that SMV is less dispersive than the two other geometries under the tested Re range. This is expected because extensional flows in SMV coexist only around the walls of the channels and in the narrow passages between the corrugated sheets (cf. Figure 31). Nevertheless, rotational flows ($\beta < 0.5$) predominate elsewhere, i.e. inside the open channels and downstream where vortices are found.

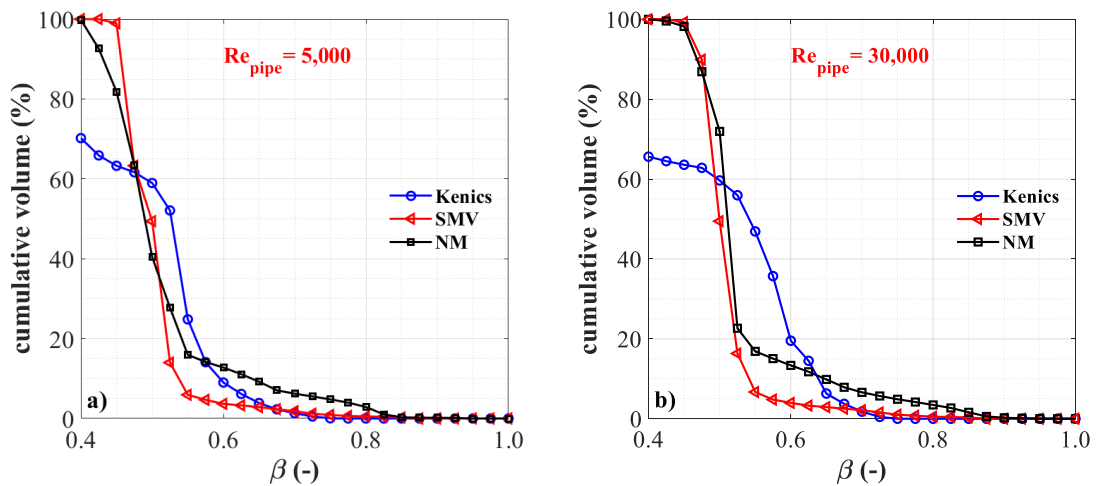


Figure 44 Volumetric cumulative extensional efficiency for the different designs at (a) $Re_{pipe} = 5,000$ and (b) $Re_{pipe} = 30,000$ over the entire mixing chamber

On the other hand, one can notice that for $0.5 < \beta < 0.64$ the curve of Kenics at $Re_{pipe} = 30,000$ always lies above those of the novel geometry with 40% of the entire volume of Kenics is being covered with $0.52 < \beta < 0.64$, whereas this same range of β is encountered in only 5% of the novel geometry volume (Figure 44b). Values of $\beta >$

0.64 are more frequent in the new mixer than in Kenics where they cover 10% of the entire volume of this new geometry at both Re_{pipe} .

The analysis of these graphs might be confusing at first because it undervalues the dispersive capabilities of the STSM that proved to be perfect for dispersions and drop breakup and coalescence according to the literature (Azizi & Al Taweel, 2011). One, however, should always recall that the novel geometry, as opposed to the two other designs encloses large empty sections dominated by rotational flow which might be affecting the results. For a fair comparison, the same graphs shown in Figure 44 are now reproduced to cover only the region of the mixers occupied by the mixing units, and the results are depicted in Figure 45.

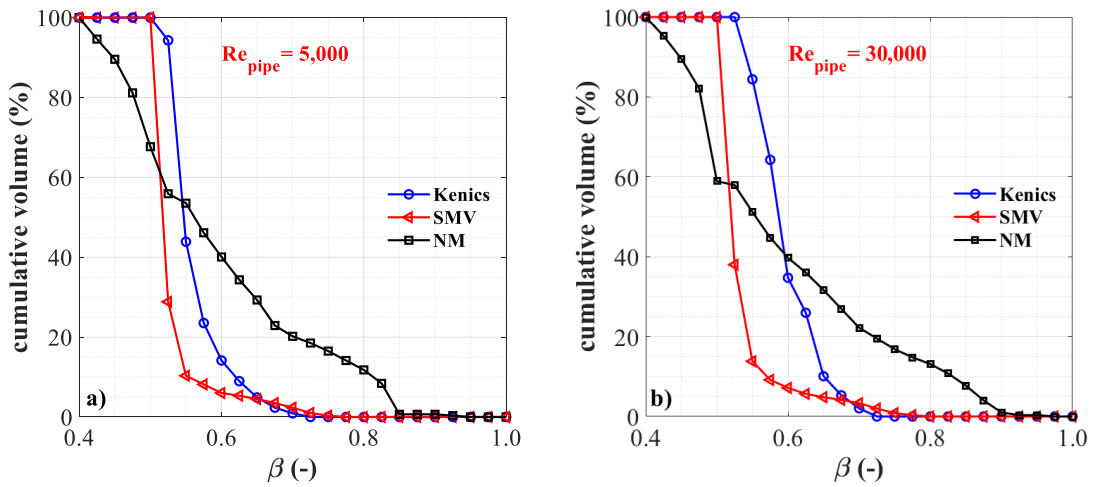


Figure 45 Volumetric cumulative extensional efficiency for the different designs at (a) $Re_{pipe} = 5,000$ and (b) $Re_{pipe} = 30,000$ over the regions of the mixers occupied by the mixing units.

The graphs in Figure 45 perfectly show that the optimized geometry of the STSM outperforms its two counterparts in terms of dispersive behavior, since for high values of β (*i.e.* $\beta > 0.55$ $0.6 < \beta < 1$) the curve of STSM is always on top of the

two others for both Re numbers. However, this outperformance is less important at high Re numbers as can be seen from Figure 45. On another note, it is worth mentioning that the flow conditions seem to only affect the dispersive behavior of Kenics where better efficiency is realized at the highest Re value.

8.2.2 CoV

To compare the distributive efficiency of the three designs, the variation of the CoV at the outlet of the mixing chambers for the various configurations over the tested Re_{pipe} range is depicted in Figure 46. First of all, it can be clearly seen that at $Re_{pipe} = 5,000$, all the mixers exhibit perfect mixing ($CoV \leq 5\%$). Beyond this Re value, the various configurations reveal distinct behaviors.

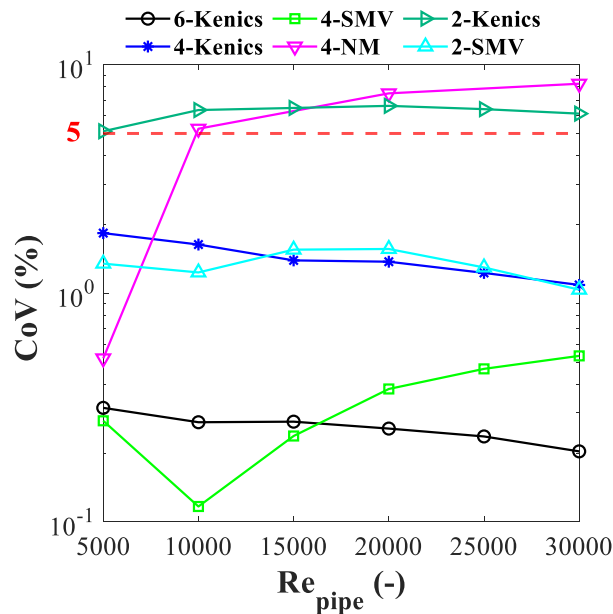


Figure 46 CoV at the exit of the mixing chamber for the various configurations versus Re_{pipe}

In the new mixer, the distributive mixing efficiency seems to diminish with an increase in Re_{pipe} where the CoV values increase from ~ 0.5 to 8% as Re_{pipe} increases from 5,000 to 30,000. This is expected since at low velocities, the fluid particles have more time to change their spatial location which confirms the ascending trend of CoV as

Re increases. This trend was also observed in the 4-SMV (for $Re_{\text{pipe}} > 10,000$) and the 2-Kenics configurations. In reality, the CoV values, for all the geometries except for the novel one, are quasi-constant over the tested Re range, and values $< 5\%$ were already reached in all the geometries except for the novel geometry and the 2-Kenics mixer (cf. Table 12).

The improved distributive mixing efficiency of SMV and Kenics compared to the novel geometry can be attributed to them being prevalent over the total length of the mixer, as opposed to the novel geometry where two consecutive elements are spaced. The flows in the conventional geometries are constantly split and rerouted and secondary flows that proved to be crucial for the distribution of the fluid particles across the mixers, are continuously induced which fosters the distributive behavior of these mixers compared to the novel geometry. However, for the same number of units, SMV results in lower CoV values than Kenics. This could be attributed to the inherent geometry of SMV which encloses corrugations and folded plates that imposes longer paths for the particle to cross.

On another note, the 4-Kenics mixer and the 2-SMV mixers have comparable distributive performances as they show almost no differences in their CoV values that fluctuate around the value of $CoV = 1.5\%$ over the tested Re range. In general, the 6-Kenics mixer achieved the lowest CoV values over the entire Re range, however could be compared to the 4-SMV mixer as they were both able to reduce the CoV to values less than 0.5% .

8.2.3 Global Comparison

To perform a global comparison between the considered cases, the CoV at $5D$ downstream of the mixing section for each configuration was plotted against the pressure drop for that respective geometry at the tested Re values in Figure 47.

It can be noticed that the novel geometry is the least efficient geometry at high velocities in distributive mixing as revealed by the combined high CoV and ΔP values at high Re . On the other hand, the 2-SMV and the 4-Kenics mixer present the optimal solution for the distributive mixing problems. When these two configurations are compared to the 4-SMV and the 6-Kenics mixers, one can notice that the mixing efficiency in these two mixers is slightly improved, but this improvement was counterbalanced by high-pressure drops. For instance, at $Re = 10,000$, the CoV values at the outlet of 2-SMV, 4-Kenics, 4-SMV, and 6-Kenics are 1.23, 1.63, 0.12, and 0.27%, respectively whereas the pressure drops were approximately twice lower in the first geometry. This slight decrease in the CoV at the cost of excessive energy consumption is irrelevant since a value of $CoV < 5\%$ is deemed acceptable for most industrial applications. As for the 2-Kenics mixer which is twice more energy efficient than the 2-SMV mixer, the CoV values at its outlet fluctuate around 5-6%. This suggests that this configuration could be used as an effective alternative for the proposed geometries if a long empty tube section is added downstream.

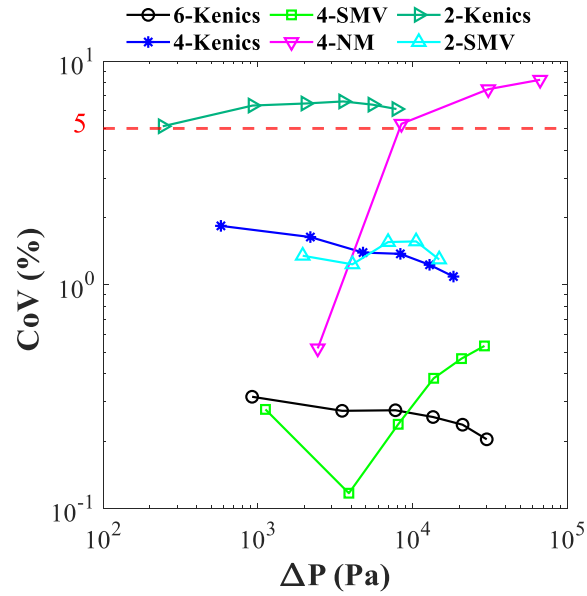


Figure 47 CoV of the various configurations versus the pressure drop they generate

To further highlight the differences between the three geometries from an energy efficiency perspective, the *CoV* was plotted against the amount of energy input per unit volume volume (E_v) in Figure 48 where E_v is computed as follows (Al-Hassan et al., 2021):

$$E_v = \frac{\Delta P \times Q}{V} \quad (36)$$

Where ΔP is the total pressure drop across the mixer (*kPa*);

Q is the volumetric flow rate (m^3/s);

V is the total volume of the mixer (m^3);

It can be clearly discerned that Kenics has the best performance among the three geometries since it can achieve the desired degree of homogeneity at low energy expenditure. At low Re numbers, SMV and the novel geometry exhibit almost similar performance however the novel geometry has the advantage of improving the dispersive mixing at the same time.

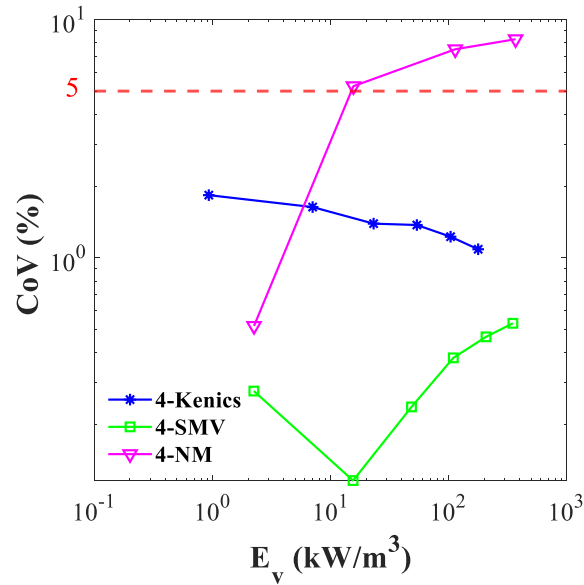


Figure 48 CoV of the different mixers versus the amount of the energy input in unit time and unit volume

Table 12 Table summarizing the results of ΔP , β and CoV for the various configurations investigated in the current study

	2-Kenics			2-SMV			4-Kenics			4-SMV			4-NM			6-Kenics		
	<i>L = 147 mm</i>			<i>L = 128 mm</i>			<i>L = 197 mm</i>			<i>L = 158 mm</i>			<i>L = 330 mm</i>			<i>L = 246 mm</i>		
Re_{pipe}	ΔP (kPa)	β_{avg} (-)	CoV (%)	ΔP (kPa)	β_{avg} (-)	CoV (%)	ΔP (kPa)	β_{avg} (-)	CoV (%)	ΔP (kPa)	β_{avg} (-)	CoV (%)	ΔP (kPa)	β_{avg} (-)	CoV (%)	ΔP (kPa)	β_{avg} (-)	CoV (%)
5,000	0.24	0.56	5.11	0.56	0.53	1.35	0.58	0.56	1.83	1.12	0.53	0.28	2.44	0.67	0.52	0.92	0.56	0.36
10,000	0.93	0.57	6.33	1.95	0.53	1.23	2.18	0.57	1.63	3.88	0.53	0.12	8.48	0.69	5.24	3.51	0.57	0.27
15,000	2.03	0.58	6.46	4.09	0.53	1.55	4.78	0.58	1.39	8.08	0.53	0.24	N/A	N/A	N/A	7.76	0.58	0.27
20,000	3.56	0.58	6.60	6.95	0.53	1.56	8.35	0.58	1.37	13.7	0.53	0.38	30.9	0.69	7.49	13.6	0.58	0.26
25,000	5.51	0.59	6.39	10.6	0.54	1.30	12.9	0.59	1.29	20.8	0.54	0.47	N/A	N/A	N/A	21.1	0.59	0.24
30,000	7.87	0.59	6.11	14.9	0.54	1.04	18.4	0.59	1.09	29.2	0.54	0.53	66.9	0.68	8.25	30.2	0.59	0.21

CHAPTER 9

CONCLUSIONS AND RECOMMENDATIONS

In this study the performance of a novel modified geometry of screen-type static (STSM) mixer was compared to two other commercial designs, namely the standard Kenics and the Sulzer SMV mixers. This was undertaken from a hydrodynamics and mixing efficiency perspectives. Various configurations were investigated where the number of mixing units was varied between 2 and 6. For this purpose, 3-dimensional CFD numerical simulations were carried out in Ansys Fluent[®] at different Re_{pipe} numbers ranging between 5,000 and 30,000. The extensional efficiency β was used to assess the dispersive behavior of the investigated mixers, whereas three other parameters, namely the coefficient of variation (CoV) and the aerial distribution of the mass fraction of the secondary fluid in addition to a parameter proposed in the literature known as the M -Number (Medina et al., 2019), were employed to quantify and qualify the distributive mixing of the three considered designs.

The predicted pressure drop across all the designs showed an excellent agreement with the available literature data and correlations. The pressure and velocity fields of the three designs were investigated for each case and the results provided insights into the mixing mechanisms. The transition region in Kenics exhibited flow reversal, boundary layer separation and formation of secondary flow structures that proved to have a great influence on the mixing behavior of this mixer. Formation of vortices at the intersecting points of two adjacent sheets and mean radial velocities were observed in the narrow channels of the SMV mixer and greatly impacted the distributive mixing behavior of this corrugated mixer. The addition of the divergent

inserts to the screen-type static mixer improved the distribution of the fluid elements as they are forced to change their direction periodically.

The comparison of the different designs was based on the pressure drop, drag coefficient (K), β , CoV and the amount of energy input per unit volume (E_v) required by each mixer to overcome the pressure losses across it. The addition of the inserts to the woven wire meshes induces an increase of ~50% in the pressure drop. The new mixer was found to generate 3 and 1.2 times more pressure losses compared to a mixer equipped with the same number of elements of Kenics and SMV, respectively. This was further confirmed by the calculated drag coefficient where the average values over the entire tested Re range were found to be equal to 2.84, 5.06, 7.34 and 11.28 for Kenics, SMV, STSM and the new mixer, respectively.

The comparison of the CoV values at $5D$ downstream of the mixing sections showed a quasi-constant behavior over the tested Re range for all the configurations except for the novel mixer that exhibits an increasing CoV trend with Re . All the mixers showed an excellent distributive mixing efficiency at the $Re_{pipe} = 5,000$ where a CoV of 5% or less was reached. At higher Re values, the novel mixer and the mixer equipped with 2 elements of Kenics ended up with a $CoV > 5\%$. The CoV results of the latter mixer suggested that the addition of a longer pipe stretch may help achieve the desired homogeneity level at lower operating costs. Moreover, it was revealed that 2 SMV and 4 Kenics units are deemed sufficient to achieve the desired homogeneity level and the addition of supplementary units would end up with a negligible increase in the level of mixedness at the expense of additional pressure losses (100% increase in the pressure drop).

The dispersive behavior showed insensitivity to Re numbers through SMV and the new mixer whereas a better performance was obtained through a Kenics mixer at higher flowrates. It was found that the flow is highly dispersive at the entrance and the leading edges of all the mixers, however highly dispersive regions prevail also within the mixing units in Kenics at higher Re numbers. Downstream of the mixing section values of $\beta < 0.5$ were encountered in all the designs. This is due to the presence of rotating structures transported from the mixing section or created in the wake region of the blunt bodies. The addition of inserts in the new mixer had a positive impact on the dispersive behavior of the screens where additional volumes with high β were encountered over the inserts regions. Overall the new mixer exhibited the best dispersive action among all the mixer followed by Kenics and then SMV with an average β of 0.68, 0.57 and 0.53, respectively.

Recommendations:

The current research was limited to numerically investigating the turbulent mixing of miscible liquids of similar physical properties under a Re range between 5,000 and 30,000. Future works may include:

- Conduct experimental work to further validate the obtained numerical results
- Test a wider Re range and including values lower than $Re_{\text{pipe}} = 5,000$ since at low velocities the new mixer exhibited excellent performance.

- Optimize the geometry of the new mixer. A different woven mesh geometry will greatly impact the pressure losses across them. In addition, the impact of changing the divergent angle of the inserts, their thickness, location, and length will also have a major impact on the results.
- Investigate the effect of the fluid density and viscosity on the mixing behavior of the three units since actual industrial processes involve the use of fluid of different properties
- Investigate the effect of the geometric properties (i.e. aspect ratio, thickness of the plate, roughness) on the mixing and energy efficiency of the mixers.

APPENDIX 1

KENICS MIXER

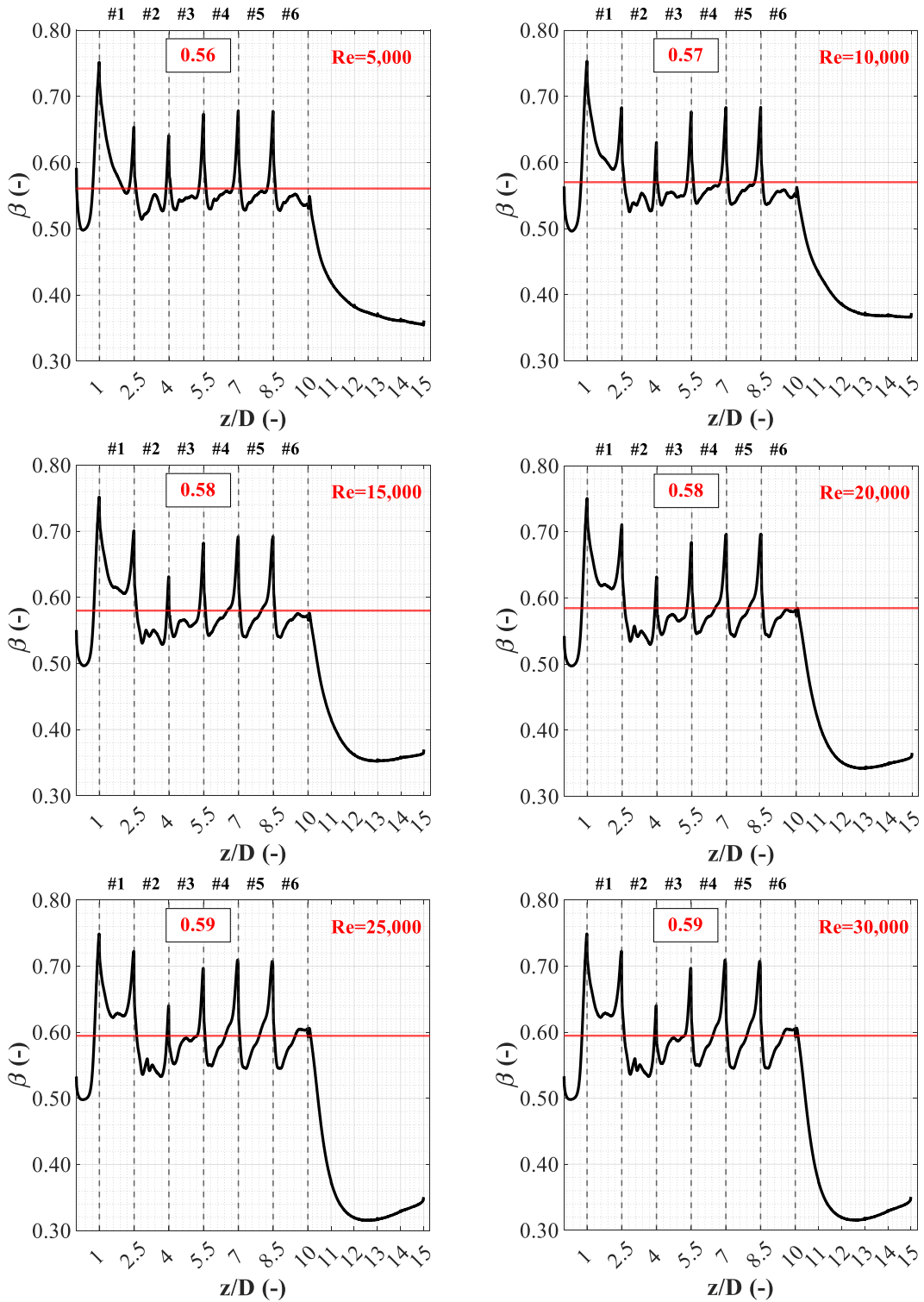


Figure 49 Axial distribution of the extensional efficiency β in kenics containing 6 elements at different Re numbers

The areal distribution MATLAB code

```
% This code plots the bar graphs of the aerial distribution of the mass
% fraction of the secondary fluid
%-----Description-----
% the excel file Kenics-d=16.37-th=1-Aerial_Distribution-Re=30k.xlsx
% contains the mass fraction and the z-area of each cell on the different
% considered cross-sections. it also contains the average mass fraction and
% the total area of the considered cross-section
%-----Remarks-----
%change the Re number in the file's name

%% Clear Data
clear all
close all
clc

%% Read data
Data=xlsread('Kenics-d=16.37-th=1-Aerial_Distribution-Re=30k.xlsx');
j=1;
for i=1:2:14
m(:,j)=Data(:,i); % Forming a matrix of the mass fraction distribution
m=fillmissing(m,'constant',0);
z_Sarea(:,j)=Data(:,i+1);%matrix of the z-face areas
z_Sarea=fillmissing(z_Sarea,'constant',0);
Sarea_tot(1,j)=Data(1,i+16);% total cross sectional area on each cross section
mbar(1,j)=Data(1,i+15); % area weighted average of the mass fraction of the
%corresponding cross-section
j=j+1;
end

%% Setting the upper and lower bounds of Mass fraction corresponding to X% level of
mixedness
% ux is the upper bound of the mass fraction corresponding to >x%--(1+(1-X))*mbar
% lx is the lower bound of the mass fraction corresponding to >x%--(1-(1-X))*mbar
u95=(2-0.95)*mbar; l95=0.95*mbar;
u90=(2-0.9)*mbar; l90=0.9*mbar;
u80=(2-0.8)*mbar; l80=0.8*mbar;
u70=(2-0.7)*mbar; l70=0.7*mbar;
u60=(2-0.6)*mbar; l60=0.6*mbar;

%% Total surface area where X% mixing is achieved

%-----Example mbar=0.5-----
% for X>=95% ---> 0.475 <= x <= 0.525
% for 90%<=X<=94% ---> 0.450 <= x < 0.475 or 0.525 <x <= 0.55
% for 80%<=X<=89% ---> 0.400 <= x < 0.45 or 0.550 < x <= 0.6
% for 70%<=X<=79% ---> 0.350 <= x < 0.40 or 0.600 < x <= 0.65
% for 60%<=X<=69% ---> 0.300 <= x < 0.35 or 0.650 < x <= 0.70
```

```

% for    X< 60% --->    x < 0.30 or    x > 0.70

%-----Defintions of the surface areas corresponding to each X%-----
% X>=95%-SA95//90%<=X<=94%-SA90//80%<=X<=89%-SA80//70%<=X<=79-
SA70//60%<=X<=69%-SA60// X< 60%-SAr

[SA95,SA90,SA80,SA70,SA60,SAr]=deal(zeros(1,7));
for j=1:7
    for i=1:size(m,1)
        if ( m(i,j)>=l95(j) && m(i,j)<=u95(j) )
            SA95(j)=SA95(j)+z_Sarea(i,j);
        elseif ( m(i,j)>=l90(j) && m(i,j)< l95(j)) || (m(i,j)>u95(j) && m(i,j)<=u90(j) )
            SA90(j)=SA90(j)+z_Sarea(i,j);

        elseif ( (m(i,j)>=l80(j) && m(i,j)< l90(j)) || (m(i,j)>u90(j) && m(i,j)<= u80(j)) )
            SA80(j)=SA80(j)+z_Sarea(i,j);

        elseif ( (m(i,j)>=l70(j) && m(i,j)< l80(j)) || (m(i,j)>u80(j) && m(i,j)<= u70(j)) )
            SA70(j)=SA70(j)+z_Sarea(i,j);

        elseif ( (m(i,j)>=l60(j) && m(i,j)< l70(j)) || (m(i,j)>u70(j) && m(i,j)<= u60(j)) )
            SA60(j)=SA60(j)+z_Sarea(i,j);

        else
            SAr(j)=SAr(j)+z_Sarea(i,j);
        end
    end
end
end
% -----Area fractions Af corresponding to each area as in the previous part %----
Af95=SA95./Sarea_tot;
Af90=SA90./Sarea_tot;
Af80=SA80./Sarea_tot;
Af70=SA70./Sarea_tot;
Af60=SA60./Sarea_tot;
Afr=SAr./Sarea_tot;

%% Plotting the bar graphs

Af=[Af95;Af90; Af80; Af70; Af60 ;Afr];% matrix containing all the area fractions
[m% ;Re]
Af(:,1)=abs(Af(:,1));
figure (1)
Mbar=bar(Af,'stacked','FaceColor','flat');
xt = get(gca, 'XTick');
set(gca, 'XTick', xt, 'XTickLabel', {'Inlet','K4','d*=1',...
'd*=2','d*=3','d*=4','Outlet',},'FontSize',18,'FontName','Times new Roman')
ylabel('Area Fraction','FontWeight','bold','FontSize',20,'FontName','Times new
Roman','FontWeight','bold');

```



```
ylim([0,1]);  
legend ('95-100%', '90-94%', '80-89%', '70-79%', '60-  
69%', '<60%', 'FontWeight', 'bold', 'FontSize', 18, 'FontName', 'Times new  
Roman', 'Location', 'SE')
```

APPENDIX 2

SMV MIXER

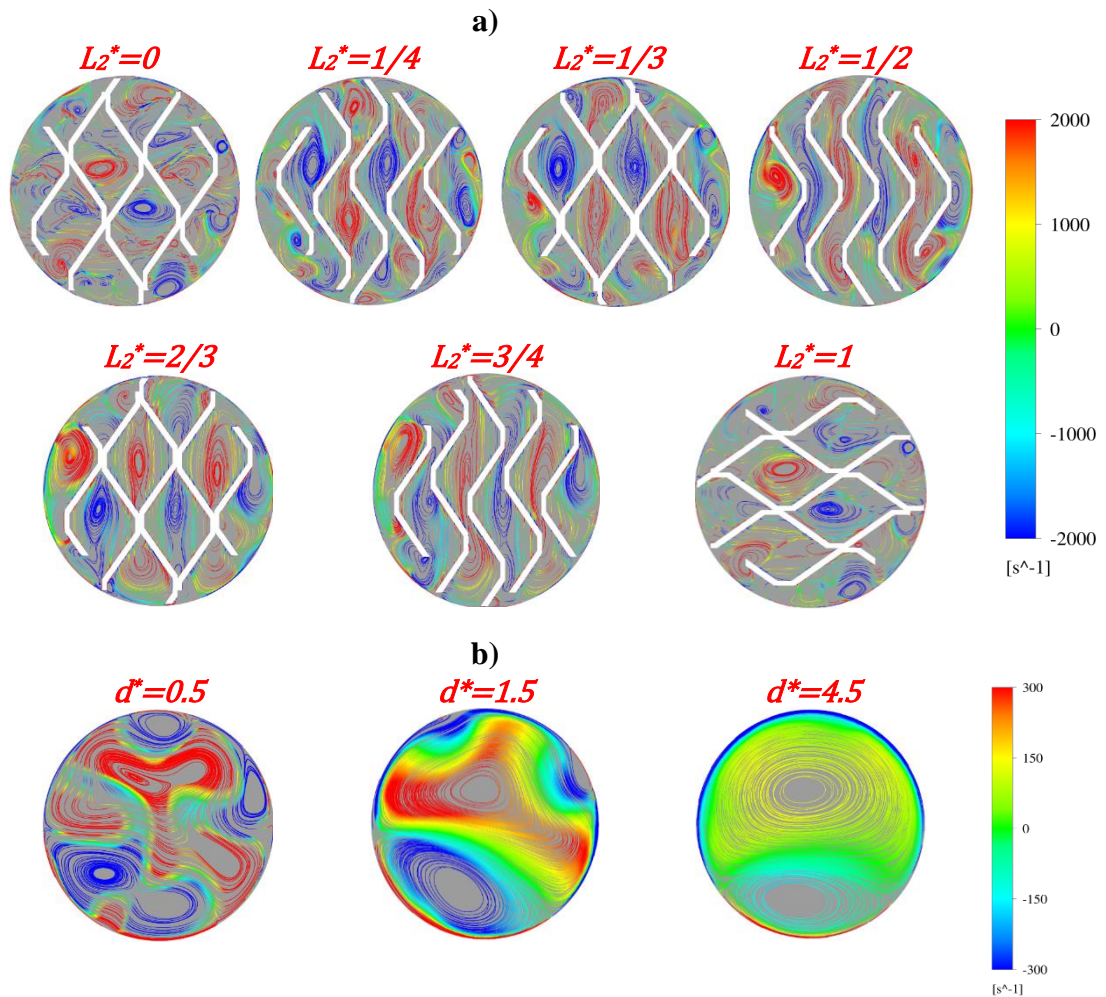


Figure 50 Planar velocity streamlines colored by the axial vorticity at different planes a) within the 2nd SMV element and b) downstream of the mixing section at $Re=30,000$

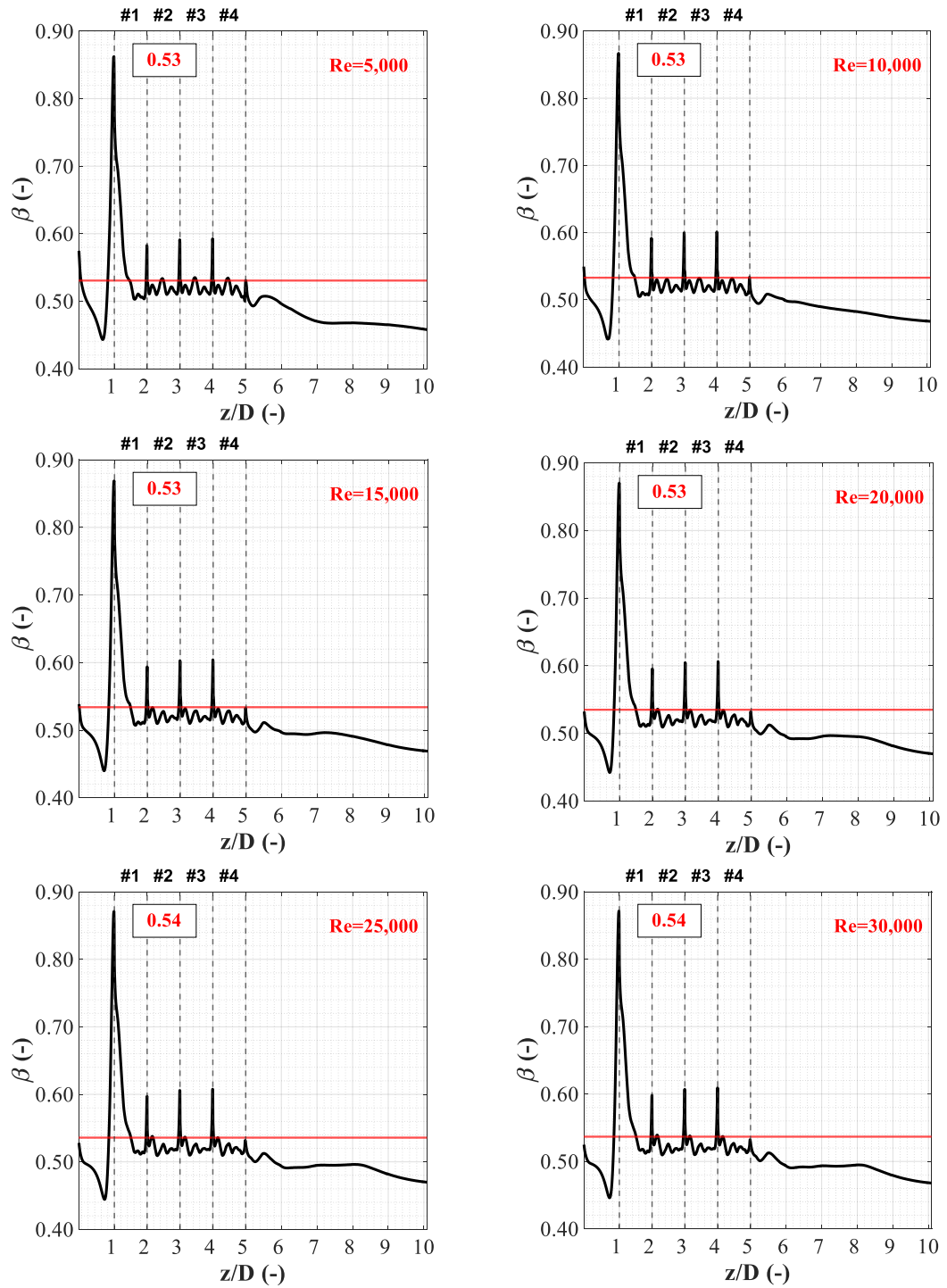


Figure 51 Axial variation of the extensional efficiency β in a 4-SMV mixer at different Re numbers

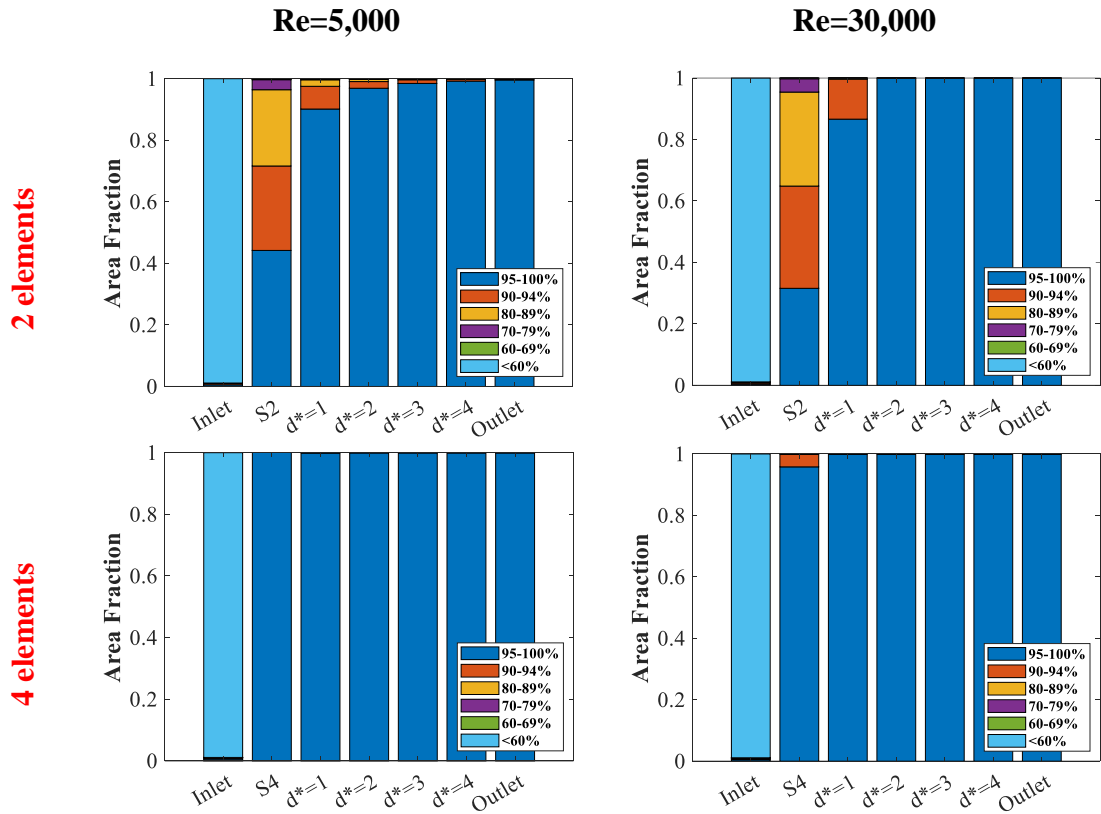


Figure 52 Stacked bar graphs showing the discrete areal distribution of the mass fraction of the secondary fluid in SMV at different locations for $Re=5,000$ (first column), $Re=30,000$ (second column), and for different numbers of mixing units: 2 elements (first row) and 4 elements (second row)

REFERENCES

- Abou-Hweij, W. (2022). Numerical Simulation of Wall-Bounded Flows through Screen-Type Static Mixers. Unpublished PhD thesis, American University of Beirut.
- Abou-Hweij, W., & Azizi, F. (2020a). CFD simulation of wall-bounded laminar flow through screens. Part I: Hydrodynamic characterization. *European Journal of Mechanics - B/Fluids*, 84, 207-232.
- Abou-Hweij, W., & Azizi, F. (2020b). CFD SIMULATION OF WALL-BOUNDED LAMINAR FLOW THROUGH SCREENS: PART II — MIXING CHARACTERIZATION. In A. S. o. M. Engineers (Ed.), *Proceedings of the ASME 2020 Fluids Engineering Division Summer Meeting FEDSM2020*. Virtual, Online: ASME.
- Abou Hweij, K., & Azizi, F. (2015). Hydrodynamics and residence time distribution of liquid flow in tubular reactors equipped with screen-type static mixers. *Chemical Engineering Journal*, 279, 948-963.
- Adamiak, I., & Jaworski, Z. (2001). An experimental investigation of the non-Newtonian liquid flow in a Kenics static mixer. *Inzynieria Chemiczna I Procesowa*, 22, 175-180.
- Al-Hassan, T., Habchi, C., Lemenand, T., & Azizi, F. (2021). CFD simulation of creeping flows in a novel split-and-recombine multifunctional reactor. *Chemical Engineering and Processing - Process Intensification*, 162.
- Alberini, F., Simmons, M. J. H., Ingram, A., & Stitt, E. H. (2014). Use of an areal distribution of mixing intensity to describe blending of non-newtonian fluids in a kenics KM static mixer using PLIF. *AIChE Journal*, 60, 332-342.
- Ansys. (2013). *ANSYS Fluent Theory Guide*. In.
- Aubin, J., Ferrando, M., & Jiricny, V. (2010). Current methods for characterising mixing and flow in microchannels. *Chemical Engineering Science*, 65, 2065-2093.
- Azizi, F. (2019). On the pressure drop of fluids through woven screen meshes. *Chemical Engineering Science*, 207, 464-478.
- Azizi, F., Abou-Hweij, W., Lebaz, N., & Sheibat-Othman, N. (2022). A numerical evaluation of flows through an SMX-Plus mixer. *Chemical Engineering Research and Design*, 178, 382-394.
- Azizi, F., & Abou Hweij, K. (2017). Liquid-phase axial dispersion of turbulent gas-liquid co-current flow through screen-type static mixers. *AIChE Journal*, 63, 1390-1403.
- Azizi, F., & Al Taweel, A. M. (2011). Hydrodynamics of Liquid Flow through Screens and Screen-Type Static Mixers. *Chemical Engineering Communications*, 198, 726-742.

- Azizi, F., & Taweel, A. M. A. (2011). Turbulently flowing liquid–liquid dispersions. Part I: Drop breakage and coalescence. *Chemical Engineering Journal*, 166, 715–725.
- Barrue, H., Karoui, A., Le Sauze, N., Costes, J., & Illy, F. (2001). Comparison of aerodynamics and mixing mechanisms of three mixers: Oxynator™ gas–gas mixer, KMA and SMI static mixers. *Chemical Engineering Journal*, 84, 343–354.
- Berkman, P., & Calabrese, R. (1988). Dispersion of Viscous Liquids by Turbulent Flow in a Static Mixer. *AIChE Journal*, 34, 602–609.
- Bigg, D. (1975). On Mixing in Polymer Flow Systems. *Polymer Engineering and Science*, 15, 684–689.
- Bourne, J., Lenzner, J., & Petrozzi, S. (1992). Micromixing in Static Mixers: An Experimental Study. *Industrial & Engineering Chemistry Research*, 31, 1216–1222.
- Celik, I., Ghia, U., Roache, P., Freitas, C., Coleman, H., & Raad, P. (2008). Procedure for Estimation and Reporting of Uncertainty Due to Discretization in CFD Applications. *Journal of Fluids Engineering*, 130.
- Çengel, y., & Cimbala, J. (2017). *Fluid Mechanics Fundamentals and Applications*. In (pp. 372): Mc Graw Hill.
- Coroneo, M., Montante, G., & Paglianti, A. (2012). Computational Fluid Dynamics Modeling of Corrugated Static Mixers for Turbulent Applications. *Industrial & Engineering Chemistry Research*, 51, 15986–15996.
- Cremaschi, S. (2014). A perspective on process synthesis. In *Proceedings of the 8th International Conference on Foundations of Computer-Aided Process Design* (pp. 35–44).
- Dančová, P., Sosnowski, M., Krzywanski, J., Grabowska, K., & Gnatowska, R. (2018). Polyhedral meshing in numerical analysis of conjugate heat transfer. *EPJ Web of Conferences*, 180.
- De La Villéon, J., Bertrand, F., Tanguy, P., Labrie, R., Bousquet, J., & Lebouvier, D. (1998). Numerical Investigation of Mixing Efficiency of Helical Ribbon. *AIChE Journal*, 44, 972–977.
- Dimotakis, P. (2005). Turbulent Mixing. *Annu. Rev. Fluid Mech.*, 37, 329–356.
- Dong, Y., Ng, W. K., Hu, J., Shen, S., & Tan, R. B. (2010). A continuous and highly effective static mixing process for antisolvent precipitation of nanoparticles of poorly water-soluble drugs. *Int J Pharm*, 386, 256–261.
- Etchells, A. W., & Meyer, C. F. (2004). Mixing in Pipelines. In E. Paul, V. Atiemo-Obeng & S. Kresta (Eds.), *Handbook of industrial mixing- Science and practice*. Canada: JOHN WILEY & SONS, INC.
- Fogler, H. S. (2016). Residence Time Distribution of Chemical Reactors. In *Elements of Chemical Reactor Engineering* (Fifth ed., pp. 802–842): Pearson Education, Inc.

- Frascari, D., Zuccaro, M., Pinelli, D., & Paglianti, A. (2008). A Pilot-Scale Study of Alkali-Catalyzed Sunflower Oil Transesterification with Static Mixing and with Mechanical Agitation. *Energy and Fuels*, 22, 1493–1501.
- Ghanem, A., Lemenand, T., Della Valle, D., & Peerhossaini, H. (2014). Static mixers: Mechanisms, applications, and characterization methods – A review. *Chemical Engineering Research and Design*, 92, 205-228.
- Godfrey, J. (1997). Static Mixers. In N. Harnby, M. F. Edwards & N. W. Nienow (Eds.), *Mixing in the Process Industries* (second edition ed., pp. 225-264): Butterworth Heinmann,.
- González-Juárez, D., Solano, J. P., Herrero-Martín, R., & Harvey, A. P. (2017). Residence time distribution in multiorifice baffled tubes: A numerical study. *Chemical Engineering Research and Design*, 118, 259-269.
- Habchi, C., & Azizi, F. (2018). Heat transfer and turbulent mixing characterization in screen-type static mixers. *International Journal of Thermal Sciences*, 134, 208-215.
- Haddadi, M. M., Hosseini, S. H., Rashtchian, D., & Olazar, M. (2020). Comparative analysis of different static mixers performance by CFD technique: An innovative mixer. *Chinese Journal of Chemical Engineering*, 28, 672-684.
- Hearn, S. (1995). Turbulent mixing mechanism in motionless mixers. University of Birmingham.
- Hirschberg, S., Koubek, R., F.Moser, & Schöck, J. (2009). An improvement of the Sulzer SMX™ static mixer significantly reducing the pressure drop. *Chemical Engineering Research and Design*, 87, 524-532.
- Hobbs, D., & Muzzio, F. (1997a). Effects of Injection Location, Flow Ratio and Geometry on Kenics Mixer Performance. *AIChE Journal*, 43, 3121-3132.
- Hobbs, D., & Muzzio, F. (1997b). The Kenics static mixer: a three-dimensional chaotic flow. *Chemical Engineering Journal*, 67, 153-166.
- Hosseini, S. M., Razzaghi, K., & Shahraki, F. (2019). Design and characterization of a Low-pressure-drop static mixer. *AIChE Journal*, 65, 1126-1133.
- Jegatheeswaran, S., Ein-Mozaffari, F., & Wu, J. (2020). Laminar mixing of non-Newtonian fluids in static mixers: process intensification perspective. *Reviews in Chemical Engineering*, 36, 423-436.
- Jiang, X., Yang, N., & Wang, R. (2021). Effect of Aspect Ratio on the Mixing Performance in the Kenics Static Mixer. *Processes*, 9.
- Joaquim, C. F., Reynol, A., Cekinski, E., Seckler, M. M., & Nunhez, J. R. (2011). Development of static mixers for miscible fluids in laminar flow with the use of computational fluid dynamics (CFD). *The Canadian Journal of Chemical Engineering*, 89, 734-744.
- Joshi, P., Nigam, K. D. P., & Nauman, E. B. (1995). The Kenics Static Mixer: New data and proposed Correlations. *The Chemical Engineering Journal*, 59, 265-271.
- Karoui, A., & Costes, J. (1998). Caractérisation de l'hydrodynamique et du mélange dans les mélangeurs statiques Sulzer SMV.

- Karoui, A., Hakenholz, F., Le Sauze, N., Costes, J., & Bertrand, J. (1998). Determination of The Mixing performanve of Sulzer SM Static Mixers by Laser Induced Fluorescence. *The Canadian Journal of Chemical Engineering*, 76.
- Krstić, D. M., Höflinger, W., Koris, A. K., & Vatai, G. N. (2007). Energy-saving potential of cross-flow ultrafiltration with inserted static mixer: Application to an oil-in-water emulsion. *Separation and Purification Technology*, 57, 134-139.
- Kukukova, A., Aubin , J., & Kresta, S. (2009). A new definition of mixing and segregation: Three dimensions of a key process variable. *Chemical Engineering Research and Design*, 87, 633-647.
- Kumar, V., Shirke, V., & Nigam, K. D. P. (2008). Performance of Kenics static mixer over a wide range of Reynolds number. *Chemical Engineering Journal*, 139, 284-295.
- Kurian, T., & Fransson, J. H. M. (2009). Grid-generated turbulence revisited. *Fluid Dynamics Research*, 41.
- Lang, E., Drtina, P., Streiff, F., & Fleischli, M. (1995). Numerical simulation of the fluid flow and the mixing process in a static mixer. *International Journal of Heat and Mass Transfer*, 38, 2239-2250.
- Lebaz, N., & Sheibat-Othman, N. (2019). Modeling Emulsification in Static Mixers: Equilibrium Correlations versus Population Balance Equations. *Chemical Engineering & Technology*.
- Lehwald, A., Janiga, G., Thévenin, D., & Zähringer, K. (2012). Simultaneous investigation of macro- and micro-mixing in a static mixer. *Chemical Engineering Science*, 79, 8-18.
- Li, H. Z., Fasol, C., & Choplin, L. (2007). Residence Time Distribution of Rheologically Complex Fluids Passing through a Sulzer Smx Static Mixer. *Chemical Engineering Communications*, 165, 1-15.
- Lim, V., Hobby, A. M., McCarthy, M. J., & McCarthy, K. L. (2015). Laminar mixing of miscible fluids in a SMX mixer evaluated by magnetic resonance imaging (MRI). *Chemical Engineering Science*, 137, 1024-1033.
- Medina, H., Thomas, M., Eldredge, T., & Adebajo, A. (2019). The M Number: A Novel Parameter to Evaluate the Performance of Static Mixers. *Journal of Fluids Engineering*, 141.
- Meng, H.-B., Song, M.-Y., Yu, Y.-F., Jiang, X.-H., Wang, Z.-Y., & Wu, J.-H. (2016). Enhancement of Laminar Flow and Mixing Performance in a Lightnin Static Mixer. *International Journal of Chemical Reactor Engineering*, 15.
- Meng, H., Han, M., Yu, Y., Wang, Z., & Wu, J. (2020). Numerical evaluations on the characteristics of turbulent flow and heat transfer in the Lightnin static mixer. *International Journal of Heat and Mass Transfer*, 156.
- Meng, H., Song, M., Yu, Y., Wang, F., & Wu, J. (2015). Chaotic mixing characteristics in static mixers with different axial twisted-tape inserts. *The Canadian Journal of Chemical Engineering*, 93, 1849-1859.

- Meng, H., Wang, F., Yu, Y., Song, M., & Wu, J. (2014). A Numerical Study of Mixing Performance of High-Viscosity Fluid in Novel Static Mixers with Multitwisted Leaves. *Industrial & Engineering Chemistry Research*, 53, 4084-4095.
- Mihailova, O., Lim, V., McCarthy, M. J., McCarthy, K. L., & Bakalis, S. (2015). Laminar mixing in a SMX static mixer evaluated by positron emission particle tracking (PEPT) and magnetic resonance imaging (MRI). *Chemical Engineering Science*, 137, 1014-1023.
- Mohammadi, A., Moghaddas, J., & Ariamanesh, A. (2014). Residence Time and Concentration Distribution in a Kenics Static Mixer. *Chemical Engineering Communications*, 202, 144-150.
- Montante, G., Coroneo, M., & Paglianti, A. (2016). Blending of miscible liquids with different densities and viscosities in static mixers. *Chemical Engineering Science*, 141, 250-260.
- Moukalled, F., Darwish, M., & Mangani, L. (2015). Turbulence Modeling. In *The Finite Volume Method in Computational Fluid Dynamics* (Vol. 133, pp. 693-742): Springer.
- Murasiewicz, H., & Jaworski, Z. (2013). Investigation of turbulent flow field in a Kenics static mixer by Laser Doppler Anemometry. *Chemical Papers*, 67.
- Murasiewicz, H., & Zakrzewska, B. (2019). Large Eddy Simulation of turbulent flow and heat transfer in a Kenics static mixer. *Chemical and Process Engineering*, 40, 87-99.
- Myers, K., Janz, E., Cathie, N., & Jones, M. (2018). *Employ Static Mixers for Process Intensifications*. American Institute of Chemical Engineers.
- Nyande, B. W., Mathew Thomas, K., & Lakerveld, R. (2021). CFD Analysis of a Kenics Static Mixer with a Low Pressure Drop under Laminar Flow Conditions. *Industrial & Engineering Chemistry Research*, 60, 5264-5277.
- Okolo, P. N., Zhao, K., Kennedy, J., & Bennett, G. J. (2019). Numerical assessment of flow control capabilities of three dimensional woven wire mesh screens. *European Journal of Mechanics - B/Fluids*, 76, 259-271.
- Paglianti, A., & Montante, G. (2013). A mechanistic model for pressure drops in corrugated plates static mixers. *Chemical Engineering Science*, 97, 376-384.
- Pianko-Oprych, P., & Jaworski, Z. (2009). CFD modelling of two-phase liquid-liquid flow in a SMX static mixer. *Polish Journal of Chemical Technology*, 11, 41-49.
- Rafiee, M., Simmons, M. J. H., Ingram, A., & Stitt, E. H. (2013). Development of positron emission particle tracking for studying laminar mixing in Kenics static mixer. *Chemical Engineering Research and Design*, 91, 2106-2113.
- Rahmani, R. K., Ayasoufi, A., & Keith, T. G. (2007). A Numerical Study of the Global Performance of Two Static Mixers. *Journal of Fluids Engineering*, 129, 338-349.
- Rahmani, R. K., Keith, T. G., & Ayasoufi, A. (2008). Numerical simulation of turbulent flow in an industrial helical static mixer. *International Journal of Numerical Methods for Heat & Fluid Flow*, 18, 675-696.

- Rauline, D., Tanguy, P., & Le Blevec, J. (1998). Numerical Investigation of The Performance of Several Static Mixers. *The Canadian Journal of Chemical Engineering*, 76, 527-535.
- Regner, M., Östergren, K., & Trägårdh, C. (2006). Effects of geometry and flow rate on secondary flow and the mixing process in static mixers—a numerical study. *Chemical Engineering Science*, 61, 6133-6141.
- Roache, P. (1986). The generation of nearly isotropic turbulence by means of grids. *Heat and Fluid Flow*, 8, 82-92.
- Simpson, T. A., Dawson, M. K., & Etchells, A. W. (2016). Update to Mixing in Pipelines. In *Advances in industrial mixing*: Wiley.
- Sir, J., & Lecjaks, Z. (1982). Pressure Drop and Homogenization Efficiency of a Motionless Mixer. *Chemical Engineering Communications*, 16, 325-334.
- Song, H.-S., & Han, S. P. (2005). A general correlation for pressure drop in a Kenics static mixer. *Chemical Engineering Science*, 60, 5696-5704.
- Stec, M., & Synowiec, P. M. (2017a). Study of fluid dynamic conditions in the selected static mixers part I- research of pressure drop. *The Canadian Journal of Chemical Engineering*, 95, 2156-2167.
- Stec, M., & Synowiec, P. M. (2017b). Study of fluid dynamic conditions in the selected static mixers part II-determination of the residence time distribution. *The Canadian Journal of Chemical Engineering*, 95, 2410-2422.
- Stec, M., & Synowiec, P. M. (2019). Study of fluid dynamic conditions in the selected static mixers part III—research of mixture homogeneity. *The Canadian Journal of Chemical Engineering*, 97, 995-1007.
- Szalai, E. S., ALVAREZ, M., & MUZZIO, F. (2004). LAMINAR MIXING: A DYNAMICA SYSTEMS APPROACH. In E. Paul, V. Atiemo-Obeng & S. Kresta (Eds.), *Hand Book of Industrial Mixing: Science and Practice* (pp. 89-141). Canada: JOHN WILEY & SONS, INC.
- Szalai, E. S., & Muzzio, F. (2003). Fundamental Approach to the Design and Optimization of Static Mixers. *AIChE Journal*, 49, 2687-2699.
- Tajima, H., Nagata, T., Abe, Y., Yamasaki, A., Kiyono, F., & Yamagiwa, K. (2010). HFC-134a Hydrate Formation Kinetics during Continuous Gas Hydrate Formation with a Kenics Static Mixer for Gas Separation. *Industrial & Engineering Chemistry Research*, 49, 2525–2532.
- Tajima, H., Yoshida, Y., Abiko, S., & Yamagiwa, K. (2010). Size adjustment of spherical temperature-sensitive hydrogel beads by liquid–liquid dispersion using a Kenics static mixer. *Chemical Engineering Journal*, 156, 479-486.
- Thakur, R. K., Vial, C., Nigam, K. D. P., Nauman, E. B., & Djelveh, G. (2003). Static Mixers in the Process Industries—A Review. *Chemical Engineering Research and Design*, 81, 787-826.
- Theron, F. (2009). Conception et mise en œuvre d'un procédé intensifié continu de microencapsulation par polycondensation interfaciale. Université de Toulouse.

- Theron, F., & Le Sauze, N. (2011). Comparison between three static mixers for emulsification in turbulent flow. *International Journal of Multiphase Flow*, 37, 488-500.
- Wadley, R., & Dawson, M. K. (2005). LIF measurements of blending in static mixers in the turbulent and transitional flow regimes. *Chemical Engineering Science*, 60, 2469-2478.
- Yenjaichon, W., Pageau, G., Bhole, M., Bennington, C. P. J., & Grace, J. R. (2011). Assessment of mixing quality for an industrial pulp mixer using electrical resistance tomography. *The Canadian Journal of Chemical Engineering*, 89, 996-1004.
- Zhuang, Z., Yan, J., Sun, C., Wang, H., Wang, Y., & Wu, Z. (2020). The numerical simulation of a new double swirl static mixer for gas reactants mixing. *Chinese Journal of Chemical Engineering*, 28, 2438-2446.